DISSERTATION

Stimulation des Stickstoffmonoxid-Signalweges durch Aktivatoren der löslichen Guanylatzyklase in kortikalen und medullären renalen Mikrogefäßen

Stimulation of the nitric oxide signaling pathway by activators of the soluble guanylyl cyclase in cortical and medullary renal microvessels

zur Erlangung des akademischen Grades

Doctor of Philosophy (PhD)

vorgelegt der Medizinischen Fakultät
Charité – Universitätsmedizin Berlin

von

Minze Xu

Erstbetreuer*in: Prof. Dr. med. Andreas Patzak

Datum der Promotion: 28.02.2025

Table of contents

List of figures

List of abbreviations

AA	- afferent arteriole
ACh	- acetylcholine
AKI	- acute kidney injury
AKD	- acute kidney disease
Ang II	- angiotensin II
cGMP	- cyclic guanosine monophosphate
CKD	- chronic kidney disease
EA	- efferent arteriole
GMP	- guanosine monophosphate
H/R	- hypoxia/re-oxygenation
KDIGO	- Kidney Disease Improving Global Outcomes
L-NAME	- N(ω)-nitro-L-arginine methyl ester
NO	- nitric oxide
NOS	- nitric oxide synthase
eNOS	- endothelial NOS
iNOS	- inducible NOS
nNOS	- neuronal NOS
PDE5	- phosphodiesterase 5
PKG	- protein kinase G
ODQ	- sGC inhibitor
ROS	- reactive oxygen species
sGC	- soluble guanylyl cyclase
SNP	- sodium nitroprusside
VSMC	- vascular smooth muscle cell

Abstract

Disturbances in renal microcirculatory function contribute to renal pathologies such as acute kidney injury (AKI), chronic kidney disease (CKD) of different origin, and rejection of kidney transplants. A main pathophysiological factor is reduced nitric oxide (NO) bioavailability in the renal vasculature. Pharmacological activation of the natural receptor for NO, the soluble guanylyl cyclase (sGC), improves the renal outcome after experimental AKI or CKD. This thesis investigates the effect of sGC-activation in renal cortical and medullary microvessels in situations with NO-deficit, oxidation of sGC, and after hypoxia/re-oxygenation.

Microvessels were dissected from freshly harvested kidney slices by hand. A customized micro-perfusion system, situated on a stage of an inverted microscope, was used for the perfusion of isolated afferent and efferent arterioles of mice as well as medullary vasa recta from rats. The reactivity of the microvessels was analysed by measuring the changes in vessel luminal diameters in response to several pharmacological and physical manipulations.

The sGC activators BAY 58-2667, runcaciguat, and BAY 60-2770 were used. They have similar pharmacological actions. BAY 58-2667 and BAY 60-2770 dilated cortical and medullary microvessels, respectively, after inhibition of endothelial and neuronal NO-synthases by L-NAME and pre-constriction with angiotensin II (Ang II). Further, BAY 58-2667 dilated contrast medium (iodixanol) treated afferent arterioles, which have reduced NO-bioavailability. ODQ was administered to oxidize the sGC, which leads to the loss of NO binding of the enzyme. Under this condition, the dilator effect of runcaciguat on afferent and efferent arterioles was stronger compared to vessels pre-treated with L-NAME. Furthermore, BAY 58-2667 and BAY 60-2770 were able to dilate efferent arterioles and vasa recta, respectively, but not afferent arterioles after strong hypoxia and re-oxygenation *in vitro*.

The data show that pharmacological sGC-activation dilates renal microvessels under the condition of NO deficiency, sGC oxidation as well as after hypoxia-re-oxygenation. The stronger effect of runcaciguat on vessels with oxidized sGC suggests improved action in kidneys with impaired redox balance as observed in AKI and CKD. The results suggest that sGC activation may compensate for NO deficiency and impaired sGC function in microvessels, which may contribute to its renoprotective effect.

Zusammenfassung

Zahlreiche Nierenpathologien wie akutes Nierenversagen (AKI), chronisches Nierenversagen (CKD) unterschiedlichster Genese sowie die Abstoßungsreaktion bei Nierentransplantaten gehen mit Störungen der renalen Mikrozirkulation einher. Ein Hauptfaktor hierbei ist die verminderte Bioverfügbarkeit von Stickstoffmonoxid (NO). Pharmakologische Aktivierung der löslichen Guanylatzyklase (sGC), dem natürlichen Rezeptor für NO, schützt die Niere bei AKI und CKD. In der vorliegenden Dissertationsschrift wird die Wirkung von sGC-Aktivierung auf kortikale und medulläre Mikrogefäße der Niere unter den Bedingungen eines NO-Defizits, der Oxidation der sGC und nach Hypoxie/Re-Oxygenierung untersucht.

Die renalen Mikrogefäße wurden aus Akutschnitten der Niere per Hand isoliert. Afferenten und efferente Arteriolen der Maus als auch medulläre Vasa recta der Ratte wurden mittels eines speziellen Perfusionssystems, welches sich auf einem Mikroskop umgekehrter Bauweise befand, perfundiert. Die Reaktionen der Gefäße auf pharmakologische und physikalische Stimuli wurden durch Messung des Gefäßlumens bewertet.

Es wurden die sGC-Aktivatoren BAY 58-2667, Runcaciguat und BAY 60-2770 verwendet. Sie haben sehr ähnliche pharmakologische Eigenschaften. BAY 58-2667 und BAY 60-2770 erweiterten kortikale bzw. medulläre Mikrogefäße nach Hemmung der endothelialen und neuronalen NO-Synthasen mittels L-NAME sowie Präkonstriktion mit Angiotensin II (Ang II). BAY 58-2667 dilatierte afferente Arteriolen, die mit einem jodhaltigen Kontrastmittel (Jodixanol) behandelt und NO-defizient waren. In weiteren Experimenten wurde die sGC durch Behandlung mit ODQ oxidiert, wodurch sie die Fähigkeit zur NO-Anlagerung verliert. Unter diesen Bedingungen war der dilatierende Effekt von Runcaciguat in afferenten und efferenten Arteriolen stärker als unter L-NAME-Vorbehandlung. BAY 58-2667 und BAY 60-2770 dilatierten efferente Arteriolen bzw. Vasa recta, jedoch nicht afferente Arteriolen, nach starker Hypoxie *in vitro* und nachfolgender Re-Oxygenierung.

Die Daten zeigen, dass pharmakologische Aktivierung der sGC renale Mikrogefäße unter den Bedingungen von NO-Mangel, Oxidation der sGC sowie nach Hypoxie/Re-Oxygenierung erweitert. Der größere Effekt von Runcaciguat in Gefäßen mit oxidierter sGC könnte mit einer besseren Wirkung dieses Medikaments in Nieren einhergehen, die ein

gestörtes Redox-Gleichgewicht haben. Oxidativer Stress ist bei AKI und CKD beschrieben worden. Insgesamt weisen die Ergebnisse auf eine kompensatorische Wirkung von sGC-Aktivatoren bei NO-Mangel und gestörter sGC-Funktion in Mikrogefäßen hin. Dieser Effekt könnte zur beobachteten renoprotektiven Aktion von sGC-Aktivatoren beitragen.

1 Introduction

1.1 Acute kidney injury, acute kidney disease, and chronic kidney disease

Acute kidney injury (AKI) affects 7 to 18% of hospitalized patients. AKI goes along with adverse long-term outcomes and increased mortality (1). The high incidence especially in developing countries motivated the International Society of Nephrology to its Oby25 initiative for eliminating preventable deaths from AKI (2). AKI patients are at high risk for transition to chronic kidney disease (3, 4). The pathological processes, which develop after AKI have been defined recently and the medical term acute kidney disease (AKD) has been introduced (4). AKD is used for patients with affected kidney function and/or structure who meet neither the definition of AKI nor chronic kidney disease (5). According to the Kidney Disease Improving Global Outcomes (KDIGO) AKI guideline of 2011, AKI is considered a subset of the AKD section (6).

The prevalence of CKD is higher than 10% worldwide (7). Thus, CKD contributes significantly to worldwide mortality, whereby CKD-associated death rates have considerably risen since 1990 (4).

These data demand for enhanced efforts for better prevention and treatment of acute and chronic kidney diseases.

1.2 Pathophysiology of AKI and CKD

1.2.1 AKI

Causes for AKI include pathophysiological events which of pre-, intra- or post-renal origin. Pre-renal AKI is often due to cardiovascular failure particularly in critically ill patients in the intensive care unit (8). Acute tubule-necrosis due to intoxication (for example iodinated contrast media) or insufficient perfusion is the main reason for intra-renal AKI (9). Post-renal AKI is often attributed to urinary obstruction (different pathologies, (10). The different forms of AKI share a number of pathophysiological mechanisms, despite of diverse causes (see Fig. 1).

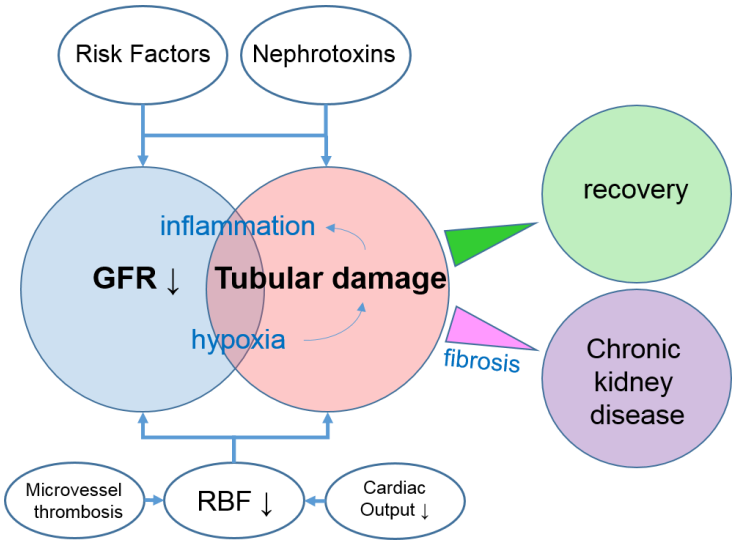

Fig. 1: Causes, important pathophysiological factors, and outcome of AKI. This is a simplified overview, which does consider neither all causes nor the complexity of the pathophysiological processes.
Modified after Pikkers P. et al. (11), GFR – glomerular filtration rate, RBF – renal blood flow.

1.2.2 CKD

The most frequent reasons for developing CKD are diabetes mellitus, systemic hypertension, glomerulonephritis, cystic kidneys, and nephrotoxic drugs. AKI is an important risk factor and can be a cause of CKD (12). CKD is characterised by gradual loss of kidney function and this may result in end-stage kidney disease. The pathogenesis of CKD differs according to the causes; however, the different forms share some basic changes such as a reduction in renal parenchyma and fibrosis (13).

1.2.3 Renal microvessels in AKI and CKD

The renal vasculature contributes to the orchestra of pathophysiological mechanisms in AKI and CKD. In the acute situation, microvessels often constrict and show thrombotic occlusions. Particularly in ischemia-reperfusion injury, as a common cause for AKI, as well as for sepsis induced AKI, peritubular capillaries and vasa recta are affected (14-16). In addition, glomerular arterioles may constrict in response to increased sympathetic nerve activity and renin-angiotensin-aldosteron system activation, which results in a decreased glomerular filtration rate. However, the experimental access to renal microvessels especially *in vivo* is still limited. Therefore, statements regarding possible

changes in microvessel function in AKI are rather hypothetically and need to be confirmed using adequate methods.

Microvessel rarefication is an important pathophysiological factor the progression from AKI to CKD (17).

Several studies suggest that the inner part of the outer medulla of the kidney is the most sensitive part concerning hypoxic damage (18). This may be due to the high demand of oxygen for resorption in the tubuli, the physiologically low perfusion combined with low oxygen pressure. The latter is due to the hair pin arrangement of vasa recta, which exclusively supplies this area with blood (19). Vasa recta are capillary like vessels without a media, but equipped with pericytes. They have similar functional properties as arterioles and contribute significantly to the control of renal medullary blood flow (20).

1.2.4 NO-sGC-cGMP-pathway for vessel dilatation

The balance between vasoconstrictory and vasodilatory substances determines the tone of renal vessels and microvessels. It changes in favour of vasoconstriction in AKI and CKD, thus contributing to a reduced renal perfusion and oxygen supply (21).

The NO-sGC-cGMP axis is a very powerful dilatory system in the renal vasculature (22). Experiments in isolated renal arterioles and vasa recta reveal the importance of the system for microvessel tone and reactivity to vasoconstrictors (23, 24). NO affecting renal microvasculature origins from different sources. The endothelial NOS (eNOS) generates the major portion, but the neuronal NOS (nNOS) in macula densa cells and NOS in epithelial cells contribute to NO bioavailability in renal microvessels (25-27). NO diffuses into vascular smooth muscle cells and activates the sGC by binding to the prosthetic group (heme), which contains a central iron atom (Fe^{2+}). Oxidative stress leads to oxidation (Fe^{3+}) and release of the heme group which goes along with a loss of function of the enzyme (28).

The activated sGC catalyses the production of cGMP, which then activates the protein kinase G (PKG). Vessel dilation results from the activation of several other kinases and channels; all of them contributing to a reduction in cytosolic Ca^{2+} (29-31). Fig. 2 shows the main signalling pathway of NO and possible effects of hypoxia/re-oxygenation.

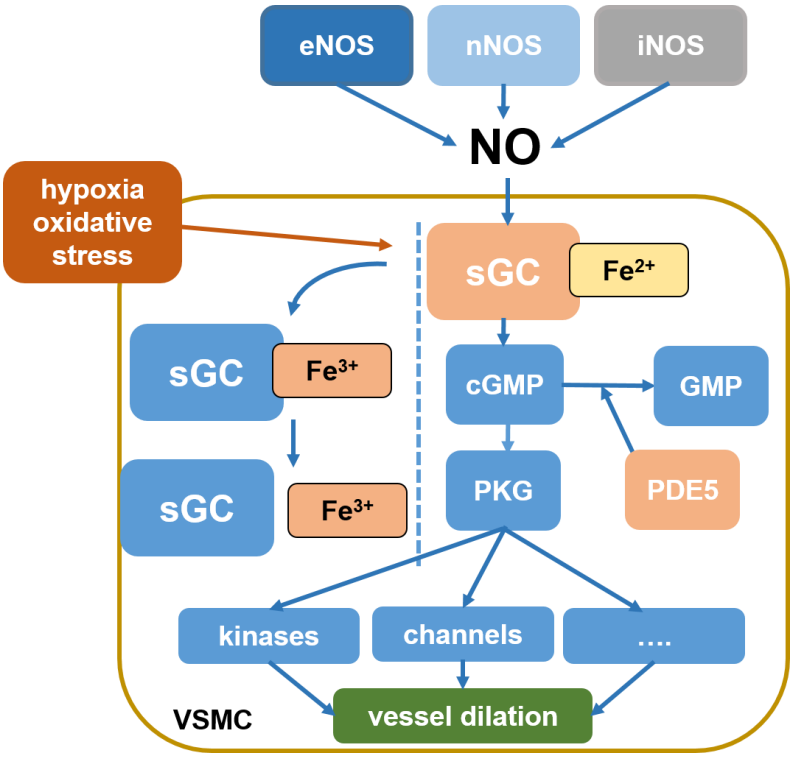

Fig. 2: Simple scheme of the NO-sGC-cGMP pathway. eNOS - endothelial nitric oxide synthase, nNOS - neuronal nitric oxide synthase, iNOS - inducible nitric oxide synthase, sGC- soluble guanylyl cyclase, cGMP – cyclic guanosin monophosphate, GMP - guanosin monophosphate, PKG – protein kinase G, PDE5 – phosphodiesterase 5, VSMC – vascular smooth muscle cell (own presentation).

1.2 sGC-stimulators and -activators

Two groups of pharmacological substances are available for sGC activation: so called stimulators and activators of sGC. Stimulators enhance the NO induced activation of the sGC. Activators work independently from NO. They do not need a heme group (32). NO bioavailability is reduced in many pathological situations. In addition, oxidation of the sGC due to oxidative stress has been described in AKI and CKD, which speaks in favour of activator application. SGC stimulators showed a protective effect in animal models of CKD (33, 34) and in heart failure with reduced ejection fraction (35). SGC activators are already used in the therapy of pulmonary hypertension (36). The protective effect of activators has been shown in different pre-clinical models of CKD and cardiovascular diseases (37-45). Activators reduced kidney damage, fibrosis, and inflammation. The exact mechanisms of their action are widely unknown. Since the NO-sGC-cGMP pathway is

important for vessel tone, one can hypothesize a protective effect via improved vasodilatation and renal perfusion.

1.3 Hypoxia – an important pathophysiological factor in AKI and CKD

Hypoxia is a broadly accepted component in the pathogenesis of multiple forms of acute kidney injury. However, reviews of the existing literature show a lack of understanding of the pathophysiological events after ischemia re-perfusion in the kidney (46, 47). Hypoxia may also be important in the transition from AKI to CKD and in the pathogenesis of CKD of different origin (48-50). Hypoxia does not only result from reduced renal (local) blood flow. Increased oxygen consumption, for example due to increased filtration in pathological situations, contributes to the observed hypoxia and low oxygenation, respectively (48). Experiments in models of ischemia/re-perfusion and hypoxia/re-oxygenation suggest a significant influence on vessel function. Renal microvessels of acute kidney slices showed higher reactivity to the vasoconstrictor angiotensin II after hypoxia/re-oxygenation (51, 52). Further, isolated renal interlobar arteries demonstrated an impaired vasorelaxation under similar experimental conditions (53). A critical role in this context plays oxidative stress, i.e. an increased concentration of reactive oxygen species (for example superoxide), which strengthens the angiotensin II signalling via MAPK kinase activation as well as scavenging of NO from endothelial and epithelial sources (54, 55). Further, oxidative stress impairs the function of the sGC in vascular smooth muscles (56). These effects contribute to increased microvessel tone and vascular resistance, which further worsen renal perfusion and oxygenation.

1.4 Hypothesis and objective

AKI and CKD are characterized by NO deficiency and oxidative stress (57, 58). Hypoxia/re-oxygenation is an important pathophysiological factor in most forms of AKI and CKD, which can induce endothelial dysfunction and excessive reactive oxygen species (oxidative stress). Activators of sGC stimulate the sGC NO- and heme-independent. We hypothesize that treatment with sGC activators dilate renal microvessel under these pathophysiological conditions and may have protective action in this context.

To test this hypothesis models of NO-deficiency and hypoxia/re-oxygenation in isolated renal cortical and medullary microvessels are used.

2 Methods

2.1 Animals

Male mice (C57Bl6J) and rats (Male Sprague-Dawley) were included in the studies. Animals were housed under standard conditions of Charité animal houses (59-61). The use of animals was approved by Landesamt für Gesundheit und Soziales Berlin (LAGeSo) and conformed to the Guide for the Care and Use of Laboratory Animals adopted by the National Institutes of Health.

2.2 Dissection and perfusion of microvessels

Details of procedures are available from our own publications (59-61). In short: Animals were anaesthetized with isoflurane and decapitated. Kidneys were removed quickly after opening the abdominal layers. They were sliced (1 mm thick) and the slices were kept at 4° Celsius in Dulbecco's modified Eagle's medium (DMEM, Gibco, Paisley, UK) with 0.1% albumin (Carl Roth GmbH, Karlsruhe, Germany). Dissection was performed using the same solution and temperature, and with the help of customized forceps (No. 5, Dumont, Switzerland). Mouse cortical microvessels were identified by their spatial position in relation to the glomerulus and by typical vessel wall patterns. Vasa recta (descending) were dissected from the outer medulla of the rat kidney and identified by their typical "bump-on-a-log" pattern (62).

Isolated microvessels were transferred to a thermo-controlled organ chamber (Vetec, Rostock, Germany) and perfused using a customized perfusion system with handmade pipettes (63, 64). Vessels were perfused with DMEM + 1% albumin and the bath solution was DMEM + 0.1% albumin. The perfusion pressure was adjusted to reach physiological perfusion rates and to distend the isolated vessel not too much. Afferent arterioles were perfused with a pressure in the pressure head of 100 mmHg, efferent arterioles with 40 mmHg and vasa recta with 15 mmHg.

Hypoxia/re-oxygenation experiments: Hypoxia (0.1% O_2, 5% CO_2) was applied to microvessels for 30 min, immediately after dissection (hypoxia chamber, Don Whitley Scientific Ltd., West Yorkshire, UK). Re-oxygenation time was 10 min and included the time needed for establishing the perfusion of the vessels.

2.3 Human vasa recta

Human DVR were isolated from human kidney tissue obtained from nephrectomy material of patients with renal cell carcinoma (Klinik für Urologie, Charité – Universitätsmedizin Berlin). All patients provided written informed consent. The study was approved by the ethical committee of the Charité – Universitätsmedizin Berlin (Approval No. EA4/65/18).

2.3 Data acquisition and analysis

Experiments were continuously monitored using a video system (Moticam 2.0, Motic Asia, Hong Kong, China) connected to an inverted microscope (Zeiss, Oberkochen, Germany).

Five pictures were taken for each experimental step in the functional steady state situation of the vessels. The pictures were analyzed with the help of ImageJ (65).The site with the strongest reactivity to vasoactive substances was used to estimate glomerular arteriolar responsiveness. In vasa recta, only sites with a pericyte were used. Vasa recta show detectable active functional reactions only where pericytes are located. The average of five pictures per experimental step was used for further analysis. For the time-response experimental part, pictures were taken for every 10 seconds for 10 minutes after the substance application.

The statistical analysis was performed using “R”, a free software package (http://www.r-project.org) and GraphPad software (San Diego, CA, USA). We tested differences in concentration dependent diameter changes between groups with the two-way, ANOVA like Brunner test for non-normal distributed data. The Wilcoxon test for independent variables served for testing differences in single parameters between two groups (GraphPad) while the Wilcoxon-test for dependent measurements was used for testing the effect of drugs within a group.

2.4 Experimental procedures

Experiments started within two hours after sacrificing the animal. Microvessels were perfused and warmed to 37° C in the chamber (organ bath) on the stage of the inverted microscope. Afferent arterioles’ viability was tested by a short application of 100 mmol/l

KCl solution, which should result in complete and sustained (10s) constriction. Other criteria for vessel viability were a preserved wall structure and a preserved vessel tone. Adaptation time for microvessels was 10 min.

N(ω)-nitro-L-arginine methyl ester (L-NAME, 10^{-4} mol/l)) was applied to inhibit NOS isoforms non-selectively. Vessel constriction ability was measured by applying angiotensin II in increasing concentrations (10^{-12}-10^{-6} mol/l). A bolus of angiotensin II (10^{-6} mol/l) was used to pre-constrict microvessels before testing the dilatory effect of agonists. Endothelial dependent dilatation was tested by application of acetylcholine in increasing concentrations (10^{-11}-10^{-4} mol/l), while endothelium independent dilatation was tested by applying the NO-donator sodium nitroprusside (SNP, 10^{-3} mol/l). Activation of the sGC was performed by applying the sGC activators cinaciguat (60) or BAY 60-2770 (59) or runcaciguat (61). The GC was inhibited by applying the selective inhibitor ODQ (5 *10^{-4} mol/l). All substances were added to the bath solution.

3. Results

3.1 The NO-sGC-cGMP system in vasa recta

L-NAME (10^{-4} mol/l) application for 15 min reduced vasa recta diameter, increased the following angiotensin II induced constriction compared to vessels not treated with L-NAME, and strongly weakened the ACh (10^{-11}-10^{-4} mol/l) induced dilation (Fig. 3). Sildenafil (10^{-9}-10^{-6} mol/l), a specific PDE5 inhibitor, dilated pre-constricted vasa recta dose dependent (Fig. 4). Further, a sildenafil bolus (10^{-7} mol/l) dilated to pre-constricted vessels 10 min after bath application completely (Fig. 4). Bay 60-2770 (10^{-6} mol/l) dilated L-NAME (10^{-4} mol/l) treated (NO deficient) and angiotensin II-pre-constricted (10^{-6} mol/l) vasa recta to about 90% of initial diameter (Fig. 5). Bay 60-2770 dilated human vasa recta after pre-constriction with angiotensin II (10^{-12}-10^{-6} mol/l) completely (Fig. 6).

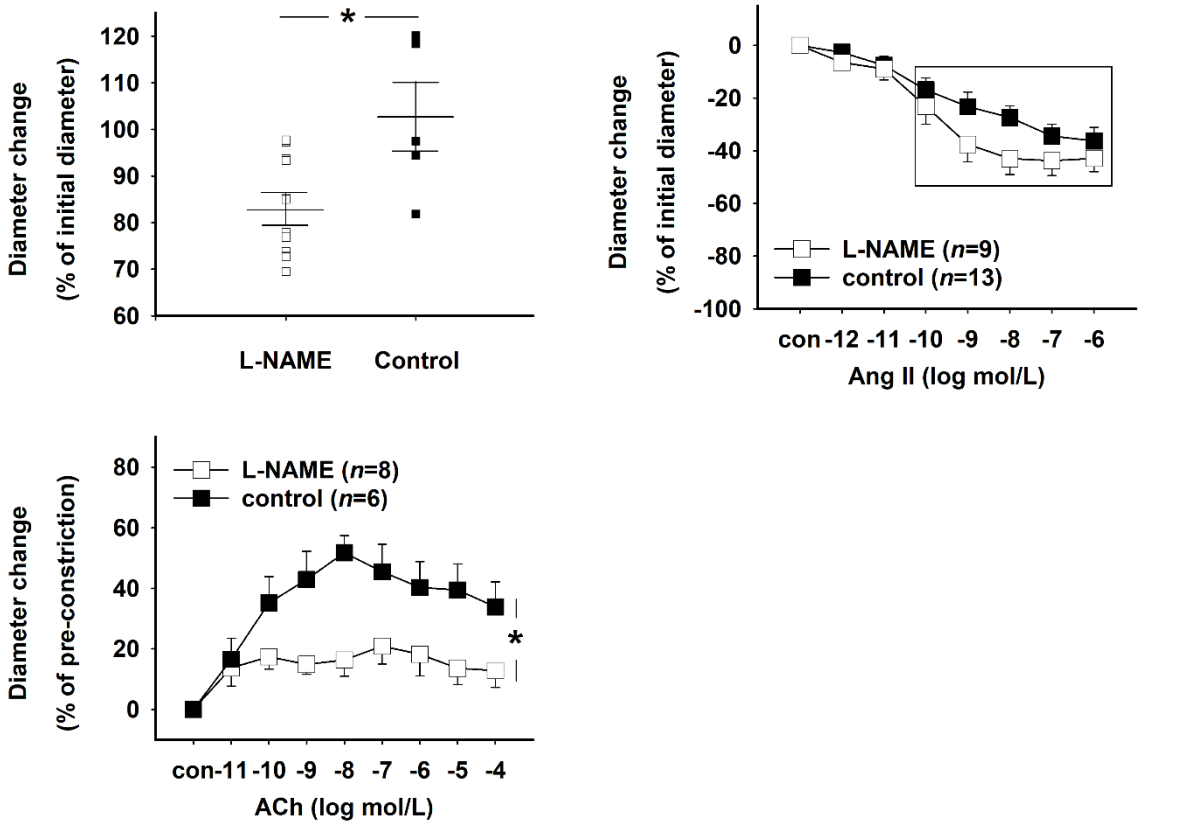

Fig. 3: L-NAME effect on vasa recta. Upper left: L-NAME reduces basal diameter. Upper right: L-NAME increases response to angiotensin II (Ang II). Lower panel: L-NAME decreases response to ACh. * indicates significant differences (Wilcoxon and Brunner test, respectively). Significant differences between the curves in the frame in the upper right diagram (Brunner test). Modified from (59)

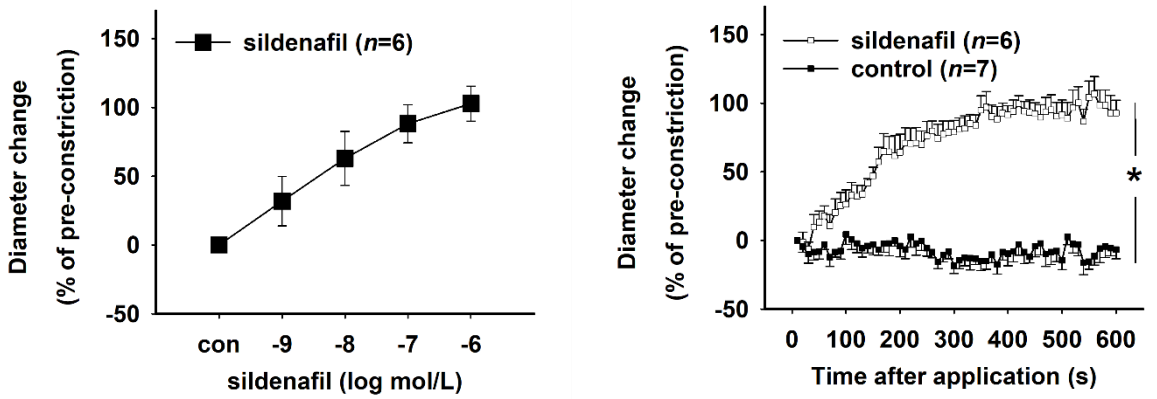

Fig: 4: Sildenafil effect in vasa recta. Left panel: Sildenafil dilates angiotensin II pre-constricted vasa recta concentration dependent. Right panel: Bolus application of sildenafil dilates the vessel. * indicates significant differences between curves (Brunner test). Modified from (59)

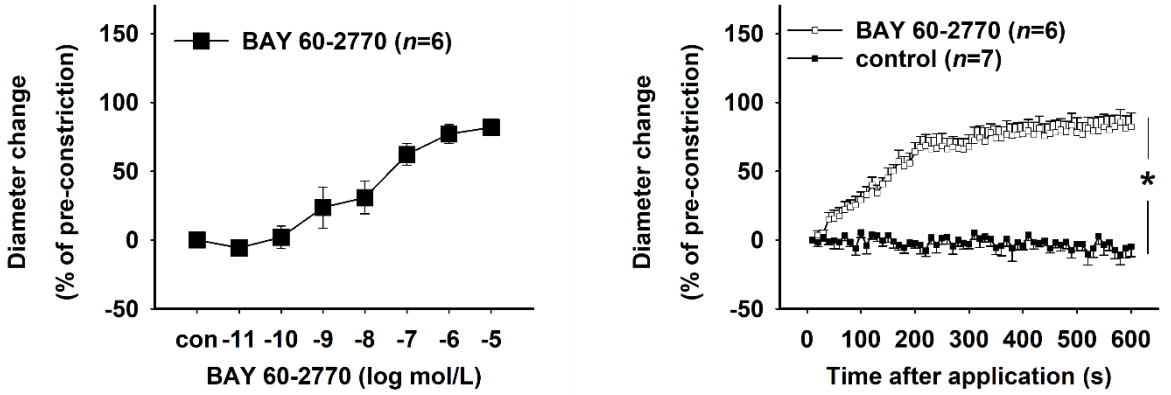

Fig. 5: Bay 60-2770 effect on L-NAME treated, angiotensin II pre-constricted vasa recta. Left panel: Bay 60-2770 dilates the vessels concentration dependent. Right panel: Bolus application of Bay 60-2770 dilates the vessels. * indicates significant differences between curves (Brunner test). Modified from (59)

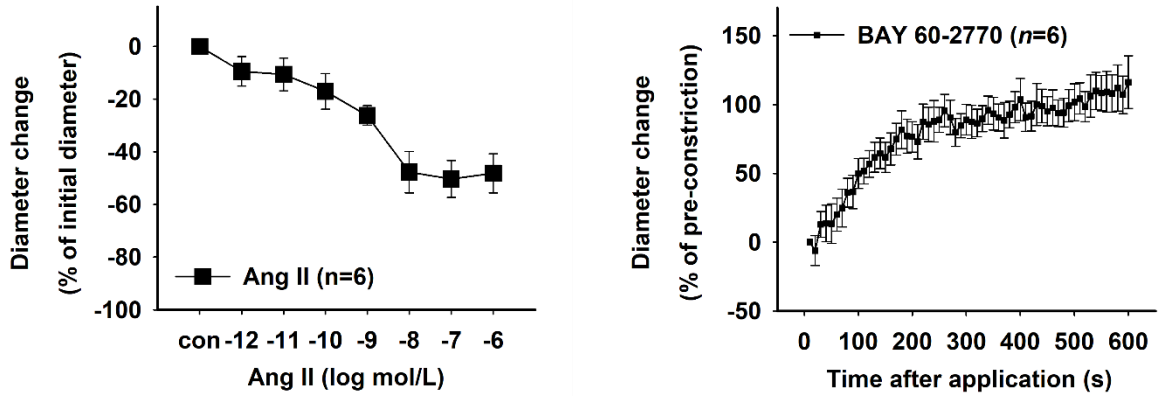

Fig. 6: Bay 60-2770 effect in human vasa recta. Left panel: Angiotensin II constricts vasa recta concentration dependent. Right panel: Dilation to Bay 60-2770 bolus application in these angiotensin II pre-constricted vessels. Modified from (59)

3.2 Effect of hypoxia/re-oxygenation in vasa recta

Severe hypoxia (0.1% O_2 for 30 min) followed by re-oxygenation increased the angiotensin II response in vasa recta and decreased the response to ACh in angiotensin II pre-constricted vessels (Fig. 7). Sildenafil (10^{-7} mol/l) did not dilate the vessels in the conditions of hypoxia/re-oxygenation, while SNP (10^{-3} mol/l) and Bay 60-2770 (10^{-6} mol/l) dilated the vessels in the same condition. The dilatory effect of Bay 60-2770 bolus application was faster than that of SNP treatment (Fig. 8).

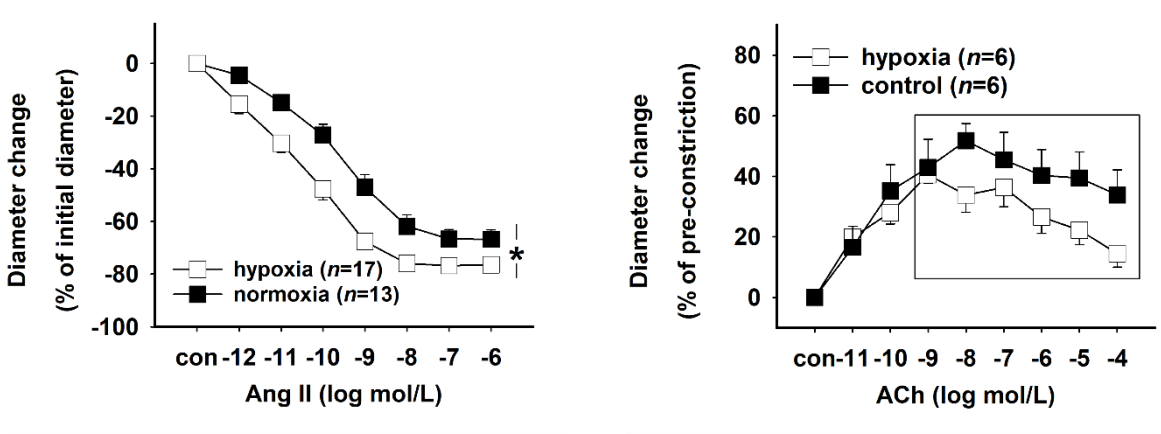

Fig. 7: Effect of hypoxia on vasa recta. Left panel: Hypoxia increase response to angiotensin II (a) Right panel: Hypoxia decreases response to ACh in angiotensin II pre-constricted vessels. * indicates significant differences between curves (Brunner test). Modified from (59)

3.3 Effect of NO deficiency and hypoxia/re-oxygenation in glomerular arterioles

Glomerular arterioles of mice have a potent NO-sGC-cGMP system (60, 64). NOS inhibition (L-NAME, 10^{-4} mol/l) increased the angiotensin II response in afferent and efferent arterioles (Fig. 9). Cinaciguat (10^{-7} mol/l) dilated the L-NAME (10^{-4} mol/l) pre-treated and pre-constricted (angiotensin II 10^{-6} mol/l) vessels. The dilation to cinaciguat was similar in control vessels without L-NAME treatment. In both protocols, efferent responded more strongly than afferent arterioles (Fig. 10 and 11). Severe hypoxia (0.1% O_2 for 30 min) followed by re-oxygenation increased the angiotensin II response in afferent and efferent vessels (Fig. 12). Cinaciguat dilated the pre-constricted efferent vessels, but not afferent arterioles (Fig. 12).

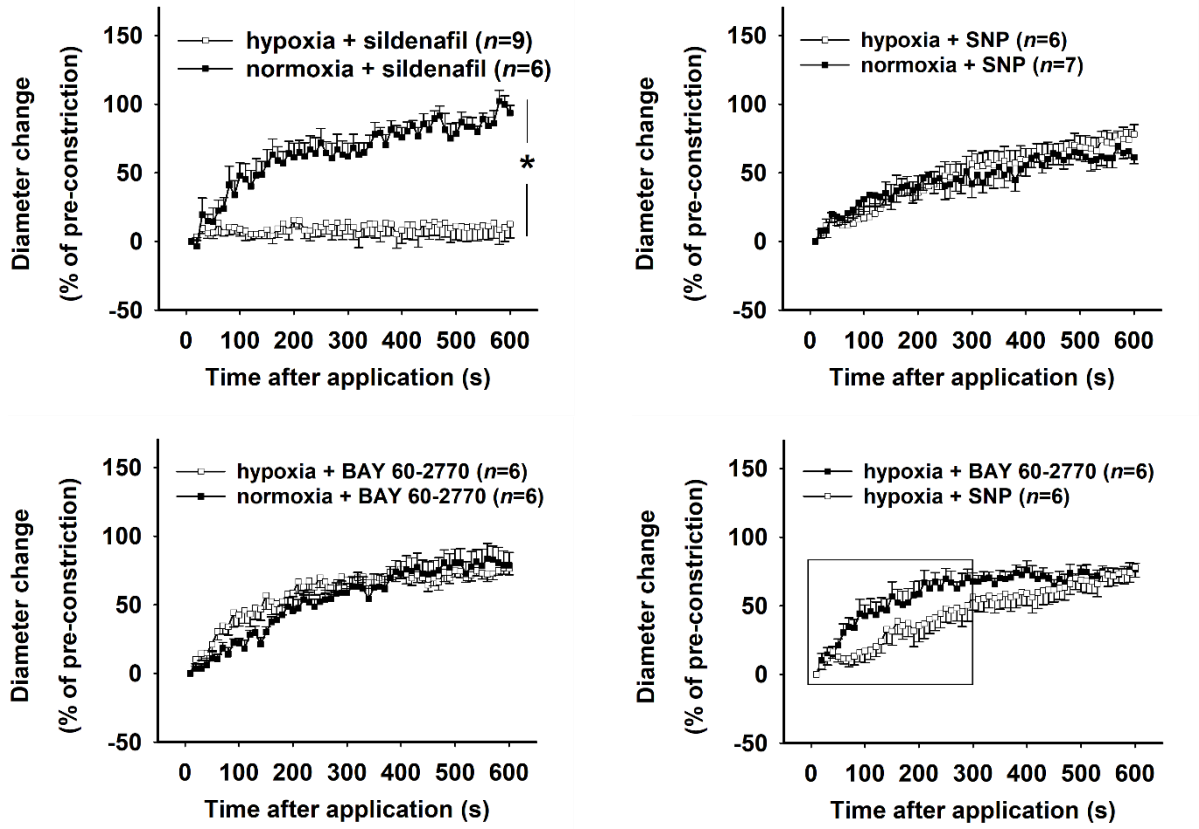

Fig. 8: Effect of hypoxia on vasa recta. Upper left: Sildenafil does not dilate angiotensin II pre-constricted vasa recta after hypoxia. Upper right: Sodium nitroprusside (SNP) bolus application dilates angiotensin II pre-constricted vasa recta under normoxia and after hypoxia similarly. Lower left: Bay 60-2770 bolus application dilates Angiotensin II- pre-constricted vasa recta under normoxia and after hypoxia similarly. Lower right: Bay 60-2770 dilates Angiotensin II- pre-constricted vasa recta faster than SNP after hypoxia. * indicates significant differences between curves (Brunner test). Modified from (59)

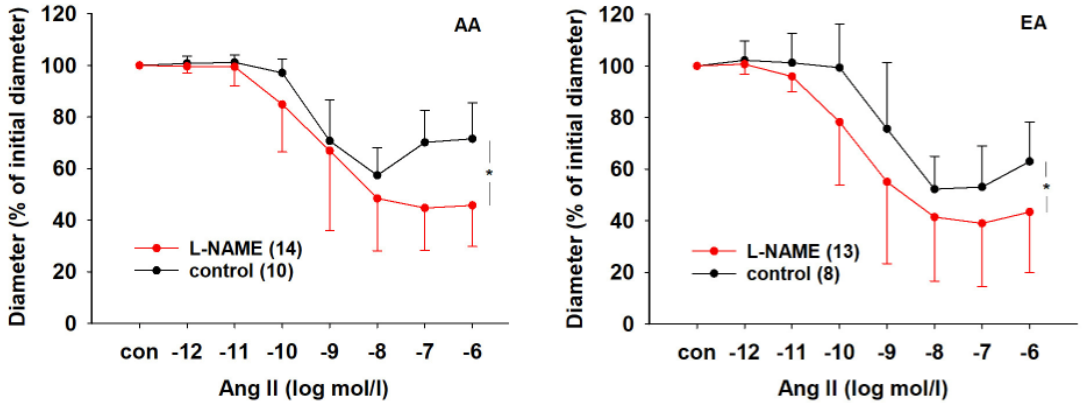

Fig. 9: Response of afferent (AA, left panel) and efferent arterioles (EA, right panel) to angiotensin II (Ang II) after pre-treatment with the NOS inhibitor L-NAME. * indicates significant differences ($p<0.05$) in the concentration response (Brunner test). Modified from (60).

3.4 Contrast medium treated afferent arterioles

Iodixanol reduces the NO-bioavailability and induces oxidative stress in the vessel wall (66). To test the effect of the sGC activator cinaciguat, vessels were pre-treated with the iodinated contrast medium iodixanol (23 mg of iodine/ml) from the luminal side. Cinaciguat (10^{-7} mol/l) dilated pre-constricted afferent arterioles under these conditions (Fig. 11).

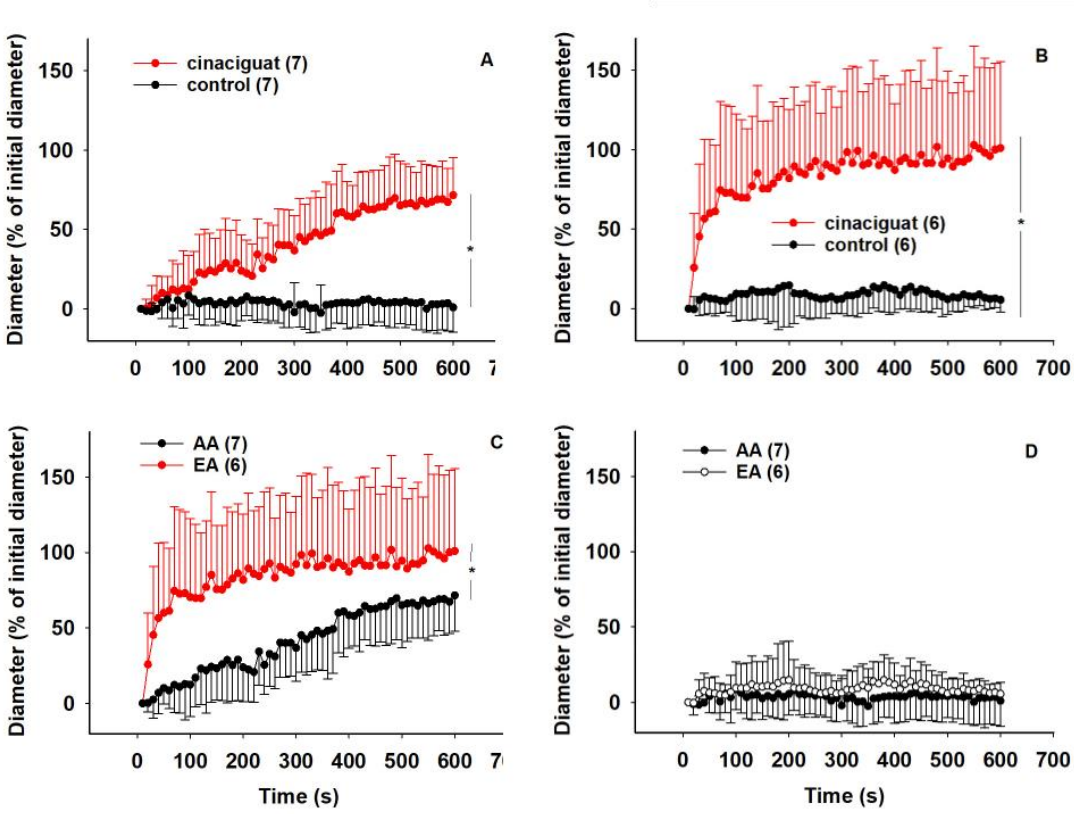

Fig.10: Effect of sGC activator cinaciguat in L-NAME pre-treated and angiotensin II-pre-constricted afferent (AA, panel A) and efferent arterioles (EA, panel B). Panel C: Comparison of cinaciguat effects in AA and EA. Panel D: Diameters of control groups for AA and EA. * indicates significant differences ($p<0.05$, Brunner test). Modified from (60).

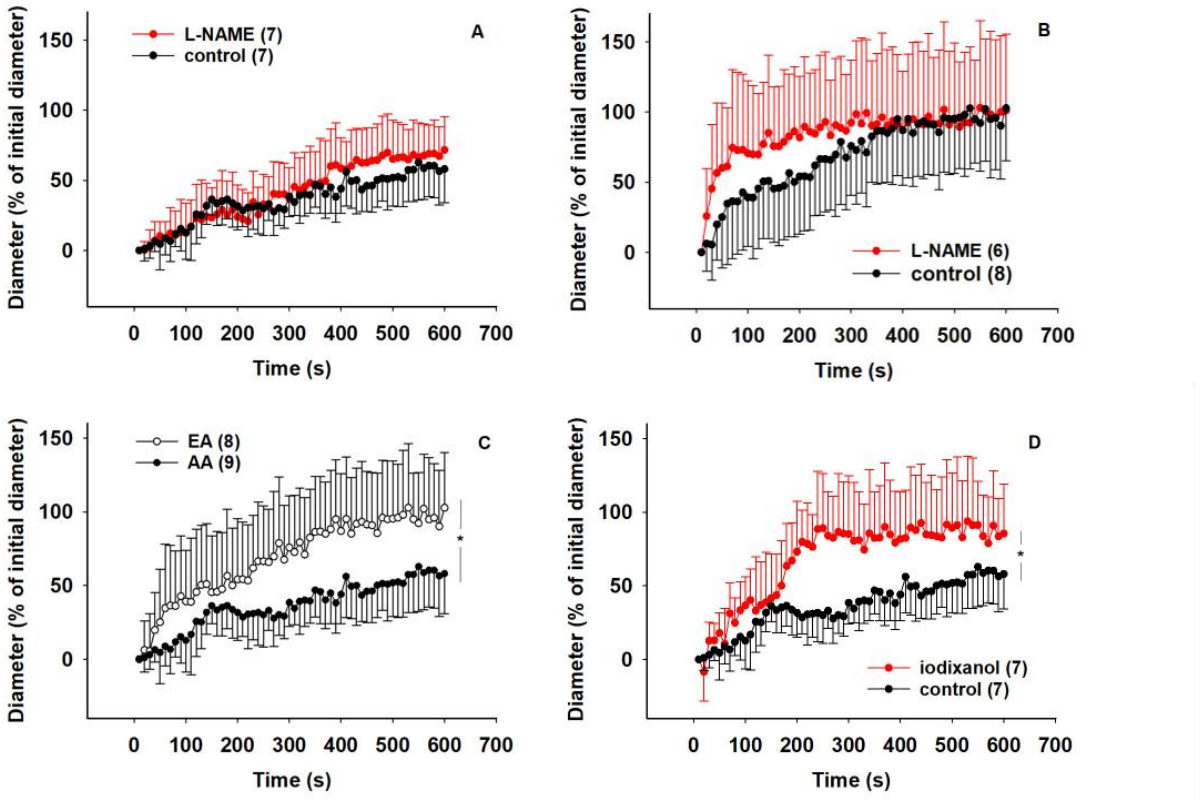

Fig. 11: Effect of cinaciguat in angiotensin II pre-treated afferent (AA, panel A) and efferent arterioles (EA, Panel B) without L-NAME pre-treatment. Panel C: Comparison of the cinaciguat effects in AA and EA. Panel D: Cinaciguat induced dilation in iodixanol-treated AA. * indicates significant differences ($p<0.05$, Brunner test). Modified from (60).

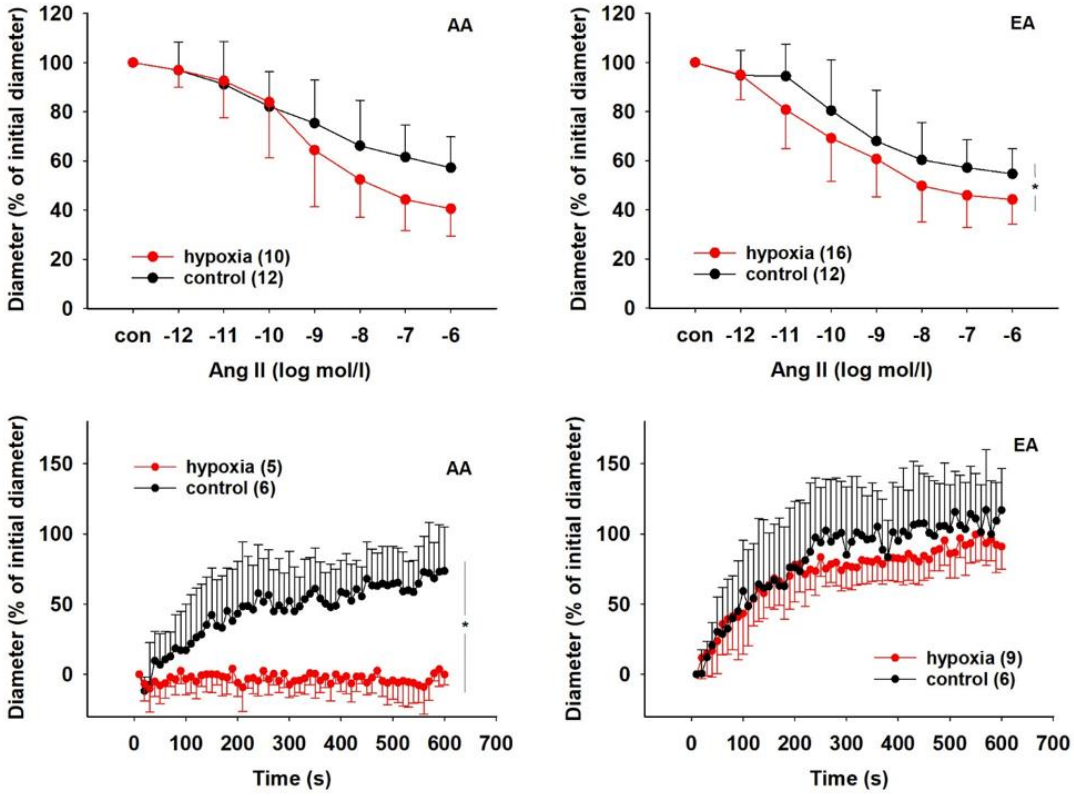

Fig. 12: Effect of hypoxia on angiotensin II (Ang II) induced constriction in afferent (AA) and efferent arterioles (EA). Lower panels: Cinaciguat effect on AA and EA after hypoxia/re-oxygenation in angiotensin II pre-treated arterioles. * indicates significant differences ($p<0.05$, Brunner test). Modified from (60).

3.5 Effect of runcaciguat on glomerular arterioles after sGC inhibition with ODQ

The sGC activator runcaciguat (10^{-6} mol/l), given as bolus, dilated L-NAME (10^{-4} mol/l) treated and angiotensin II (10^{-6} mol/l) pre-constricted afferent and efferent arterioles (Fig. 13). After application of ODQ, an inhibitor of sGC, which oxidizes the enzyme, runcaciguat was more effective compared to the L-NAME treated group as shown in concentration response curves (Fig. 14).

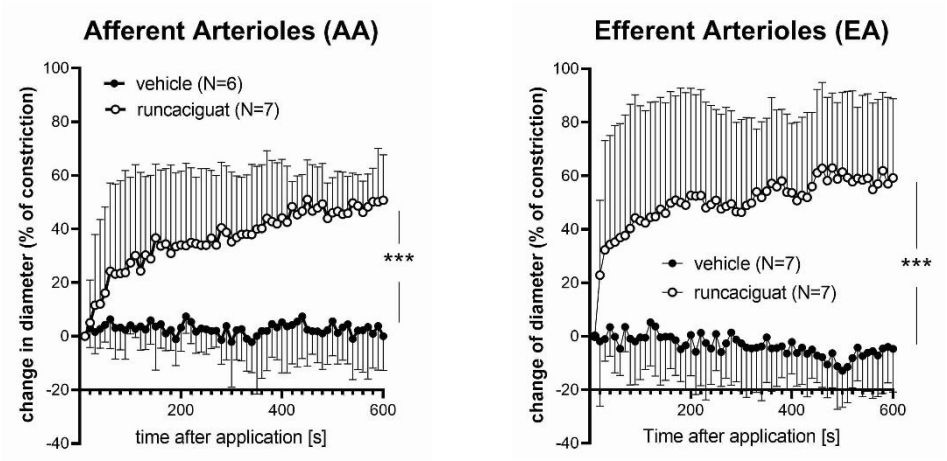

Fig. 13: Effect of runcaciguat given as bolus in L-NAME treated and angiotensin II-pre-constricted afferent and efferent arterioles. *** indicates significant differences between the curves ($p<0.001$, Brunner test; figure modified from (61).

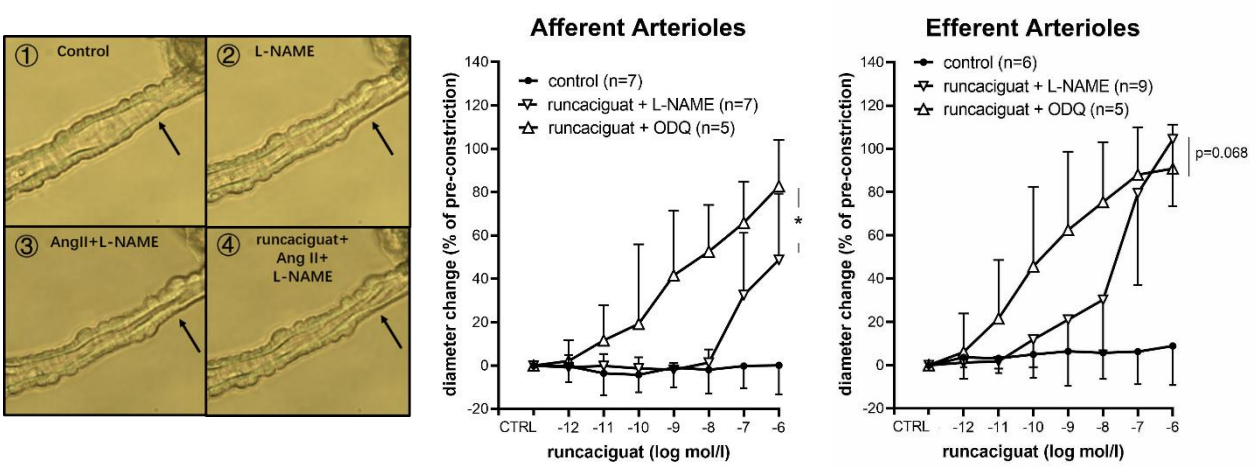

Fig. 14: Effect of runcaciguat on angiotensin II-pre-constricted afferent and efferent arterioles after L-NAME or ODQ treatment. Left panel: Video-microscopic pictures demonstrating “1” an afferent arteriole in the control situation, “2” after 15 min treatment with L-NAME , “3” after additional pre-constriction with Angiotensin II (10^{-4} mol/l), “4” and after additional application of runcaciguat. The black arrow indicates the site of measurement of the arteriolar luminal diameter. * indicates significant differences between both curves ($p<0.05$, Brunner test, figure modified from (61).

4. Discussion

4.1 Short summary of results

The thesis presents data about the action of sGC activators under different pathophysiological conditions in renal microvessels. Activators of the sGC dilated glomerular arterioles and outer medullary descending vasa recta after inhibition of NOS, i.e. under NO deficiency. The sGC activation induced stronger dilatory effects in efferent compared to afferent arterioles. Renal pathologies go along with hypoxia or hypoxia/re-oxygenation and an increased concentration of reactive oxygen species, which may lead to impaired sGC function. Hypoxia/re-oxygenation *in vitro* increased angiotensin II responses in glomerular and medullary microvessels and reduced the dilation to ACh in vasa recta. SGC activators dilated efferent arterioles and vasa recta after hypoxia/re-oxygenation as well as afferent arterioles after ODQ treatment (oxidized sGC). However, cinaciguat did not dilate afferent arterioles after strong hypoxia-re-oxygenation. The studies confirm our hypothesis that sGC activators act under NO-deficiency and sGC oxygenation in isolated renal microvessels.

4.2 Interpretation of results

4.2.1 NO deficiency in renal microvessels

Luminal diameters decreased in arterioles and vasa recta after L-NAME treatment (NOS inhibition). The response to angiotensin II, which is a strong constrictor in the renal vasculature, was increased in glomerular arterioles and in vasa recta. Further, ACh dilatation was reduced in the vasa recta. These results suggest an important role of the NO-sGC-cGMP system for renal microvessel dilation and tone, respectively. The results confirm observations in renal afferent arterioles and vasa recta from previous studies (27, 67). The sGC activators used in this thesis were able to dilate pre-constricted vessels with NO-deficiency. These substances can activate the sGC NO-independently. Several other studies showed activator induced dilation in NO-deficient vessels. For example, Bay 58-2667, an sGC activator, dilated iliac arteries in aged rats better than an sGC stimulator or PDE5 inhibitor (sildenafil) did (68), suggesting that this class of substances can be useful in situations where NO bioavailability is reduced in organs and vessels, respectively. Interestingly, our data support the idea of a stronger NO-sGC-cGMP system in efferent

arterioles compared to mouse afferent vessels (24). Results of a study in NOS deficient mice also indicated a stronger NO-system in efferent arterioles (27). In contrast, the observation of a stronger reaction of efferent arterioles to angiotensin II has been related to a weaker NO-system in these microvessels in rabbits (69, 70). Results may depend on experimental conditions and species. Ultimately, the low number of investigations does not allow a conclusion regarding the differential role of the NO-system in glomerular arterioles.

4.2.2 Hypoxia/re-oxygenation

Glomerular arteriolar and vasa recta response to angiotensin II increased after hypoxia/re-oxygenation and the ACh response diminished in vasa recta. This indicates an increased microvascular tone in pathological situation of ischemia/reperfusion. The mechanisms behind the hypoxia-induced changes in microvessels function are not fully understood. Oxidative stress may scavenge NO and activate signalling pathways, which increase the calcium sensitivity of the contractile machinery (52). In addition, hypoxia/re-oxygenation may decrease eNOS expression in mesenteric arteries, which can contribute to NO reduction (53). Authors found a reduced response to the NO donor SNP, suggesting that the sGC or downstream pathways are affected, as well. Increased concentration of reactive oxygen species after hypoxia/re-oxygenation can oxidize the sGC. Oxidation inhibits NO-heme interaction and leads to loss of the heme group and loss of function. In the *in vitro* study in isolated mesenteric arteries, superoxide-related fluorescence was not increased (53). However, superoxide and several other ROS are generated in the renal parenchyma in hypoxia and re-oxygenation, which are able to oxidize the sGC (49, 71-73). In the chronic disease situation, oxidative stress may lead and induces hypoxia; for example in diabetic nephropathy (74). Renal microvessels constrict under these conditions and aggravate hypoxia.

NO deficiency and sGC oxidation with the consequence of microvessel constriction and blood flow reduction demand pharmacological interventions with the aim to dilate vessels and improve renal perfusion. Although, sGC stimulators showed protective action in models of CKD (33, 34, 38), activators seem to be superior because of their NO-and hem-independent action.

Our finding that runcaciguat dilates vasa recta better after treatment with ODQ compared to ODQ untreated vessels is important in this context, because it suggests that activators preferentially activate the sGC in tissue with oxidative stress. Further, in the kidney the

area most prone to hypoxic damage, namely the inner part of the outer medulla including the vasa recta, will be targeted. Several studies in non-renal vessel also revealed a better function of sGC activators when sGC oxidation was induced or assumed. ODQ impaired the vessel response to the activator riociguat, while it enhanced the response to cinaciguat in the aorta and pulmonary arteries in rats (75). Further, ODQ potentiated the response to Bay 58-2667 (cinaciguat) in heme-free sGC (apo-sGC) and in arteries of diabetic mice compared to controls (76). Treatment with Bay 54-6544 (sGC activator) improved pulmonary vessel function in a mouse model of sickle cell disease, while sildenafil, while a sGC stimulator did not (77). This finding indicates an oxidized sGC in this disease model. In isolated monkey coronary arteries, the activator Bay 60-2770 relaxed the vessels better than the stimulator Bay 41-2272 (75). The free radical scavenger tempol prevented this effect, suggesting a change in the redox state by hypoxia/re-oxygenation.

4.3 Embedding the results into the current state of research

Renal cortical and medullary microvessels are important not only for renal perfusion and oxygen supply but are directly connected to renal filtration and concentration function. Glomerular afferent arterioles contribute 50% to renal resistance and determine the glomerular filtration rate. In addition, afferent and possibly efferent arterioles are effectors in the tubuloglomerular feedback mechanisms (78). Afferent arterioles' myogenic response is a one of the three mechanisms of renal autoregulation (79). Only one tenth of medullary perfusion reaches the renal medulla via juxtamedullary efferent arterioles. Nevertheless, medullary perfusion is independent of cortical perfusion to a certain extent (80). Outer medullary descending vasa recta are important in this context. They are the only vessels, which provide blood to the medulla. Vasa recta resistance is variable. The contractile elements of the vasa recta are pericytes (20).

Several systems including the sympathetic nervous system, the local and systemic renin-angiotensin-system as well as many other autocrine and paracrine substances influence vasa recta and cortical glomerular arteriolar tone (81). Glomerular arterioles react differentially to agonists thereby controlling glomerular filtration rate (81). Surrounding tubuli release a variety of vasoactive substances and metabolites, which interact in controlling renal perfusion, glomerular filtration rate and medullary functions (82, 83). Endothelial dilatory systems such as the NO-system, arachidonic acid derivates and the hyperpolar-

izing factor contribute significantly to microvessel tone (84). The balance between vasoconstrictors (norepinephrine, angiotensin II, endothelin, and more) and dilatory substances gets lost under pathological situations. In AKI, the sympathetic nervous systems is activated and thus the renin-angiotensin-system (85). At the same time, endothelial dysfunction promotes vasoconstriction. Taken together, both systems increase renal vascular resistance and lower renal perfusion and oxygenation (18).

Enormous efforts have been undertaken to develop an adequate and specific treatment for AKI and CKD. The overwhelming part of the experimental studies aimed at pathophysiological components in epithelial cells, thereby reducing early damage, inflammation, apoptosis, and fibrosis. Although, many of the study results were promising they have not been transferred into clinical use.

Impaired renal perfusion has been identified as a pathophysiological factor in AKI and CKD (86). However, details of the pathophysiological action of the renal microvasculature are not well known. The thesis show that NO-deficiency and hypoxia/re-oxygenation increase vessel tone and reactivity to vasoconstrictors *in vitro*. Further, the beneficial action of the sGC activators in models of NO-deficiency and sGC impairment suggests a therapeutic potential for this substance group.

4.4 Strengths and weaknesses of the studies

The studies of this thesis demonstrate the beneficial action of sGC activators *in vitro* models of NO deficiency and sGC dysfunction. The studies included three hemodynamically most important types of microvessels: cortical glomerular arterioles and medullary vasa recta. These results extend our knowledge about pathophysiological aspects and offers new therapeutic options for the treatment of AKI and CKD.

Most experiments of this thesis were performed in animal models, which limits the translation into the human situation. Importantly, we could show the principal beneficial action of a sGC activator in human vasa recta.

4.5 Implications for practice and/or future research

Performing experiments in isolated microvessels was a step forward to a better understanding of pathophysiological mechanisms and in testing a new class of vasoactive substances in this context. Clinical studies for the application of sGC activators in human medicine (treatment of CKD) already started. Therefore, it is important to understand the

mechanisms behind the protective effects. Future work should focus on investigating sGC activator effects on renal vasculature function *ex vivo* in different models of AKI and CKD.

5. Conclusions

The results of the thesis provide evidence for a strong dilator effect of sGC activators in renal microvessels under conditions of NO-deficiency due to NOS-inhibition or treatment with an iodinized contrast medium. Further, data suggest an even enhanced action of sGC activators (runcaciguat) when the sGC is oxidized. The findings indicate renal protection by sGC activators via reduced renal hemodynamic resistance and improved renal perfusion.

Reference list

1. Lewington AJ, Cerda J, Mehta RL. Raising awareness of acute kidney injury: a global perspective of a silent killer. Kidney Int. 2013;84(3):457-67.
2. Mehta RL, Cerda J, Burdmann EA, Tonelli M, Garcia-Garcia G, Jha V, Susantitaphong P, Rocco M, Vanholder R, Sever MS, Cruz D, Jaber B, Lameire NH, Lombardi R, Lewington A, Feehally J, Finkelstein F, Levin N, Pannu N, Thomas B, Aronoff-Spencer E, Remuzzi G. International Society of Nephrology's 0by25 initiative for acute kidney injury (zero preventable deaths by 2025): a human rights case for nephrology. Lancet. 2015;385(9987):2616-43.
3. Tao Li PK, Burdmann EA, Mehta RL. Acute kidney injury: global health alert. Int J Organ Transplant Med. 2013;4(1):1-8.
4. Chawla LS, Bellomo R, Bihorac A, Goldstein SL, Siew ED, Bagshaw SM, Bittleman D, Cruz D, Endre Z, Fitzgerald RL, Forni L, Kane-Gill SL, Hoste E, Koyner J, Liu KD, Macedo E, Mehta R, Murray P, Nadim M, Ostermann M, Palevsky PM, Pannu N, Rosner M, Wald R, Zarbock A, Ronco C, Kellum JA, Acute Disease Quality Initiative W. Acute kidney disease and renal recovery: consensus report of the Acute Disease Quality Initiative (ADQI) 16 Workgroup. Nat Rev Nephrol. 2017;13(4):241-57.
5. Lameire NH, Levin A, Kellum JA, Cheung M, Jadoul M, Winkelmayer WC, Stevens PE, Conference P. Harmonizing acute and chronic kidney disease definition and classification: report of a Kidney Disease: Improving Global Outcomes (KDIGO) Consensus Conference. Kidney Int. 2021;100(3):516-26.
6. Section 2: AKI Definition. Kidney Int Suppl (2011). 2012;2(1):19-36.
7. Kovesdy CP. Epidemiology of chronic kidney disease: an update 2022. Kidney Int Suppl (2011). 2022;12(1):7-11.
8. Selby NM. A Comment on the Diagnosis and Definition of Acute Kidney Injury. Nephron. 2019;141(3):203-6.
9. Sanz AB, Sanchez-Nino MD, Ramos AM, Ortiz A. Regulated cell death pathways in kidney disease. Nat Rev Nephrol. 2023;19(5):281-99.
10. Ronco C, Bellomo R, Kellum JA. Acute kidney injury. Lancet. 2019;394(10212):1949-64.
11. Pickkers P, Darmon M, Hoste E, Joannidis M, Legrand M, Ostermann M, Prowle JR, Schneider A, Schetz M. Acute kidney injury in the critically ill: an updated review on pathophysiology and management. Intensive Care Med. 2021;47(8):835-50.

12. Kurzhagen JT, Dellepiane S, Cantaluppi V, Rabb H. AKI: an increasingly recognized risk factor for CKD development and progression. J Nephrol. 2020;33(6):1171-87.
13. Khwaja A, El Kossi M, Floege J, El Nahas M. The management of CKD: a look into the future. Kidney Int. 2007;72(11):1316-23.
14. Freitas F, Attwell D. Pericyte-mediated constriction of renal capillaries evokes no-reflow and kidney injury following ischaemia. Elife. 2022;11.
15. Bougle A, Duranteau J. Pathophysiology of sepsis-induced acute kidney injury: the role of global renal blood flow and renal vascular resistance. Contrib Nephrol. 2011;174:89-97.
16. Verma SK, Molitoris BA. Renal endothelial injury and microvascular dysfunction in acute kidney injury. Semin Nephrol. 2015;35(1):96-107.
17. Chen Q, Yu J, Rush BM, Stocker SD, Tan RJ, Kim K. Ultrasound super-resolution imaging provides a noninvasive assessment of renal microvasculature changes during mouse acute kidney injury. Kidney Int. 2020;98(2):355-65.
18. Scholz H, Boivin FJ, Schmidt-Ott KM, Bachmann S, Eckardt KU, Scholl UI, Persson PB. Kidney physiology and susceptibility to acute kidney injury: implications for renoprotection. Nat Rev Nephrol. 2021;17(5):335-49.
19. Pallone TL, Edwards A, Mattson DL. Renal medullary circulation. Compr Physiol. 2012;2(1):97-140.
20. Kennedy-Lydon TM, Crawford C, Wildman SS, Peppiatt-Wildman CM. Renal pericytes: regulators of medullary blood flow. Acta Physiol (Oxf). 2013;207(2):212-25.
21. Panizo N, Rubio-Navarro A, Amaro-Villalobos JM, Egido J, Moreno JA. Molecular Mechanisms and Novel Therapeutic Approaches to Rhabdomyolysis-Induced Acute Kidney Injury. Kidney Blood Press Res. 2015;40(5):520-32.
22. Alberola AM, Salazar FJ, Nakamura T, Granger JP. Interaction between angiotensin II and nitric oxide in control of renal hemodynamics in conscious dogs. Am J Physiol. 1994;267(6 Pt 2):R1472-8.
23. Patzak A, Lai E, Persson PB, Persson AE. Angiotensin II-nitric oxide interaction in glomerular arterioles. Clin Exp Pharmacol Physiol. 2005;32(5-6):410-4.
24. Patzak A, Kleinmann F, Lai EY, Kupsch E, Skelweit A, Mrowka R. Nitric oxide counteracts angiotensin II induced contraction in efferent arterioles in mice. Acta Physiol Scand. 2004;181(4):439-44.

25. Mundel P, Bachmann S, Bader M, Fischer A, Kummer W, Mayer B, Kriz W. Expression of nitric oxide synthase in kidney macula densa cells. Kidney Int. 1992;42(4):1017-9.

26. Bachmann S, Mundel P. Nitric oxide in the kidney: synthesis, localization, and function. Am J Kidney Dis. 1994;24(1):112-29.

27. Patzak A, Steege A, Lai EY, Brinkmann JO, Kupsch E, Spielmann N, Gericke A, Skalweit A, Stegbauer J, Persson PB, Seeliger E. Angiotensin II response in afferent arterioles of mice lacking either the endothelial or neuronal isoform of nitric oxide synthase. Am J Physiol Regul Integr Comp Physiol. 2008;294(2):R429-37.

28. Sandner P, Follmann M, Becker-Pelster E, Hahn MG, Meier C, Freitas C, Roessig L, Stasch JP. Soluble GC stimulators and activators: Past, present and future. Br J Pharmacol. 2021.

29. Lucas KA, Pitari GM, Kazerounian S, Ruiz-Stewart I, Park J, Schulz S, Chepenik KP, Waldman SA. Guanylyl cyclases and signaling by cyclic GMP. Pharmacol Rev. 2000;52(3):375-414.

30. Carrier GO, Fuchs LC, Winecoff AP, Giulumian AD, White RE. Nitrovasodilators relax mesenteric microvessels by cGMP-induced stimulation of Ca-activated K channels. Am J Physiol. 1997;273(1 Pt 2):H76-84.

31. Liu T, Schroeder HJ, Zhang M, Wilson SM, Terry MH, Longo LD, Power GG, Blood AB. S-nitrosothiols dilate the mesenteric artery more potently than the femoral artery by a cGMP and L-type calcium channel-dependent mechanism. Nitric Oxide. 2016;58:20-7.

32. Xiao S, Li Q, Hu L, Yu Z, Yang J, Chang Q, Chen Z, Hu G. Soluble Guanylate Cyclase Stimulators and Activators: Where are We and Where to Go? Mini Rev Med Chem. 2019;19(18):1544-57.

33. Stasch JP, Schlossmann J, Hocher B. Renal effects of soluble guanylate cyclase stimulators and activators: a review of the preclinical evidence. Curr Opin Pharmacol. 2015;21:95-104.

34. Sravani S, Saifi MA, Godugu C. Riociguat ameliorates kidney injury and fibrosis in an animal model. Biochem Biophys Res Commun. 2020;530(4):706-12.

35. Lombardi CM, Cimino G, Pagnesi M, Dell'Aquila A, Tomasoni D, Ravera A, Inciardi R, Carubelli V, Vizzardi E, Nodari S, Emdin M, Aimo A. Vericiguat for Heart Failure with Reduced Ejection Fraction. Curr Cardiol Rep. 2021;23(10):144.

36. Grzesk G, Witczynska A, Weglarz M, Wolowiec L, Nowaczyk J, Grzesk E, Nowaczyk A. Soluble Guanylyl Cyclase Activators-Promising Therapeutic Option in the Pharmacotherapy of Heart Failure and Pulmonary Hypertension. Molecules. 2023;28(2).
37. Benardeau A, Kahnert A, Schomber T, Meyer J, Pavkovic M, Kretschmer A, Lawrenz B, Hartmann E, Mathar I, Hueser J, Kraehling JR, Eitner F, Hahn MG, Stasch JP, Sandner P. Runcaciguat, a novel soluble guanylate cyclase activator, shows renoprotection in hypertensive, diabetic, and metabolic preclinical models of chronic kidney disease. Naunyn Schmiedebergs Arch Pharmacol. 2021;394(12):2363-79.
38. Krishnan SM, Kraehling JR, Eitner F, Benardeau A, Sandner P. The Impact of the Nitric Oxide (NO)/Soluble Guanylyl Cyclase (sGC) Signaling Cascade on Kidney Health and Disease: A Preclinical Perspective. Int J Mol Sci. 2018;19(6).
39. Reinhart GA, Harrison PC, Lincoln K, Chen H, Sun P, Hill J, Qian HS, McHugh MC, Clifford H, Ng KJ, Wang H, Fowler D, Gueneva-Boucheva K, Brenneman JB, Bosanac T, Wong D, Fryer RM, Sarko C, Boustany-Kari CM, Pullen SS. The Novel, Clinical-Stage Soluble Guanylate Cyclase Activator BI 685509 Protects from Disease Progression in Models of Renal Injury and Disease. J Pharmacol Exp Ther. 2023;384(3):382-92.
40. Lee KH, Lee SR, Cho H, Woo JS, Kang JH, Jeong YM, Cheng XW, Kim WS, Kim W. Cardioprotective effects of PKG activation by soluble GC activator, BAY 60-2770, in ischemia-reperfusion-injured rat hearts. PLoS One. 2017;12(7):e0180207.
41. Loganathan S, Korkmaz-Icoz S, Radovits T, Li S, Mikles B, Barnucz E, Hirschberg K, Karck M, Szabo G. Effects of soluble guanylate cyclase activation on heart transplantation in a rat model. J Heart Lung Transplant. 2015;34(10):1346-53.
42. Fraccarollo D, Galuppo P, Motschenbacher S, Ruetten H, Schafer A, Bauersachs J. Soluble guanylyl cyclase activation improves progressive cardiac remodeling and failure after myocardial infarction. Cardioprotection over ACE inhibition. Basic Res Cardiol. 2014;109(4):421.
43. Tsou CY, Chen CY, Zhao JF, Su KH, Lee HT, Lin SJ, Shyue SK, Hsiao SH, Lee TS. Activation of soluble guanylyl cyclase prevents foam cell formation and atherosclerosis. Acta Physiol (Oxf). 2014;210(4):799-810.
44. Vandendriessche B, Rogge E, Goossens V, Vandenabeele P, Stasch JP, Brouckaert P, Cauwels A. The soluble guanylate cyclase activator BAY 58-2667 protects against morbidity and mortality in endotoxic shock by recoupling organ systems. PLoS One. 2013;8(8):e72155.

45. Irvine JC, Ganthavee V, Love JE, Alexander AE, Horowitz JD, Stasch JP, Kemp-Harper BK, Ritchie RH. The soluble guanylyl cyclase activator bay 58-2667 selectively limits cardiomyocyte hypertrophy. PLoS One. 2012;7(11):e44481.

46. Evans RG, Ow CP, Bie P. The chronic hypoxia hypothesis: the search for the smoking gun goes on. Am J Physiol Renal Physiol. 2015;308(2):F101-2.

47. Ow CPC, Ngo JP, Ullah MM, Barsha G, Meex RC, Watt MJ, Hilliard LM, Koeners MP, Evans RG. Absence of renal hypoxia in the subacute phase of severe renal ischemia-reperfusion injury. Am J Physiol Renal Physiol. 2018;315(5):F1358-F69.

48. Singh P, Ricksten SE, Bragadottir G, Redfors B, Nordquist L. Renal oxygenation and haemodynamics in acute kidney injury and chronic kidney disease. Clin Exp Pharmacol Physiol. 2013;40(2):138-47.

49. Palm F, Cederberg J, Hansell P, Liss P, Carlsson PO. Reactive oxygen species cause diabetes-induced decrease in renal oxygen tension. Diabetologia. 2003;46(8):1153-60.

50. Welch WJ, Baumgartl H, Lubbers D, Wilcox CS. Renal oxygenation defects in the spontaneously hypertensive rat: role of AT1 receptors. Kidney Int. 2003;63(1):202-8.

51. Braun D, Dietze S, Pahlitzsch TMJ, Wennysia IC, Persson PB, Ludwig M, Patzak A. Short-term hypoxia and vasa recta function in kidney slices. Clin Hemorheol Microcirc. 2017;67(3-4):475-84.

52. Pahlitzsch T, Liu ZZ, Al-Masri A, Braun D, Dietze S, Persson PB, Schunck WH, Blum M, Kupsch E, Ludwig M, Patzak A. Hypoxia-reoxygenation enhances murine afferent arteriolar vasoconstriction by angiotensin II. Am J Physiol Renal Physiol. 2018;314(3):F430-F8.

53. Braun D, Zollbrecht C, Dietze S, Schubert R, Golz S, Summer H, Persson PB, Carlstrom M, Ludwig M, Patzak A. Hypoxia/Reoxygenation of Rat Renal Arteries Impairs Vasorelaxation via Modulation of Endothelium-Independent sGC/cGMP/PKG Signaling. Front Physiol. 2018;9:480.

54. Kaufmann J, Martinka P, Moede O, Sendeski M, Steege A, Fahling M, Hultstrom M, Gaestel M, Moraes-Silva IC, Nikitina T, Liu ZZ, Zavaritskaya O, Patzak A. Noradrenaline enhances angiotensin II responses via p38 MAPK activation after hypoxia/re-oxygenation in renal interlobar arteries. Acta Physiol (Oxf). 2015;213(4):920-32.

55. Stevenson MD, Vendrov AE, Yang X, Chen Y, Navarro HA, Moss N, Runge MS, Arendshorst WJ, Madamanchi NR. Reactivity of renal and mesenteric resistance vessels

to angiotensin II is mediated by NOXA1/NOX1 and superoxide signaling. Am J Physiol Renal Physiol. 2023;324(4):F335-F52.

56. Makrynitsa GI, Argyriou AI, Zompra AA, Salagiannis K, Vazoura V, Papapetropoulos A, Topouzis S, Spyroulias GA. Mapping of the sGC Stimulator BAY 41-2272 Binding Site on H-NOX Domain and Its Regulation by the Redox State of the Heme. Front Cell Dev Biol. 2022;10:925457.

57. Fontecha-Barriuso M, Lopez-Diaz AM, Guerrero-Mauvecin J, Miguel V, Ramos AM, Sanchez-Nino MD, Ruiz-Ortega M, Ortiz A, Sanz AB. Tubular Mitochondrial Dysfunction, Oxidative Stress, and Progression of Chronic Kidney Disease. Antioxidants (Basel). 2022;11(7).

58. Zhang X, Agborbesong E, Li X. The Role of Mitochondria in Acute Kidney Injury and Chronic Kidney Disease and Its Therapeutic Potential. Int J Mol Sci. 2021;22(20).

59. Xu M, Lichtenberger FB, Erdogan C, Lai E, Persson PB, Patzak A, Khedkar PH. Nitric Oxide Signalling in Descending Vasa Recta after Hypoxia/Re-Oxygenation. Int J Mol Sci. 2022;23(13).

60. Wennysia IC, Zhao L, Schomber T, Braun D, Golz S, Summer H, Benardeau A, Lai EY, Lichtenberger FB, Schubert R, Persson PB, Xu MZ, Patzak A. Role of soluble guanylyl cyclase in renal afferent and efferent arterioles. Am J Physiol Renal Physiol. 2021;320(2):F193-F202.

61. Stehle D, Xu MZ, Schomber T, Hahn MG, Schweda F, Feil S, Kraehling JR, Eitner F, Patzak A, Sandner P, Feil R, Benardeau A. Novel soluble guanylyl cyclase activators increase glomerular cGMP, induce vasodilation and improve blood flow in the murine kidney. Br J Pharmacol. 2022;179(11):2476-89.

62. Crawford C, Kennedy-Lydon T, Sprott C, Desai T, Sawbridge L, Munday J, Unwin RJ, Wildman SS, Peppiatt-Wildman CM. An intact kidney slice model to investigate vasa recta properties and function in situ. Nephron Physiol. 2012;120(3):p17-31.

63. Sendeski MM, Liu ZZ, Perlewitz A, Busch JF, Ikromov O, Weikert S, Persson PB, Patzak A. Functional characterization of isolated, perfused outermedullary descending human vasa recta. Acta Physiol (Oxf). 2013;208(1):50-6.

64. Patzak A, Mrowka R, Storch E, Hocher B, Persson PB. Interaction of angiotensin II and nitric oxide in isolated perfused afferent arterioles of mice. J Am Soc Nephrol. 2001;12(6):1122-7.

65. Schneider CA, Rasband WS, Eliceiri KW. NIH Image to ImageJ: 25 years of image analysis. Nat Methods. 2012;9(7):671-5.

66. Liu ZZ, Schmerbach K, Lu Y, Perlewitz A, Nikitina T, Cantow K, Seeliger E, Persson PB, Patzak A, Liu R, Sendeski MM. Iodinated contrast media cause direct tubular cell damage, leading to oxidative stress, low nitric oxide, and impairment of tubuloglomerular feedback. Am J Physiol Renal Physiol. 2014;306(8):F864-72.
67. Cao C, Edwards A, Sendeski M, Lee-Kwon W, Cui L, Cai CY, Patzak A, Pallone TL. Intrinsic nitric oxide and superoxide production regulates descending vasa recta contraction. Am J Physiol Renal Physiol. 2010;299(5):F1056-64.
68. Justo AFO, de Oliveira MG, Calmasini FB, Alexandre EC, Bertollotto GM, Jacintho FF, Antunes E, Monica FZ. Preserved activity of soluble guanylate cyclase (sGC) in iliac artery from middle-aged rats: Role of sGC modulators. Nitric Oxide. 2021;106:9-16.
69. Edwards RM, Trizna W. Modulation of glomerular arteriolar tone by nitric oxide synthase inhibitors. J Am Soc Nephrol. 1993;4(5):1127-32.
70. Ito S, Arima S, Ren YL, Juncos LA, Carretero OA. Endothelium-derived relaxing factor/nitric oxide modulates angiotensin II action in the isolated microperfused rabbit afferent but not efferent arteriole. J Clin Invest. 1993;91(5):2012-9.
71. Clanton TL. Hypoxia-induced reactive oxygen species formation in skeletal muscle. J Appl Physiol (1985). 2007;102(6):2379-88.
72. Guzy RD, Mack MM, Schumacker PT. Mitochondrial complex III is required for hypoxia-induced ROS production and gene transcription in yeast. Antioxid Redox Signal. 2007;9(9):1317-28.
73. Welch WJ, Baumgartl H, Lubbers D, Wilcox CS. Nephron pO2 and renal oxygen usage in the hypertensive rat kidney. Kidney Int. 2001;59(1):230-7.
74. Schiffer TA, Friederich-Persson M. Mitochondrial Reactive Oxygen Species and Kidney Hypoxia in the Development of Diabetic Nephropathy. Front Physiol. 2017;8:211.
75. Tawa M, Yamashita Y, Masuoka T, Nakano K, Yoshida J, Nishio M, Ishibashi T. Responsiveness of rat aorta and pulmonary artery to cGMP generators in the presence of thiol or heme oxidant. J Pharmacol Sci. 2019;140(1):43-7.
76. Goulopoulou S, Hannan JL, Matsumoto T, Ogbi S, Ergul A, Webb RC. Reduced vascular responses to soluble guanylyl cyclase but increased sensitivity to sildenafil in female rats with type 2 diabetes. Am J Physiol Heart Circ Physiol. 2015;309(2):H297-304.
77. Potoka KP, Wood KC, Baust JJ, Bueno M, Hahn SA, Vanderpool RR, Bachman T, Mallampalli GM, Osei-Hwedieh DO, Schrott V, Sun B, Bullock GC, Becker-Pelster EM, Wittwer M, Stampfuss J, Mathar I, Stasch JP, Truebel H, Sandner P, Mora AL, Straub AC, Gladwin MT. Nitric Oxide-Independent Soluble Guanylate Cyclase Activation

Improves Vascular Function and Cardiac Remodeling in Sickle Cell Disease. Am J Respir Cell Mol Biol. 2018;58(5):636-47.

78. Schnermann J, Traynor T, Yang T, Arend L, Huang YG, Smart A, Briggs JP. Tubuloglomerular feedback: new concepts and developments. Kidney Int Suppl. 1998;67:S40-5.

79. Seeliger E, Wronski T, Ladwig M, Dobrowolski L, Vogel T, Godes M, Persson PB, Flemming B. The renin-angiotensin system and the third mechanism of renal blood flow autoregulation. Am J Physiol Renal Physiol. 2009;296(6):F1334-45.

80. Evans RG, Eppel GA, Anderson WP, Denton KM. Mechanisms underlying the differential control of blood flow in the renal medulla and cortex. J Hypertens. 2004;22(8):1439-51.

81. Navar LG, Inscho EW, Majid SA, Imig JD, Harrison-Bernard LM, Mitchell KD. Paracrine regulation of the renal microcirculation. Physiol Rev. 1996;76(2):425-536.

82. Cowley AW, Jr. Renal medullary oxidative stress, pressure-natriuresis, and hypertension. Hypertension. 2008;52(5):777-86.

83. Jin C, Hu C, Polichnowski A, Mori T, Skelton M, Ito S, Cowley AW, Jr. Effects of renal perfusion pressure on renal medullary hydrogen peroxide and nitric oxide production. Hypertension. 2009;53(6):1048-53.

84. Carlstrom M, Wilcox CS, Arendshorst WJ. Renal autoregulation in health and disease. Physiol Rev. 2015;95(2):405-511.

85. Grisk O. The sympathetic nervous system in acute kidney injury. Acta Physiol (Oxf). 2020;228(2):e13404.

86. Kwiatkowska E, Kwiatkowski S, Dziedziejko V, Tomasiewicz I, Domanski L. Renal Microcirculation Injury as the Main Cause of Ischemic Acute Kidney Injury Development. Biology (Basel). 2023;12(2).

Statutory Declaration

“I, Minze Xu, by personally signing this document in lieu of an oath, hereby affirm that I prepared the submitted dissertation on the topic “Stimulation of the nitric oxide signaling pathway by activators of the soluble guanylyl cyclase in cortical and medullary renal microvessels“, “Stimulation des Stickstoffmonoxid-Signalweges durch Aktivatoren der löslichen Guanylatzyklase in kortikalen und medullären renalen Mikrogefäßen”, independently and without the support of third parties, and that I used no other sources and aids than those stated.
All parts which are based on the publications or presentations of other authors, either in letter or in spirit, are specified as such in accordance with the citing guidelines. The sections on methodology (in particular regarding practical work, laboratory regulations, statistical processing) and results (in particular regarding figures, charts and tables) are exclusively my responsibility.

Furthermore, I declare that I have correctly marked all of the data, the analyses, and the conclusions generated from data obtained in collaboration with other persons, and that I have correctly marked my own contribution and the contributions of other persons (cf. declaration of contribution). I have correctly marked all texts or parts of texts that were generated in collaboration with other persons.

My contributions to any publications to this dissertation correspond to those stated in the below joint declaration made together with the supervisor. All publications created within the scope of the dissertation comply with the guidelines of the ICMJE (International Committee of Medical Journal Editors; http://www.icmje.org) on authorship. In addition, I declare that I shall comply with the regulations of Charité – Universitätsmedizin Berlin on ensuring good scientific practice.

I declare that I have not yet submitted this dissertation in identical or similar form to another Faculty.

The significance of this statutory declaration and the consequences of a false statutory declaration under criminal law (Sections 156, 161 of the German Criminal Code) are known to me.”

Date Signature

Declaration of your own contribution to the publications

Minze Xu contributed the following to the below listed publications:

1. **Xu M**, Lichtenberger FB, Erdoğan C, Lai E, Persson PB, Patzak A, Khedkar PH. Nitric Oxide Signalling in Descending Vasa Recta after Hypoxia/Re-Oxygenation. Int J Mol Sci. 2022 Jun 24;23(13):7016. doi: 10.3390/ijms23137016.

- designed the project together with Andreas Patzak and Pratik Khedkar
- performed the experiments in vasa recta, analyzed the videomicroscopic pictures, created the Excel tables.
- contributed to the main parts of the statistical analysis
- created the figures for the publication,
- wrote all parts of the first draft of the manuscript
- created figures 1 to 7 of this publication based on the generated data
- contributed to revisions of the manuscript

2. Stehle D, **Xu MZ**, Schomber T, Hahn MG, Schweda F, Feil S, Kraehling JR, Eitner F, Patzak A, Sandner P, Feil R, Bénardeau Novel soluble guanylyl cyclase activators increase glomerular cGMP, induce vasodilation and improve blood flow in the murine kidney. A. Br J Pharmacol. 2022 Jun;179(11):2476-2489. doi: 10.1111/bph.15586.

- performed experiments in three groups of L-NAME-pre-treated, isolated afferent and efferent arterioles (control, runcaciguat, and ODEQ + runcaciguat).
- investigated the bolus effect of runcaciguat in two groups of L-NAME pre-treated afferent as well as efferent arterioles
- created figures 3 (A-D) and 4 (A, B)
- wrote parts of the method-, results- and discussion section
- performed experiments in afferent arterioles using the NO-donor SNAP or the calcium channel inhibitor cilnidipine
- created the data for figure S2 of the supplemental material to this publication

3. Wennysia IC, Zhao L, Schomber T, Braun D, Golz S, Summer H, Benardeau A, Lai EY, Lichtenberger FB, Schubert R, Persson PB, **Xu MZ**, Patzak A.Role of soluble guanylyl cyclase in renal afferent and efferent arterioles Am J Physiol Renal Physiol. 2021 Feb 1;320(2):F193-F202. doi: 10.1152/ajprenal.00272.2020.

- performed the experiments in isolated glomerular arterioles together with Inggrid C. Wennysia
- did the statistical analysis on base of the data prepared by I.C.W.
- contributed to the data generation for Figures 2-8
- contributed to the revisions of the manuscript

_____

Signature, date and stamp of first supervising university professor / lecturer

_____

Signature of doctoral candidate

Excerpt from Journal Summary List

Journal Data Filtered By: **Selected JCR Year: 2021** Selected Editions: SCIE,SSCI
Selected Categories: **"BIOCHEMISTRY and MOLECULAR BIOLOGY"** Selected
Category Scheme: WoS
Gesamtanzahl: 296 Journale

Rank	Full Journal Title	Total Cites	Journal Impact Factor	Eigenfaktor
1	NATURE MEDICINE	141,857	87.241	0.23255
2	CELL	362,236	66.850	0.53397
3	Molecular Cancer	32,250	41.444	0.03386
4	Signal Transduction and Targeted Therapy	11,026	38.104	0.01781
5	Annual Review of Biochemistry	25,139	27.258	0.01962
6	Molecular Plant	20,242	21.949	0.02339
7	MOLECULAR CELL	94,258	19.328	0.13937
8	NUCLEIC ACIDS RESEARCH	284,490	19.160	0.33755
9	NATURE STRUCTURAL & MOLECULAR BIOLOGY	33,999	18.361	0.04689
10	TRENDS IN MICROBIOLOGY	19,957	18.230	0.02015
11	CYTOKINE & GROWTH FACTOR REVIEWS	9,002	17.660	0.00625
12	MOLECULAR ASPECTS OF MEDICINE	8,986	16.337	0.00615
13	Nature Chemical Biology	31,125	16.174	0.04456
14	TRENDS IN MOLECULAR MEDICINE	14,585	15.272	0.01381
15	NATURAL PRODUCT REPORTS	14,564	15.111	0.01079
16	PROGRESS IN LIPID RESEARCH	7,962	14.673	0.00444
17	TRENDS IN BIOCHEMICAL SCIENCES	22,957	14.264	0.02170
18	EMBO JOURNAL	80,536	14.012	0.05438
19	MOLECULAR PSYCHIATRY	33,324	13.437	0.04914
20	Molecular Systems Biology	11,036	13.068	0.01483
21	EXPERIMENTAL AND MOLECULAR MEDICINE	12,199	12.153	0.01698

Rank	Full Journal Title	Total Cites	Journal Impact Factor	Eigenfaktor
22	PLANT CELL	67,319	12.085	0.02964
23	CELL DEATH AND DIFFERENTIATION	31,035	12.067	0.02639
24	BIOCHIMICA ET BIOPHYSICA ACTA-REVIEWS ON CANCER	8,255	11.414	0.00673
25	Cell Systems	8,047	11.091	0.03332
26	CURRENT BIOLOGY	85,124	10.900	0.10641
27	Redox Biology	20,557	10.787	0.02390
28	International Journal of Biological Sciences	14,100	10.750	0.01488
29	MATRIX BIOLOGY	9,415	10.447	0.00856
30	PLOS BIOLOGY	44,888	9.593	0.05920
31	Cell and Bioscience	4,564	9.584	0.00524
32	Science Signaling	17,426	9.517	0.02046
33	GENOME RESEARCH	51,169	9.438	0.05153
34	CELLULAR AND MOLECULAR LIFE SCIENCES	38,745	9.207	0.03204
35	Journal of Integrative Plant Biology	8,456	9.106	0.00730
36	EMBO REPORTS	21,705	9.071	0.02695
37	Cell Chemical Biology	6,651	9.039	0.01870
38	CURRENT OPINION IN CHEMICAL BIOLOGY	12,464	8.972	0.01277
39	MOLECULAR BIOLOGY AND EVOLUTION	67,311	8.800	0.07228
40	ONCOGENE	81,646	8.756	0.05014
41	CELLULAR & MOLECULAR BIOLOGY LETTERS	2,684	8.702	0.00250
42	CRITICAL REVIEWS IN BIOCHEMISTRY AND MOLECULAR BIOLOGY	5,108	8.697	0.00477
43	Molecular Ecology Resources	15,145	8.678	0.01553

Selected JCR Year: 2021; Selected Categories: "BIOCHEMISTRY and MOLECULAR BIOLOGY"

Rank	Full Journal Title	Total Cites	Journal Impact Factor	Eigenfaktor
44	Plant Communications	743	8.625	0.00148
45	FREE RADICAL BIOLOGY AND MEDICINE	55,523	8.101	0.02824
46	INTERNATIONAL JOURNAL OF BIOLOGICAL MACROMOLECULES	112,372	8.025	0.09445
47	Biomedical Journal	2,388	7.892	0.00301
48	CURRENT OPINION IN STRUCTURAL BIOLOGY	13,407	7.786	0.01689
49	AMERICAN JOURNAL OF RESPIRATORY CELL AND MOLECULAR BIOLOGY	16,259	7.748	0.01386
50	Antioxidants	21,453	7.675	0.01946
51	EXPERT REVIEWS IN MOLECULAR MEDICINE	2,282	7.615	0.00062
52	Reviews of Physiology Biochemistry and Pharmacology	920	7.500	0.00043
53	ANTIOXIDANTS & REDOX SIGNALING	29,117	7.468	0.01390
54	Essays in Biochemistry	4,569	7.258	0.00691
55	Genes & Diseases	2,732	7.243	0.00322
56	Open Biology	5,227	7.124	0.00994
57	PROTEIN SCIENCE	18,673	6.993	0.02822
58	BIOMACROMOLECULES	46,963	6.978	0.02347
59	JOURNAL OF PHOTOCHEMISTRY AND PHOTOBIOLOGY B-BIOLOGY	18,610	6.814	0.01229
60	JOURNAL OF LIPID RESEARCH	29,128	6.676	0.01485
61	BIOCHIMICA ET BIOPHYSICA ACTA-MOLECULAR BASIS OF DISEASE	22,719	6.633	0.01820
62	MOLECULAR ECOLOGY	45,664	6.622	0.03311
63	AMYLOID-JOURNAL OF PROTEIN FOLDING DISORDERS	2,335	6.571	0.00312

Selected JCR Year: 2021; Selected Categories: "BIOCHEMISTRY and MOLECULAR BIOLOGY"

Rank	Full Journal Title	Total Cites	Journal Impact Factor	Eigenfaktor
64	BIOFACTORS	5,614	6.438	0.00307
65	International Review of Cell and Molecular Biology	3,388	6.420	0.00314
66	MOLECULAR MEDICINE	7,039	6.376	0.00402
67	Food & Function	27,282	6.317	0.02290
68	Biochimica et Biophysica Acta-Gene Regulatory Mechanisms	8,926	6.304	0.00707
69	INTERNATIONAL JOURNAL OF MOLECULAR SCIENCES	211,517	6.208	0.24907
70	Computational and Structural Biotechnology Journal	6,436	6.155	0.00945
71	JOURNAL OF MOLECULAR BIOLOGY	66,672	6.151	0.03581
72	JOURNAL OF NUTRITIONAL BIOCHEMISTRY	15,277	6.117	0.00837
73	Frontiers in Molecular Biosciences	6,864	6.113	0.01068
74	BIOCONJUGATE CHEMISTRY	19,624	6.069	0.01508
75	Biomolecules	21,742	6.064	0.02602
76	GLYCOBIOLOGY	10,212	5.954	0.00650
77	STRUCTURE	17,734	5.871	0.01779
78	MACROMOLECULAR BIOSCIENCE	9,240	5.859	0.00565
79	FASEB JOURNAL	59,831	5.834	0.04452
80	ACS Chemical Neuroscience	12,168	5.780	0.01655
81	BIOELECTROCHEMISTRY	7,093	5.760	0.00463
82	JOURNAL OF ENZYME INHIBITION AND MEDICINAL CHEMISTRY	8,156	5.756	0.00580
83	Journal of Genetics and Genomics	3,129	5.723	0.00327
84	Acta Crystallographica Section D-Structural Biology	23,006	5.699	0.02041
85	REDOX REPORT	2,247	5.696	0.00082

Selected JCR Year: 2021; Selected Categories: "BIOCHEMISTRY and MOLECULAR BIOLOGY"

Printing copies of the publications

International Journal of *Molecular Sciences*

MDPI

Article

Nitric Oxide Signalling in Descending Vasa Recta after Hypoxia/Re-Oxygenation

Minze Xu [1], Falk-Bach Lichtenberger [1], Cem Erdoğan [1], Enyin Lai [2], Pontus B. Persson [1], Andreas Patzak [1,*] and Pratik H. Khedkar [1]

[1] Institute of Translational Physiology, Charité—Universitätsmedizin Berlin, Corporate Member of Freie Universität Berlin and Humboldt-Universität zu Berlin, Charitéplatz 1, 10117 Berlin, Germany; minze.xu@charite.de (M.X.); falk.lichtenberger@charite.de (F.-B.L.); cem.erdogan@charite.de (C.E.); pontus.persson@charite.de (P.B.P.); pratik.khedkar@charite.de (P.H.K.)

[2] Department of Physiology, Zhejiang University School of Medicine, Hangzhou 310058, China; laienyin@zju.edu.cn

* Correspondence: andreas.patzak@charite.de

Abstract: Reduced renal medullary oxygen supply is a key factor in the pathogenesis of acute kidney injury (AKI). As the medulla exclusively receives blood through descending vasa recta (DVR), dilating these microvessels after AKI may help in renoprotection by restoring renal medullary blood flow. We stimulated the NO-sGC-cGMP signalling pathway in DVR at three different levels before and after hypoxia/re-oxygenation (H/R). Rat DVR were isolated and perfused under isobaric conditions. The phosphodiesterase 5 (PDE5) inhibitor sildenafil (10^{-6} mol/L) impaired cGMP degradation and dilated DVR pre-constricted with angiotensin II (Ang II, 10^{-6} mol/L). Dilations by the soluble guanylyl cyclase (sGC) activator BAY 60-2770 as well as the nitric oxide donor sodium nitroprusside (SNP, 10^{-3} mol/L) were equally effective. Hypoxia (0.1% O_2) augmented DVR constriction by Ang II, thus potentially aggravating tissue hypoxia. H/R left DVR unresponsive to sildenafil, yet sGC activation by BAY 60-2770 effectively dilated DVR. Dilation to SNP under H/R is delayed. In conclusion, H/R renders PDE5 inhibition ineffective in dilating the crucial vessels supplying the area at risk for hypoxic damage. Stimulating sGC appears to be the most effective in restoring renal medullary blood flow after H/R and may prove to be the best target for maintaining oxygenation to this vulnerable area of the kidney.

Keywords: descending vasa recta; hypoxia; re-oxygenation; soluble guanylyl cyclase; nitric oxide

Citation: Xu, M.; Lichtenberger, F.-B.; Erdoğan, C.; Lai, E.; Persson, P.B.; Patzak, A.; Khedkar, P.H. Nitric Oxide Signalling in Descending Vasa Recta after Hypoxia/Re-Oxygenation. *Int. J. Mol. Sci.* **2022**, *23*, 7016. https://doi.org/10.3390/ijms23137016

Academic Editor: Tzong-Shyuan Lee

Received: 31 May 2022
Accepted: 21 June 2022
Published: 24 June 2022

1. Introduction

Despite its energy-intensive functions of resorption and concentration, the renal medulla receives a considerably small amount (~10%) of the renal blood flow (RBF). It is exclusively perfused through descending vasa recta (DVR), which are capillary-like, long vessels originating from the juxtamedullary nephrons. DVR are lined with pericytes on their outer surface [1–3]. DVR supply the most energy-consuming cells, while warranting minimum perfusion to glycolytic cells in remote regions of the inner medulla. Highly oxygen-consuming structures, such as the S3 segment and the thick ascending limb of Henle, rely on vasa recta anastomosis for their oxygen supply. On the other hand, blood supply to deeper structures in the papilla must be minimal to prevent osmolyte washout. High oxygen demand combined with low perfusion renders the inner part of the outer medulla particularly susceptible to hypoxic damage in pathological events such as acute kidney injury (AKI) and chronic kidney disease (CKD) [4]. As DVR are the only vessels supplying blood to these renal areas at risk of hypoxia, maintaining blood supply is uniquely demanding and is key to providing renoprotection.

The physiological functions of DVR have been extensively characterized over the last two decades and the specific role that pericytes play in this context has also been

described (for review see [5–7]). It is the response of pericytes to various stimuli, such as sympathetic nervous activity, circulating and local hormones, and metabolites generated by neighbouring tubuli, that enables DVR to constrict and relax [5,8,9].

While experimental ischemia/re-perfusion reduces the overall RBF, its effect on the blood flow and oxygenation of the medulla is significantly prolonged compared to the cortex [10,11]. Moreover, the damage is especially severe in the inner part of the outer medulla [12]. These findings suggest that medullary blood flow plays an important role in the genesis of renal damage in various renal pathologies. RBF is critically regulated by nitric oxide (NO) through its vasodilatory effect. NO is probably the strongest antagonist of several vasoconstrictors, including angiotensin II (Ang II), and plays an important role in the physiology and pathophysiology of renal perfusion [13–16]. Experimentally induced NO deficiency has been shown to reduce RBF and cause renal damage in several species [17,18]. NO deficiency is a hallmark of AKI and CKD and may contribute to the imbalance of vasoconstrictor and dilator mechanisms that increase renal vascular resistance and reduce cortical and medullary RBF [19]. Therefore, improving RBF, especially the medullary flow, by restoring NO production and signalling may be a protective and therapeutic tool in AKI and CKD. Pharmacological approaches have indeed been successful in animal experiments; however, they have not been translated to the clinical setting to date.

Cyclic GMP (cGMP) is the mediator of the NO system in vascular smooth muscle cells. Several pharmacological agents developed during the last two decades aim at modulating the effects of the NO system by increasing cellular levels of cGMP. The most prominent categories of such agents are phosphodiesterase 5 (PDE5) inhibitors and soluble guanylyl cyclase (sGC) stimulators and activators [20,21]. Some of them are already used in the clinic, e.g., to treat pulmonary hypertension [22]. Their dilatory capabilities in microvessels of the renal cortex have recently been demonstrated [23]. Interestingly, the sGC activator cinaciguat has been shown to dilate glomerular efferent but not afferent arterioles in mice after strong hypoxia and subsequent re-oxygenation [24]. This indicates that NO signalling after hypoxia is differently regulated in the two different types of glomerular arterioles. However, little is known about the influence of hypoxia on microvascular NO signalling in the renal medulla. Therefore, we investigated the dilatory capacity of the NO system in DVR and tested the ability of an sGC activator to dilate these microvessels after hypoxia/re-oxygenation (H/R). This could provide a new approach for protection and therapy in AKI and CKD.

2. Results

2.1. Pharmacological Characterization of NO-sGC-System in Rat DVR

2.1.1. Effect of NOS Inhibition

NO deficiency was induced in isolated rat DVR by treating them with an inhibitor of NO synthases (NOS)—Nω-nitro-L-arginine methyl ester hydrochloride (L-NAME, 10^{-4} mol/L)—for 15 min. While a control group of vessels incubated under similar conditions did not show a significant change in diameter, vessels treated with L-NAME were significantly constricted (Figure 1A).

L-NAME-treated and untreated control vessels were subjected to increasing concentrations of Ang II (10^{-12}–10^{-6} mol/L) to study the effect of NOS inhibition on vasoconstriction. L-NAME-treated vessels showed a significantly stronger constriction in response to higher concentrations of Ang II (10^{-10}–10^{-6} mol/L) compared to control vessels (Figure 1B). The absolute initial diameters of L-NAME-treated vessels (mean ± SEM: 7.17 ± 0.99 µm) were similar to control vessels (7.87 ± 0.70 µm, Mann–Whitney test, $p > 0.05$). To assess if NOS inhibition also affects vasodilation, L-NAME-treated and untreated control vessels were pre-constricted using 10^{-6} mol/L Ang II followed by treatment with cumulatively increasing concentrations of acetylcholine (ACh, 10^{-11}–10^{-4} mol/L). The dilatory response of L-NAME-treated vessels was, indeed, significantly weaker compared to control vessels (Figure 1C). The absolute initial diameters of the vessels after pre-constriction were not

significantly different between the L-NAME-treated and control groups (mean ± SEM: 1.97 ± 0.41 µm (L-NAME) vs. 1.80 ± 0.11 µm (control), Mann–Whitney test, $p > 0.05$).

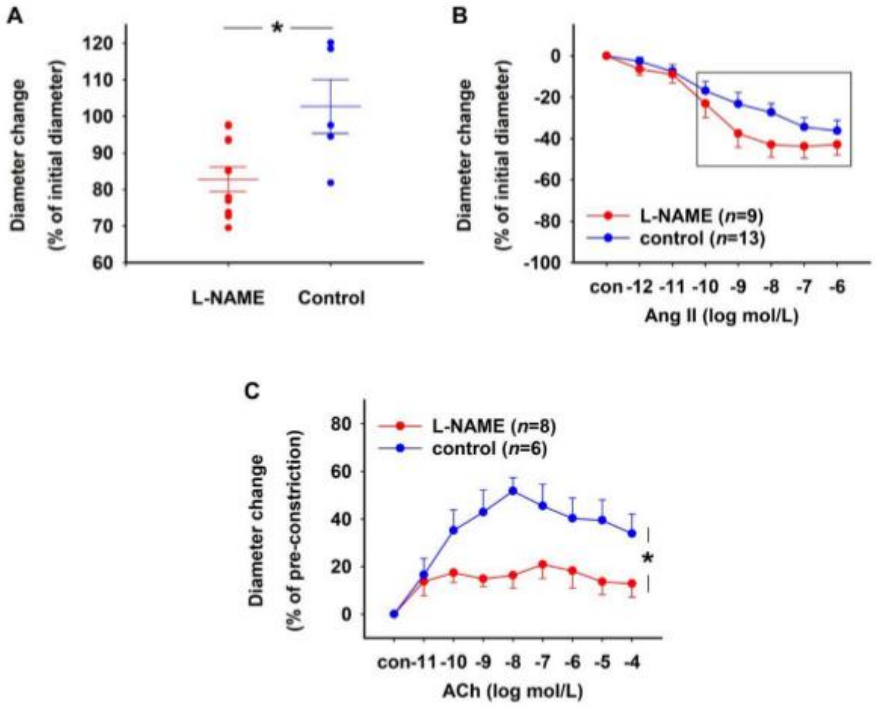

Figure 1. Effect of L-NAME on rat DVR. (**A**) Vessels treated with L-NAME (10^{-4} mol/L) for 15 min ($n = 12$) showed significant constriction compared to untreated control ($n = 5$) vessels (Mann–Whitney test, * $p < 0.05$). Vessel diameters in both groups before treatment were not significantly different (mean ± SEM: 8.48 ± 0.84 µm (L-NAME) vs. 7.84 ± 0.83 µm (control), Mann–Whitney test, $p > 0.05$). (**B**) Concentration–response curves showing the constriction induced by Ang II in DVR with and without 10^{-4} mol/L L-NAME pre-treatment for 15 min. L-NAME-treated DVR constricted significantly more in response to higher Ang II concentrations (highlighted in a box) than the control group (Brunner test, * $p < 0.001$). (**C**) Concentration–response curves showing the relaxation induced by 10^{-11}–10^{-4} mol/L acetylcholine (ACh) in DVR with and without pre-treatment with 10^{-4} mol/L L-NAME for 15 min. L-NAME-treated vessels showed a lower maximum response to ACh compared to the control group (Brunner test, * $p < 0.01$).

2.1.2. Effect of PDE5 Inhibition

Vasodilation was tested by subjecting isolated rat DVR to cumulatively increasing concentrations of sildenafil (10^{-9}–10^{-6} mol/L). Vessels were pre-constricted using Ang II (10^{-6} mol/L) and had a mean diameter ± SEM of 3.65 ± 0.32 µm. The pre-constricted vessels showed concentration-dependent dilation in response to sildenafil (Figure 2A). Bolus application of sildenafil (10^{-7} mol/L) to Ang II pre-constricted vessels resulted in 100% dilation of vessels in 5 min, while control vessels, which did not receive a bolus, remained constricted throughout the experimental duration of 10 min (Figure 2B). Both sildenafil-treated and untreated control vessels had comparable absolute diameters after Ang II pre-constriction (mean ± SEM: 3.53 ± 0.44 µm (sildenafil) vs. 3.37 ± 0.47 µm (control), Mann–Whitney test, $p > 0.05$).

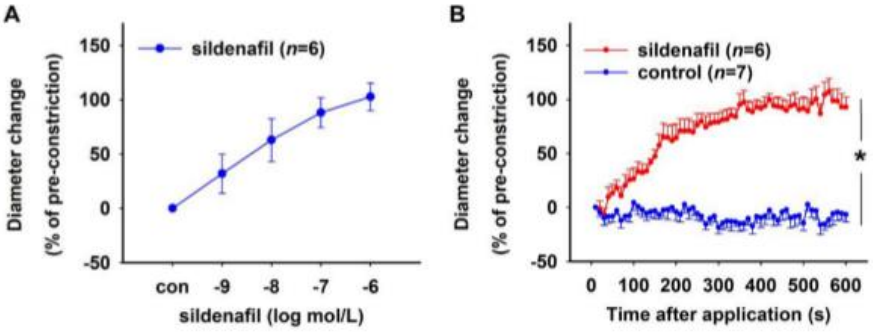

Figure 2. Effect of the PDE5 inhibitor sildenafil. Rat DVR were pre-constricted with 10^{-6} mol/L Ang II. (**A**) Concentration–response curve showing vasorelaxation induced by 10^{-9} to 10^{-6} mol/L sildenafil. Vessel diameter did not change in the absence of sildenafil (con). (**B**) Time–response curves showing relaxation induced by 10^{-7} mol/L sildenafil over a period of 10 min. Sildenafil caused an almost instantaneous relaxation of the vessels with 100% relaxation achieved in 5 min (Brunner test, * $p < 0.001$). Control vessels without sildenafil treatment remained constricted throughout the experiment.

2.1.3. Effect of sGC Activation in NO-Deficient Vessels

sGC was activated using increasing concentrations of the NO-independent activator BAY 60-2770. Rat DVR were pre-treated with 10^{-4} mol/L L-NAME followed by a pre-constriction with 10^{-6} mol/L Ang II. A concentration-dependent dilation was seen in response to BAY 60-2770 (Figure 3A). The absolute initial diameter of vessels after pre-constriction was 3.59 ± 0.32 µm (mean ± SEM). In another set of experiments, L-NAME-treated Ang-II-constricted vessels that received a bolus of 10^{-6} mol/L BAY 60-2770 showed maximum dilation in 6 min, while the vessels that did not receive the bolus remained constricted throughout the duration of the experiment (10 min, Figure 3B). Both groups of vessels had comparable initial diameters after pre-constriction with Ang II (mean ± SEM: 3.22 ± 0.38 µm (BAY 60-2770) vs. 2.90 ± 0.54 µm (control), Mann–Whitney test, $p > 0.05$).

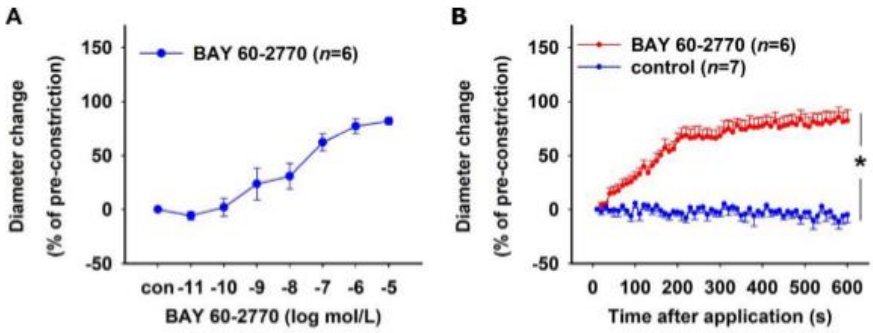

Figure 3. Effect of the soluble guanylyl cyclase activator—BAY 60-2770. Rat DVR were pre-treated with 10^{-4} mol/L L-NAME and pre-constricted with 10^{-6} mol/L Ang II. (**A**) Concentration–response curve showing relaxation induced by 10^{-11}–10^{-5} mol/L BAY 60-2770. Vessel diameter did not change in the absence of BAY 60-2770 (con). (**B**) Time–response curves showing relaxation induced by 10^{-6} mol/L BAY 60-2770 over a period of 10 min. Control vessels without BAY 60-2770 treatment remained constricted throughout the experiment (Brunner test, * $p < 0.001$).

2.2. Characterization of Human DVR

Human DVR were isolated from tissue samples obtained from nephrectomies. The viability of the vessels was tested by treating them with increasing concentrations of Ang II (10^{-12}–10^{-6} mol/L). The vessels constricted in a concentration-dependent fashion in response to Ang II (Figure 4A). The initial absolute diameter of the vessels was 11.29 ± 0.88 µm (mean ± SEM). To test the effect of sGC activation on human DVR, Ang II pre-constricted vessels were treated with a bolus of BAY 60-2770 (10^{-6} mol/L). The vessels achieved maximum relaxation 3 min post bolus application (Figure 4B).

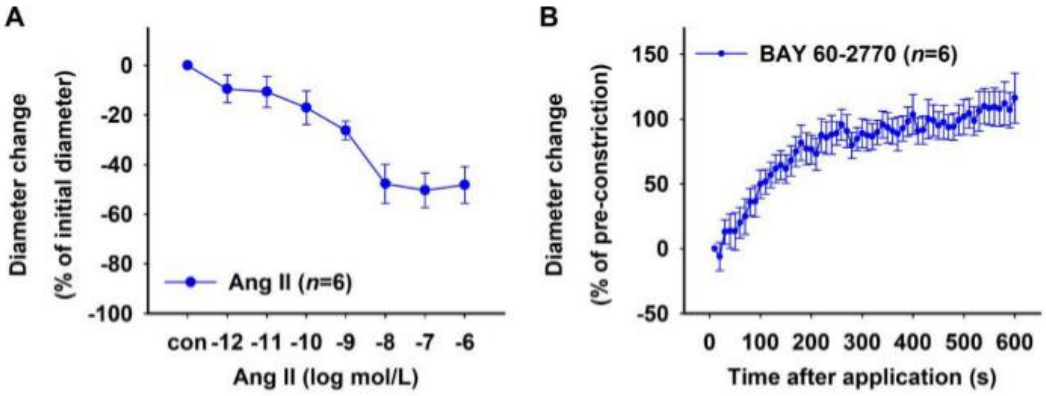

Figure 4. sGC activation in human DVR. (**A**) Concentration–response curve showing constriction induced by 10^{-12}–10^{-6} mol/L Ang II. Vessel diameters did not change in the absence of Ang II (con). (**B**) Time–response curve showing relaxation induced by 10^{-6} mol/L BAY 60-2770. Vessels were pre-constricted with 10^{-6} mol/L Ang II. BAY 60-2770 caused an almost instantaneous relaxation of the vessels with maximum relaxation achieved in 3 min.

2.3. Effect of H/R on Rat DVR

Isolated rat DVR were incubated in a 0.1% O_2 environment (hypoxia) or a 20.9% O_2 environment (normoxia) for 30 min. Hypoxia did not affect the resting diameters of the vessels (mean ± SEM: 7.31 ± 0.45 µm (hypoxia) vs. 7.91 ± 0.50 µm (normoxia), Mann–Whitney test, $p > 0.05$). To study the effect of hypoxia on vasoconstriction, both groups of vessels were treated with increasing concentrations of Ang II. Hypoxic vessels showed a significantly stronger constriction in response to Ang II (Figure 5A). The effect of hypoxia on vasodilation was analysed by pre-constricting hypoxic and normoxic vessels with 10^{-6} mol/L Ang II followed by treatment with cumulatively increasing concentrations of ACh. While both groups had similar diameters after pre-constriction (mean ± SEM: 1.48 ± 0.10 µm (hypoxia) vs. 1.97 ± 0.41 µm (control), Mann–Whitney test, $p > 0.05$), hypoxic vessels showed a significantly weaker relaxation in response to ACh compared to normoxic vessels (Figure 5B). In another set of experiments, hypoxic and normoxic vessels pre-constricted using 10^{-6} mol/L Ang II received a bolus of 10^{-6} mol/L sildenafil. While PDE5 inhibition with sildenafil resulted in the complete relaxation of normoxic vessels, hypoxic vessels remained constricted throughout the experimental duration of 10 min (Figure 5C). The initial diameters of hypoxic vessels after pre-constriction (mean ± SEM: 2.65 ± 0.47 µm) were not significantly different compared to normoxic vessels (3.53 ± 0.44 µm, Mann–Whitney test, $p > 0.05$).

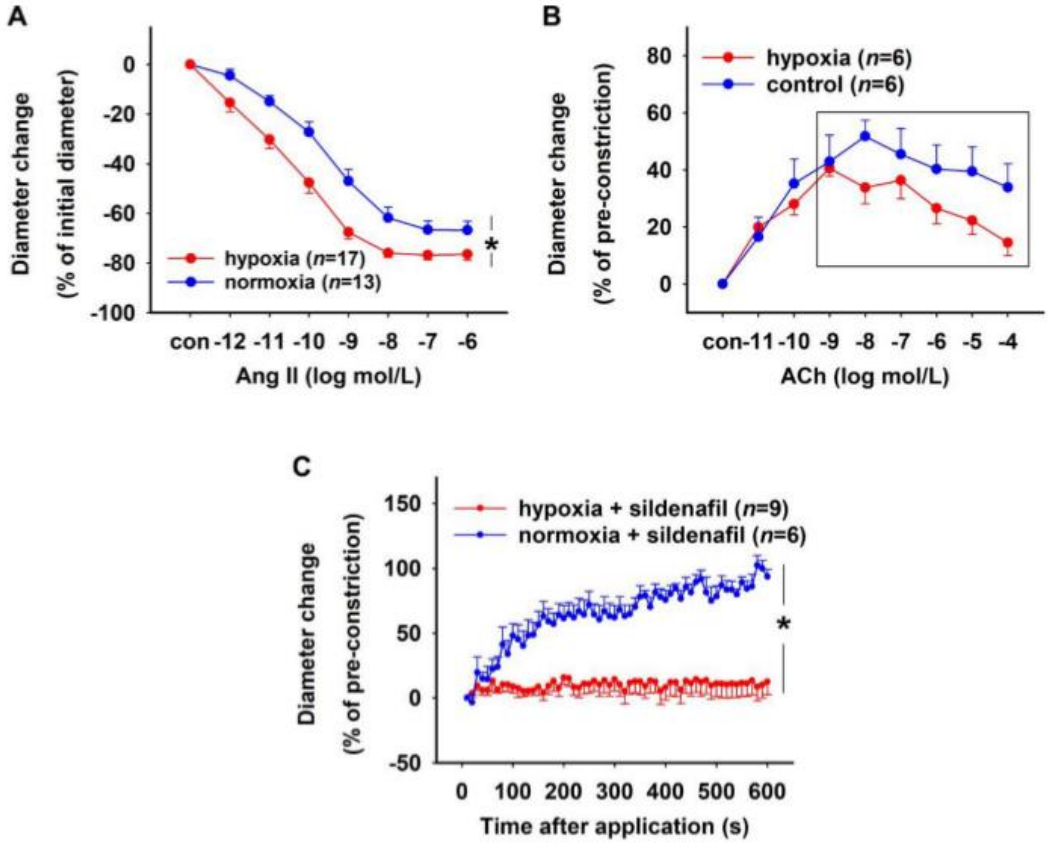

Figure 5. Effect of hypoxia/re-oxygenation on rat DVR. Vessels were pre-incubated either in a 0.1% oxygen (O_2) atmosphere (hypoxia) or in a 20.9% O_2 atmosphere (normoxia) for 30 min. (**A**) Concentration–response curves showing constriction induced by 10^{-12}–10^{-6} mol/L Ang II in hypoxic and normoxic vessels. Hypoxia/re-oxygenation group of vessels showed a significantly stronger constriction in response to Ang II compared to the normoxia group (Brunner test, * $p < 0.001$). (**B**) Concentration–response curve showing relaxation induced by 10^{-11}–10^{-4} mol/L ACh in hypoxic and normoxic vessels pre-constricted with 10^{-6} mol/L Ang II. Hypoxic vessels relaxed significantly less in response to higher concentrations of ACh (10^{-9}–10^{-4} mol/L, highlighted in a box) compared to normoxic vessels (Brunner test, * $p < 0.05$). (**C**) Time–response curves showing the effect of PDE inhibition using 10^{-6} mol/L sildenafil on hypoxic and normoxic vessels pre-constricted with 10^{-6} mol/L Ang II. Sildenafil caused normoxic vessels to relax, while no relaxation was observed in hypoxic vessels for the entire duration of the experiment (Brunner test, * $p < 0.001$).

The effect of sGC activation on hypoxic vessels was analysed using the NO donor sodium nitroprusside (SNP) and the NO-independent sGC activator BAY 60-2770. To determine the concentration response, SNP was used in cumulatively increasing concentrations to treat isolated rat DVR that were pre-constricted with 10^{-6} mol/L Ang II and pre- treated with 10^{-4} mol/L L-NAME (mean diameter ± SEM after pre-constriction: 3.59 ± 0.32 µm). The vessels relaxed in a dose-dependent manner and 100% relaxation was achieved with 10^{-3} mol/L SNP (Figure 6A).

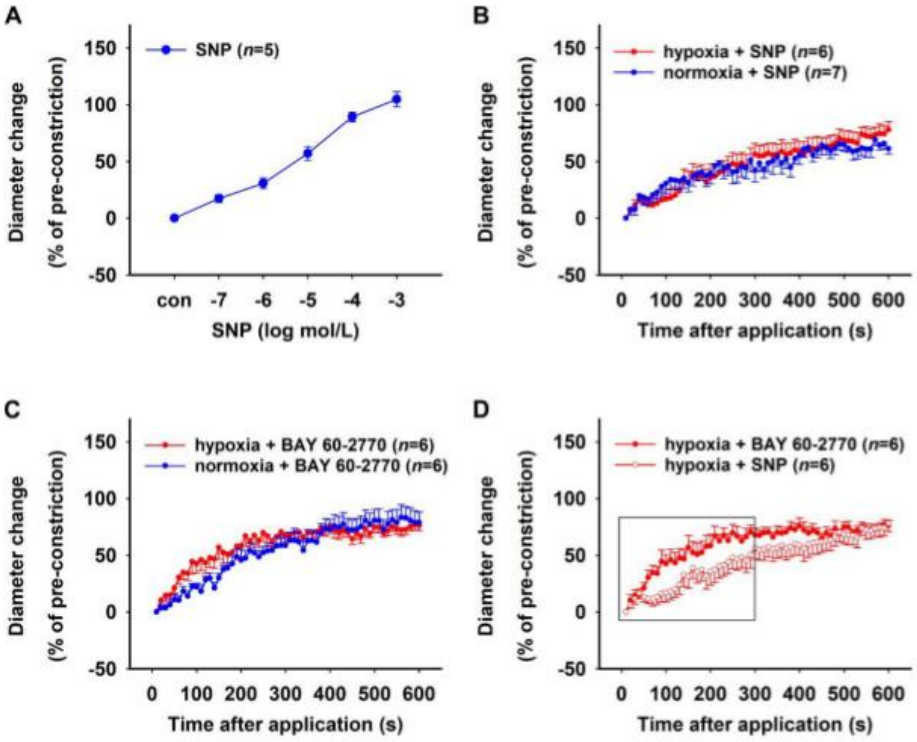

Figure 6. Effects of sodium nitroprusside (SNP) and BAY 60-2770 on hypoxic rat DVR. (**A**) Concentration–response curve showing relaxation induced by 10^{-11}–10^{-5} mol/L sodium nitroprusside (SNP) in rat vasa recta. Vessel diameter did not change under control conditions (con), i.e., in the absence of BAY 60-2770. Time–response curves showing the effect of (**B**) the NO donor SNP (10^{-3} mol/L) and (**C**) the NO-independent sGC activator BAY 60-2770 (10^{-6} mol/L) on hypoxic and normoxic vessels over a period of 10 min. Vessels were pre-incubated either in a 0.1% oxygen (O_2) atmosphere (hypoxia) or in a 20.9% O_2 atmosphere (normoxia) with 10^{-4} mol/L L-NAME for 30 min followed by a pre-constriction with 10^{-6} mol/L Ang II. Relaxation to SNP and BAY 60-2770 were similar in hypoxic and normoxic vessels, respectively. However, (**D**) hypoxic vessels showed faster relaxation in response to BAY 60-2770 compared to SNP (Brunner test, $p < 0.05$, same data as (**B**,**C**)).

Isolated DVR were subjected to hypoxia or normoxia for 30 min in the presence of 10^{-4} mol/L L-NAME to inhibit cellular NOS, followed by pre-constriction with 10^{-6} mol/L Ang II. Both groups of vessels had comparable diameters after pre-constriction (mean ± SEM: 2.72 ± 0.82 µm (hypoxia) vs. 2.51 ± 0.53 µm (normoxia), Mann–Whitney test, $p > 0.05$). A bolus of 10^{-3} mol/L SNP was then applied to these vessels to study the effect of hypoxia on the NO-dependent activation of sGC. Both groups of vessels showed similar relaxation in response to the bolus over a period of 10 min (Figure 6B). The effect of the NO-independent activation of sGC was similarly analysed by applying a bolus of 10^{-6} mol/L BAY 60-2770 to L-NAME-treated hypoxic and normoxic vessels that were pre-constricted using 10^{-6} mol/L Ang II. Both groups of vessels showed similar relaxation in response to BAY 60-2770 over a period of 10 min (Figure 6C). The absolute initial diameters of hypoxic vessels after pre-constriction (mean ± SEM: 1.70 ± 0.19 µm) were smaller compared to normoxic vessels (2.47 ± 0.24 µm, Mann–Whitney test, $p < 0.05$). However, the NO-independent activator BAY 60-2770 caused a significantly quicker relaxation in L-NAME-treated pre-constricted hypoxic vessels compared to the NO donor

SNP (Figure 6D). The absolute initial diameters of pre-constricted hypoxic vessels treated with BAY 60-2770 (mean ± SEM: 1.70 ± 0.19 µm) were not significantly different than the SNP-treated vessels (2.72 ± 0.82 µm, Mann–Whitney test, $p > 0.05$).

3. Discussion

In this study, we analysed the function of isolated, perfused outer medullary DVR to demonstrate the importance of the NO system for vascular tone. Under physiological conditions, DVR constricted strongly in response to Ang II and relaxed completely in response to the ACh treatment that followed. Moreover, the dilatory function of DVR could be substantially enhanced by pharmacological modulation of the NO system, as evident from their strong dilatory responses to the PDE5 inhibitor sildenafil and the sGC activator BAY 60-2770. After exposure to a strong and acute hypoxia, DVR response to Ang II showed a significant increase, while there was a reduction in ACh-mediated dilation. This corresponds to the imbalance between vasoconstriction and dilation that leads to reduced renal (medullary) perfusion seen in ischemia/reperfusion models of AKI. Interestingly, the natural agonist of sGC, NO, as well as the sGC activator could dilate DVR after H/R, but sildenafil could not. Although all of these pharmacological agents increase cellular cGMP levels, their ability to do so seems to be differently affected by H/R.

We used isolated, perfused DVR to characterize the NO-sGC-cGMP system and to test the dilatory potency of pharmacological substances. This method is rarely applied due to its technically demanding nature that necessitates long-term training. Nevertheless, it is a well-established method and has been used in functional, electrophysiological, and imaging studies [25,26]. It has several advantages compared to the living kidney slice technique. For instance, while living kidney slices suffer from a lack of oxygen in the inner parts owing to their commonly used thickness of 200–300 µm, isolated, perfused DVR allow for sufficient oxygenation. This lack of oxygen in the slices may lead to metabolic changes in the tubuli and vessels, resulting in a release of a cocktail of substances with potentially vasoactive properties. In the case of isolated, perfused DVR, however, the experimental conditions can be uniformly controlled with the help of the bath and perfusion solutions. They can also be easily exposed to hypoxia and re-oxygenated in a precise and controlled fashion. Moreover, the perfusion also closely simulates physiological conditions as the flow itself is an important determinant of endothelial function.

The responses of isolated, perfused rat DVR to Ang II and ACh in our experiments were consistent with previously published studies [27–29]. The inhibition of NOS clearly enhanced Ang II response and diminished ACh-induced dilation, suggesting that NO is an important regulator of DVR diameter. NO activates sGC in vascular smooth muscle cells and pericytes, leading to cGMP production. This cGMP then activates protein kinase G, which phosphorylates several proteins that reduce the levels of cytosolic calcium, which in turn causes vasodilation [30].

While NO is the natural agonist of sGC, pharmacological agents can activate sGC independently of NO. These sGC activators are functional with both oxidized and haem-free variants of sGC [22]. We tested the sGC activator BAY 60-2770 in DVR, in which NO was depleted using L-NAME. BAY 60-2770 was indeed able to dilate pre-constricted DVR in a dose-dependent manner. This observation indicates that BAY 60-2770 may have a high potency to dilate NO-deficient DVR in vivo. Cinaciguat, another sGC activator, has also been shown to normalize renal resistance and blood flow in rats after L-NAME treatment [31]. However, activators are considered to exert a systemic action, which may reduce the overall arterial blood pressure and reverse the intended restoration of renal perfusion in pathological situations [31,32]. We also tested BAY 60-2770 on *human* DVR; however, these tests were without L-NAME pre-treatment due to the limited time available for acute experiments after harvesting the tissue and its subsequent transport to the laboratory. Nevertheless, BAY 60-2770 very effectively dilated pre-constricted human DVR and has potential for clinical application. In addition to sGC, cGMP levels are also regulated by PDEs. Here, we showed that PDE5 is an important component of the

NO-sGC-cGMP system, and its inhibition had a strong dilatory effect on DVR under physiological conditions.

After characterizing the NO-sGC-cGMP system, we tested the ability of sildenafil, BAY 60-2770, and the NO donor SNP to dilate DVR after H/R. In most models of renal pathologies, including AKI and CKD, H/R is a major contributor to the pathogenesis of renal damage [33]. Animal models of ischemia/re-perfusion injury show reduced oxygenation and perfusion of the kidney. Furthermore, the restoration of blood flow and oxygenation after ischaemia is remarkably delayed in the renal medulla compared to the cortex [34,35]. This delay does not only indicate that the regulation of medullary perfusion after ischaemia is at least partly independent of that of the cortex, but also underscores the critical role that DVR play in it. Likely reasons for this medullary malperfusion could be a combination of functional changes such as the thrombotic occlusion of microvessels and an increased DVR tone [34]. The latter seems to be caused by an imbalance between vasoconstrictors and dilators. An increase in NO production and a reduced response to Ang II, as seen in ex vivo functional experiments in rat DVR, 48 h after warm renal ischaemia/re-perfusion, can be interpreted as a compensatory reaction to this imbalance. A rise in iNOS expression may trigger the increase in NO-bioavailability [26]. In kidney slices, fixed immediately following acute H/R (1 h each), vasa recta have been shown to have reduced diameters at pericyte sites and disruptions in their fluorescent dye-filled lumina [34]. Interestingly, the diameters of isolated DVR in the present study after 30 min of hypoxia followed by 10 min of re-oxygenation did not differ significantly from those of normoxic controls in the absence of vasoactive substances. However, the vessel response to Ang II was stronger, and ACh-induced dilation was weaker. Ang II activates NO synthase via Ang II receptor type I, resulting in NO release. This NO then dampens the Ang II-induced vasoconstriction in renal microvessels [36]. This crosstalk between Ang II and the NO system may be impaired after H/R, contributing to the stronger Ang II response and diminished ACh response. Another important factor that comes into play in this context is oxidative stress. Superoxide, a prominent representative of reactive oxygen species, does not only increase the Ang II response, since it is a part of the signalling, but also scavenges NO at the same time [37–39]. A similar increase in the Ang II response of DVR after H/R has also been observed in living kidney slices [40]. Taken together, functional changes in the outer medullary DVR seem to play a critical role in the disruption of medullary perfusion caused by ischaemia/re-perfusion.

Since the acute period is characterized by an increased tone and reactivity to Ang II, accompanied by reduced dilatory capacity, restoring vasodilation would be protective for the kidney. The NO donor SNP showed a full dilatory potency. This was unexpected because increased ROS generation after H/R may oxidize sGC, thereby rendering it less responsive to NO [37,41]. The NO-independent activation of sGC using BAY 60-2770 also led to complete DVR dilation, which was faster than the SNP-induced dilation. Surprisingly, sildenafil did not affect the DVR diameter after H/R at all, which may at least partly be due to low cGMP levels, as indicated by the significantly reduced response to ACh. However, direct damage to the enzyme due to the strong hypoxia cannot be ruled out.

Our findings suggest a beneficial effect of NO donors and sGC activators in hypoxia-damaged DVR in an acute pathological situation, where dilation is reduced and reactivity to Ang II is increased. While the period of re-oxygenation was relatively short in our experiments, prolonged re-oxygenation periods following strong hypoxia have also been shown to increase Ang II response in cortical microvessels in living kidney slices [42]. Therefore, one can speculate that longer re-oxygenation periods in vivo induce oxidative stress, resulting in stronger oxidation of sGC, making it unfit to be activated by NO. In such a situation, sGC activators are especially beneficial as they activate oxidized sGC more efficiently [43]. Therefore, the effect of sGC activators might be more pronounced in kidneys damaged by ischaemia/reperfusion, suggesting potential for therapeutic application.

4. Materials and Methods

4.1. Experimental Animals

Male Sprague Dawley rats were maintained at the animal facility of the Charité—Universitätsmedizin Berlin under a 12 h light/dark cycle. They were housed in enriched cages and were allowed free access to rat chow and tap water.

4.2. Dissection of DVR

To isolate DVR, rats (250 g) were anesthetized with isoflurane and then decapitated. The left kidney was then taken out immediately and sliced along the corticomedullary axis. A customized set of forceps (No. 5, Dumont, Switzerland) was used to isolate DVR from the renal outer medulla. A single DVR was then transferred to a perfusion chamber assembled on the stage of an inverted microscope. For some of the experiments, small bundles of DVR were dissected and pre-treated, e.g., in a hypoxic chamber, so that they could be easily retrieved after the pre-treatment to isolate single DVR for perfusion experiments. To follow the 3R principle of 'reduce', multiple DVR were isolated from each animal; however, no more than one DVR per animal was used for the same experimental protocol. Dulbecco's modified Eagle's medium (DMEM, Gibco, Paisley, UK) with 0.1% albumin (Carl Roth GmbH, Karlsruhe, Germany) was used as a bath solution for dissections as well as in the perfusion chamber.

4.3. Human DVR

Human DVR were isolated from non-malignant outer medullary renal tissue. The tissue was obtained from 6 patients who underwent nephrectomies due to renal cell carcinoma at the Klinik für Urologie, Charité—Universitätsmedizin Berlin between October 2019 and March 2022. All patients provided written informed consent. The study was approved by the ethical committee of the Charité—Universitätsmedizin Berlin (Approval No. EA4/65/18).

4.4. Perfusion of Isolated DVR

A set of handmade glass pipettes were used to perfuse the DVR. In the perfusion chamber, a single DVR was fixed in place using a holding pipette on each end. A smaller pipette placed inside the left holding pipette (inner pipette) was advanced into the lumen of the vessel (Figure 7A). The vessel was then perfused with DMEM supplemented with 1% albumin. The perfusion was carried out under a pressure of 15 mm Hg using a pressure head. This pressure is suitable to open the lumen of the DVR without any sign of overstretching. After warming to 37 °C, vessels were allowed to adapt for 5 min before starting the experiment. All experiments were performed within 2 h after the animals were sacrificed.

4.5. Measurement of DVR Diameters

During the experiments, vessels were continuously displayed on a computer screen using a video camera (Moticam 2.0, Motic Asia, Hong Kong, China). Luminal diameters served for the estimation of vascular tone and reactivity and were measured using the freeware ImageJ at the site where the reaction to the agonist being tested was the strongest [44]. DVR do not react to agonists uniformly across their length since pericytes, their vasoactive parts, do not completely cover their outer surface (Figure 7B,C). To analyse the effects of pre-treatments and for concentration–response curves, an image was taken every second and average vessel diameters were calculated using measurements from five consecutive images. For time–response curves, diameters were measured from single images taken every 10 s over a period of 10 min.

4.6. Protocols

All chemicals and drugs were purchased from Sigma-Aldrich (Darmstadt, Germany), unless otherwise specified. Stock solutions of substances insoluble in distilled water were prepared in dimethyl sulfoxide (DMSO, purity > 99.7%, Bellefonte, PA, USA). The final concentration of DMSO did not exceed 0.1% in any of the experiments. All chemicals were stored at −20 °C. Concentrations are given as final molar concentration in the bath solution.

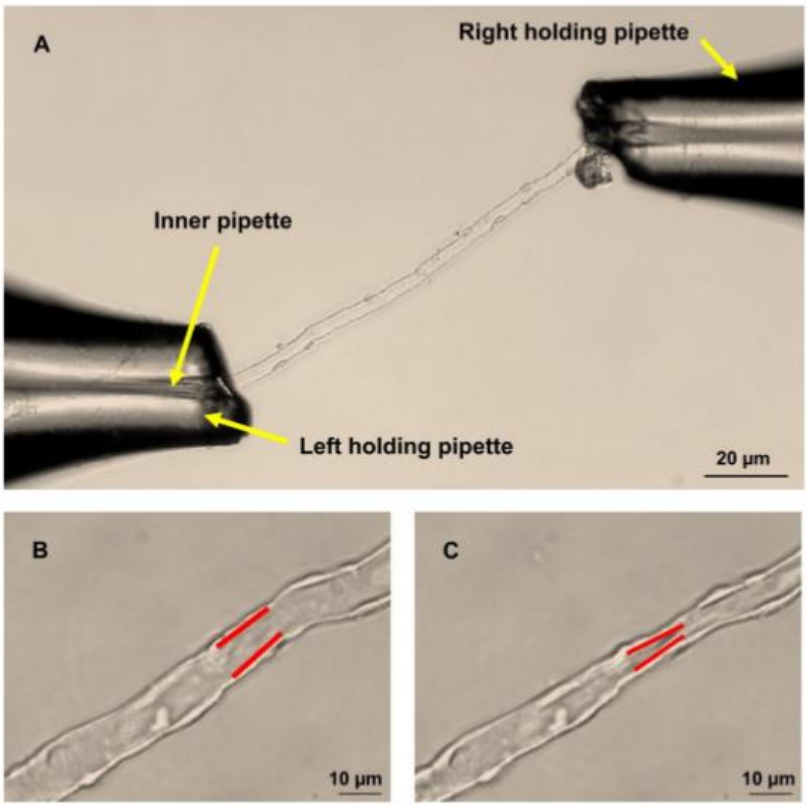

Figure 7. (**A**) Microperfusion of rat DVR using holding and perfusion pipettes. (**B**) Resting and (**C**) constricted DVR with the site of constriction marked in red.

4.6.1. Pharmacological Characterization of NO-sGC System

To test the contribution of the NO system to the DVR tone, vessels were incubated in bath solution with or without L-NAME (10^{-4} mol/L) for 15 min. Then, Ang II was given in increasing concentrations (10^{-12} to 10^{-6} mol/L, 2 min each). After reaching a stable constriction, ACh was applied in cumulatively increasing concentrations (10^{-11} to 10^{-4} mol/L, 3 min each).

The effect of PDE5 inhibition on DVR was tested using sildenafil (Biomol GmbH, Hamburg, Germany). Isolated rat DVR were pre-constricted using 10^{-6} mol/L Ang II followed by treatment with increasing concentrations of sildenafil (10^{-9}–10^{-6} mol/L, 3 min each) to obtain the concentration–response curves. The dynamics of vessel dilation were investigated by applying a bolus of sildenafil (10^{-7} mol/L) or a corresponding amount of DMSO (solvent control) and tracking the changes in vessel diameters over a period of 10 min.

To study the effect of sGC activation, isolated rat DVR were pre-treated with 10^{-4} mol/L L-NAME for 15 min followed by pre-constriction with 10^{-6} mol/L Ang II. A concentration–response curve was then obtained by applying the sGC activator BAY 60-2770 (Bayer AG, Wuppertal, Germany) in cumulatively increasing concentrations (10^{-11} to 10^{-5} mol/L, 3 min each). To obtain the time–response curve, L-NAME-treated Ang II pre-constricted DVR were treated with a bolus of 10^{-6} mol/L BAY 60-2770 or a corresponding amount of DMSO (solvent control) and the changes in vessel diameters were tracked over a period of 10 min.

4.6.2. Human DVR

To check vessel viability and simultaneously pre-constrict the DVR, Ang II was applied in increasing concentrations (10^{-12} to 10^{-6} mol/L, 2 min each). After reaching a stable constriction, BAY 60-2770 (10^{-6} mol/L) was applied and the changes in the diameter were tracked over a period of 10 min.

4.6.3. Effect of Hypoxia on the NO System

To investigate how hypoxia influences the NO system, DVR were incubated in an environment with either 0.1% O_2 (hypoxia) or 20.9% O_2 (normoxia) for 30 min. Hypoxic conditions were achieved using a hypoxia chamber (H35 hypoxystation, Don Whitley Scientific Ltd., West Yorkshire, UK). After a re-oxygenation period of 10 min, Ang II concentration–responses (10^{-12} to 10^{-6} mol/L, 2 min each) were measured. In an additional series of experiments, ACh was applied (10^{-11} to 10^{-4} mol/L, 3 min each) after pre-constriction with Ang II (10^{-6} mol/L) to obtain the concentration–response for ACh in normoxic and hypoxic DVR. Sildenafil was applied as bolus (10^{-7} mol/L) after H/R and pre-constriction with Ang II (10^{-6} mol/L). Changes in vessel diameters were tracked over a period of 10 min.

The NO donor SNP was used to test the natural stimulation of sGC. The concentration–response was measured after L-NAME (10^{-4} mol/L) pre-treatment and Ang II (10^{-6} mol/L) pre-constriction. Furthermore, the time response to bolus application of SNP (10^{-3} mol/L) was measured in normoxic and hypoxic DVR. Time–responses to the sGC activator BAY 60-2770 were measured after Ang II (10^{-6} mol/L) pre-constriction and L-NAME (10^{-4} mol/L) pre-treatment in DVR after H/R or normoxia.

4.7. Statistics

Mean and standard error of the mean (SEM) were calculated using GraphPad Prism 9.3.1 (GraphPad software, San Diego, CA, USA). Data were tested for normal distribution using the Shapiro–Wilk test. Although most data were normally distributed, we used nonparametric statistical tests in this study as they provide the most robust testing. Differences between concentration- or time-dependent changes in vascular diameters were tested by Brunner test for repeated measurements, provided by the "R" project, which is a nonparametric counterpart of the two-way ANOVA [45]. Differences between initial diameters were tested by using the Mann–Whitney test for independent measurements. The effect of L-NAME on vascular diameters was tested using the Wilcoxon test for dependent measurements (GraphPad Prism 9.3.1). Differences were assumed to be significant if p-values were <0.05.

Author Contributions: A.P., M.X., P.B.P. and P.H.K. designed the project. M.X., P.H.K., F.-B.L. and C.E. acquired and analysed the data. M.X., P.H.K., A.P., P.B.P. and E.L. wrote the manuscript. All authors have read and agreed to the published version of the manuscript.

Funding: This work was supported by grants awarded to A.P. and P.B.P., and a Mercator Fellowship awarded to E.L. by the Deutsche Forschungsgemeinschaft (DFG, German Research Foundation, Projektnummer 394046635, SFB 1365 "Renoprotection").

Institutional Review Board Statement: Animal housing, care and experimental procedures conformed to the European Convention for the protection of vertebrate animals used for experimental and other scientific purposes (Council of Europe No. 123, Strasbourg 1985) and were approved by the State Office of Health and Social Affairs, Berlin, Germany (LAGeSO, approval no. T 0003/06). The ethical committee of the Charité—Universitätsmedizin Berlin approved experiments involving human tissue samples (Approval No. EA4/065/18). Samples were collected between October 2019 and March 2022.

Informed Consent Statement: All patients provided written informed consent.

Data Availability Statement: The data presented in the study are contained within the article.

Acknowledgments: The authors thank Jonas Busch and Bettina Ergün from the *Klinik für Urologie*, Christian Hinze from the Medizinische Klinik m.S. Nephrologie und Internistische Intensivmedizin and Ines Görmar of the Institut für Pathologie, Charité—Universitätsmedizin Berlin, Germany for the organization of human sample collection.

Conflicts of Interest: All authors declare no conflicts of interest.

References

1. Kriz, W. Structural Organization of the Renal Medulla: Comparative and Functional Aspects. *Am. J. Physiol.* **1981**, *241*, R3–RS16. [CrossRef] [PubMed]
2. Pallone, T.L.; Silldorff, E.P.; Turner, M.R. Intrarenal Blood Flow: Microvascular Anatomy and the Regulation of Medullary Perfusion. *Clin. Exp. Pharmacol. Physiol.* **1998**, *25*, 383–392. [CrossRef]
3. Ren, H.; Gu, L.; Andreasen, A.; Thomsen, J.S.; Cao, L.; Christensen, E.I.; Zhai, X.Y. Spatial Organization of the Vascular Bundle and the Interbundle Region: Three-Dimensional Reconstruction at the Inner Stripe of the Outer Medulla in the Mouse Kidney. *Am. J. Physiol. Ren. Physiol.* **2014**, *306*, 321–326. [CrossRef] [PubMed]
4. Heyman, S.N.; Brezis, M.; Reubinoff, C.A.; Greenfeld, Z.; Lechene, G.; Epstein, F.H.; Rosen, S. Acute Renal Failure with Selective Medullary Injury in the Rat. *J. Clin. Investig.* **1988**, *82*, 401–412. [CrossRef] [PubMed]
5. Kennedy-Lydon, T.M.; Crawford, C.; Wildman, S.S.P.; Peppiatt-Wildman, C.M. Renal Pericytes: Regulators of Medullary Blood Flow. *Acta Physiol.* **2013**, *207*, 212–225. [CrossRef] [PubMed]
6. Pallone, T.L.; Edwards, A.; Mattson, D.L. Renal Medullary Circulation. *Compr. Physiol.* **2012**, *2*, 97–140. [CrossRef]
7. Pallone, T.L.; Silldorff, E.P. Pericyte Regulation of Renal Medullary Blood Flow. *Exp. Nephrol.* **2001**, *9*, 165–170. [CrossRef]
8. Crawford, C.; Wildman, S.S.P.; Kelly, M.C.; Kennedy-Lydon, T.M.; Peppiatt-Wildman, C.M. Sympathetic Nerve-Derived ATP Regulates Renal Medullary Vasa Recta Diameter via Pericyte Cells: A Role for Regulating Medullary Blood Flow? *Front. Physiol.* **2013**, *4*, 307. [CrossRef]
9. Crawford, C.; Kennedy-Lydon, T.; Sprott, C.; Desai, T.; Sawbridge, L.; Munday, J.; Unwin, R.J.; Wildman, S.S.P.; Peppiatt-Wildman, C.M. An Intact Kidney Slice Model to Investigate Vasa Recta Properties and Function in Situ. *Nephron Physiol.* **2012**, *120*, 17–31. [CrossRef]
10. Pohlmann, A.; Hentschel, J.; Fechner, M.; Hoff, U.; Bubalo, G.; Arakelyan, K.; Cantow, K.; Seeliger, E.; Flemming, B.; Waiczies, H.; et al. High Temporal Resolution Parametric MRI Monitoring of the Initial Ischemia/Reperfusion Phase in Experimental Acute Kidney Injury. *PLoS ONE* **2013**, *8*, e57411. [CrossRef]
11. Cantow, K.; Arakelyan, K.; Seeliger, E.; Niendorf, T.; Pohlmann, A. Assessment of Renal Hemodynamics and Oxygenation by Simultaneous Magnetic Resonance Imaging (MRI) and Quantitative Invasive Physiological Measurements. In *Kidney Research: Experimental Protocols*; Hewitson, T.D., Smith, E.R., Holt, S.G., Eds.; Springer: New York, NY, USA, 2016; pp. 129–154. ISBN 978-1-4939-3353-2.
12. Moore, J.K.; Chen, J.; Pan, H.; Gaut, J.P.; Jain, S.; Wickline, S.A. Quantification of Vascular Damage in Acute Kidney Injury with Fluorine Magnetic Resonance Imaging and Spectroscopy. *Magn. Reson. Med.* **2018**, *79*, 3144–3153. [CrossRef] [PubMed]
13. Emans, T.W.; Janssen, B.J.; Joles, J.A.; Krediet, C.T.P. Nitric Oxide Synthase Inhibition Induces Renal Medullary Hypoxia in Conscious Rats. *J. Am. Heart Assoc.* **2018**, *7*, e009501. [CrossRef] [PubMed]
14. Baumann, J.E.; Persson, P.B.; Ehmke, H.; Nafz, B.; Kirchheim, H.R. Role of Endothelium-Derived Relaxing Factor in Renal Autoregulation in Conscious Dogs. *Am. J. Physiol.* **1992**, *263*, F208–F213. [CrossRef] [PubMed]
15. Stegbauer, J.; Kuczka, Y.; Vonend, O.; Quack, I.; Sellin, L.; Patzak, A.; Steege, A.; Langnaese, K.; Rump, L.C. Endothelial Nitric Oxide Synthase Is Predominantly Involved in Angiotensin II Modulation of Renal Vascular Resistance and Norepinephrine Release. *Am. J. Physiol. Regul. Integr. Comp. Physiol.* **2008**, *294*, R421–R428. [CrossRef]
16. Patzak, A.; Mrowka, R.; Storch, E.; Hocher, B.; Persson, P.B. Interaction of Angiotensin II and Nitric Oxide in Isolated Perfused Afferent Arterioles of Mice. *J. Am. Soc. Nephrol.* **2001**, *12*, 1122–1127. [CrossRef]
17. Hu, L.; Sealey, J.E.; Chen, R.; Zhou, Y.; Merali, C.; Shi, Y.; Laragh, J.H.; Catanzaro, D.F. Nitric Oxide Synthase Inhibition Accelerates the Pressor Response to Low-Dose Angiotensin II, Exacerbates Target Organ Damage, and Induces Renin Escape. *Am. J. Hypertens.* **2004**, *17*, 395–403. [CrossRef]
18. Navarro-Cid, J.; Maeso, R.; Rodrigo, E.; Muñoz-García, R.; Ruilope, L.M.; Lahera, V.; Cachofeiro, V. Renal and Vascular Consequences of the Chronic Nitric Oxide Synthase Inhibition: Effects of Antihypertensive Drugs. *Am. J. Hypertens.* **1996**, *9*, 1077–1083. [CrossRef]
19. Araujo, M.; Welch, W.J. Oxidative Stress and Nitric Oxide in Kidney Function. *Curr. Opin. Nephrol. Hypertens.* **2006**, *15*, 72–77. [CrossRef]
20. Breitenstein, S.; Roessig, L.; Sandner, P.; Lewis, K.S. Novel SGC Stimulators and SGC Activators for the Treatment of Heart Failure. *Handb. Exp. Pharmacol.* **2017**, *243*, 225–247. [CrossRef]
21. Stasch, J.P.; Schlossmann, J.; Hocher, B. Renal Effects of Soluble Guanylate Cyclase Stimulators and Activators: A Review of the Preclinical Evidence. *Curr. Opin. Pharmacol.* **2015**, *21*, 95–104. [CrossRef]
22. Sandner, P.; Zimmer, D.P.; Milne, G.T.; Follmann, M.; Hobbs, A.; Stasch, J.-P. Soluble Guanylate Cyclase Stimulators and Activators. *Handb. Exp. Pharmacol.* **2021**, *264*, 355–394. [CrossRef] [PubMed]

23. Stehle, D.; Xu, M.Z.; Schomber, T.; Hahn, M.G.; Schweda, F.; Feil, S.; Kraehling, J.R.; Eitner, F.; Patzak, A.; Sandner, P.; et al. Novel Soluble Guanylyl Cyclase Activators Increase Glomerular CGMP, Induce Vasodilation and Improve Blood Flow in the Murine Kidney. *Br. J. Pharmacol.* **2022**, *179*, 2476–2489. [CrossRef] [PubMed]
24. Wennysia, I.C.; Zhao, L.; Schomber, T.; Braun, D.; Golz, S.; Summer, H.; Benardeau, A.; Lai, E.Y.; Lichtenberger, F.B.; Schubert, R.; et al. Role of Soluble Guanylyl Cyclase in Renal Afferent and Efferent Arterioles. *Am. J. Physiol. Ren. Physiol.* **2021**, *320*, F193–F202. [CrossRef] [PubMed]
25. Pallone, T.L. Microdissected Perfused Vessels. In *Renal Disease: Techniques and Protocols*; Goligorsky, M.S., Ed.; Humana Press: Totowa, NJ, USA, 2003; pp. 443–456. ISBN 978-1-59259-392-7.
26. Zhang, Z.; Payne, K.; Pallone, T.L. Adaptive Responses of Rat Descending Vasa Recta to Ischemia. *Am. J. Physiol. Renal Physiol.* **2018**, *314*, F373–F380. [CrossRef]
27. Sendeski, M.; Patzak, A.; Pallone, T.L.; Cao, C.; Persson, A.E.; Persson, P.B. Iodixanol, Constriction of Medullary Descending Vasa Recta, and Risk for Contrast Medium-Induced Nephropathy. *Radiology* **2009**, *251*, 697–704. [CrossRef]
28. Sendeski, M.M.; Liu, Z.Z.; Perlewitz, A.; Busch, J.F.; Ikromov, O.; Weikert, S.; Persson, P.B.; Patzak, A. Functional Characterization of Isolated, Perfused Outermedullary Descending Human Vasa Recta. *Acta Physiol.* **2013**, *208*, 50–56. [CrossRef]
29. Yang, S.; Silldorff, E.P.; Pallone, T.L. Effect of Norepinephrine and Acetylcholine on Outer Medullary Descending Vasa Recta. *Am. J. Physiol.* **1995**, *269*, H710–H716. [CrossRef]
30. McDonald, L.J.; Murad, F. Nitric Oxide and Cyclic GMP Signaling. *Proc. Soc. Exp. Biol. Med.* **1996**, *211*, 1–6. [CrossRef]
31. Dautzenberg, M.; Kahnert, A.; Stasch, J.-P.; Just, A. Role of Soluble Guanylate Cyclase in Renal Hemodynamics and Autoregulation in the Rat. *Am. J. Physiol. Renal Physiol.* **2014**, *307*, F1003–F1012. [CrossRef]
32. Wilck, N.; Markó, L.; Balogh, A.; Kräker, K.; Herse, F.; Bartolomaeus, H.; Szijártó, I.A.; Gollasch, M.; Reichhart, N.; Strauss, O.; et al. Nitric Oxide-Sensitive Guanylyl Cyclase Stimulation Improves Experimental Heart Failure with Preserved Ejection Fraction. *JCI Insight* **2018**, *3*, e96006. [CrossRef]
33. Legrand, M.; Mik, E.G.; Johannes, T.; Payen, D.; Ince, C. Renal Hypoxia and Dysoxia after Reperfusion of the Ischemic Kidney. *Mol. Med.* **2008**, *14*, 502–516. [CrossRef] [PubMed]
34. Freitas, F.; Attwell, D. Pericyte-Mediated Constriction of Renal Capillaries Evokes No-Reflow and Kidney Injury Following Ischaemia. *Elife* **2022**, *11*, e74211. [CrossRef] [PubMed]
35. Cantow, K.; Flemming, B.; Ladwig-wiegard, M.; Persson, P.B. Low Dose Nitrite Improves Reoxygenation Following Renal Ischemia in Rats. *Sci. Rep.* **2017**, *7*, 14597. [CrossRef] [PubMed]
36. Patzak, A.; Lai, E.Y.; Mrowka, R.; Steege, A.; Persson, P.B.; Persson, A.E.G. AT1 Receptors Mediate Angiotensin II-Induced Release of Nitric Oxide in Afferent Arterioles. *Kidney Int.* **2004**, *66*, 1949–1958. [CrossRef] [PubMed]
37. Elias-Miró, M.; Jiménez-Castro, M.B.; Rodés, J.; Peralta, C. Current Knowledge on Oxidative Stress in Hepatic Ischemia/Reperfusion. *Free Radic. Res.* **2013**, *47*, 555–568. [CrossRef] [PubMed]
38. Just, A.; Olson, A.J.M.; Whitten, C.L.; Arendshorst, W.J. Superoxide Mediates Acute Renal Vasoconstriction Produced by Angiotensin II and Catecholamines by a Mechanism Independent of Nitric Oxide. *Am. J. Physiol. Hear. Circ. Physiol.* **2007**, *292*, H83–H92. [CrossRef]
39. Carlström, M.; Lai, E.Y.; Ma, Z.; Patzak, A.; Brown, R.D.; Persson, A.E.G. Role of NOX2 in the Regulation of Afferent Arteriole Responsiveness. *Am. J. Physiol. Regul. Integr. Comp. Physiol.* **2009**, *296*, R72–R79. [CrossRef]
40. Braun, D.; Zollbrecht, C.; Dietze, S.; Schubert, R.; Golz, S.; Summer, H.; Persson, P.B.; Carlström, M.; Ludwig, M.; Patzak, A. Hypoxia/Reoxygenation of Rat Renal Arteries Impairs Vasorelaxation via Modulation of Endothelium-Independent SGC/CGMP/PKG Signaling. *Front. Physiol.* **2018**, *9*, 480. [CrossRef]
41. Krishnan, S.M.; Kraehling, J.R.; Eitner, F.; Sandner, P.; Ignarro, L. The Impact of the Nitric Oxide (NO)/Soluble Guanylyl Cyclase (SGC) Signaling Cascade on Kidney Health and Disease: A Preclinical Perspective. *Int. J. Mol. Sci.* **2018**, *19*, 1712. [CrossRef]
42. Braun, D.; Dietze, S.; Pahlitzsch, T.M.J.; Wennysia, I.C.; Persson, P.B.; Ludwig, M.; Patzak, A. Short-Term Hypoxia and Vasa Recta Function in Kidney Slices. *Clin. Hemorheol. Microcirc.* **2017**, *67*, 475–484. [CrossRef]
43. Zhao, Y.; Brandish, P.E.; Di Valentin, M.; Schelvis, J.P.; Babcock, G.T.; Marletta, M.A. Inhibition of Soluble Guanylate Cyclase by ODQ. *Biochemistry* **2000**, *39*, 10848–10854. [CrossRef] [PubMed]
44. Schneider, C.A.; Rasband, W.S.; Eliceiri, K.W. NIH Image to ImageJ: 25 Years of Image Analysis. *Nat. Methods* **2012**, *9*, 671–675. [CrossRef] [PubMed]
45. *R: A Language and Environment for Statistical Computing*; R Foundation for Statistical Computing: Vienna, Austria, 2014. Available online: http://www.r-project.org/ (accessed on 15 April 2022).

Received: 26 November 2020 | Revised: 7 April 2021 | Accepted: 23 May 2021

DOI: 10.1111/bph.15586

Themed Issue: cGMP Signalling in Cell Growth and Survival

RESEARCH PAPER - THEMED ISSUE

Novel soluble guanylyl cyclase activators increase glomerular cGMP, induce vasodilation and improve blood flow in the murine kidney

Daniel Stehle[1] | Min Ze Xu[2] | Tibor Schomber[3] | Michael G. Hahn[3] | Frank Schweda[4] | Susanne Feil[1] | Jan R. Kraehling[3] | Frank Eitner[3,5] | Andreas Patzak[2] | Peter Sandner[3,6] | Robert Feil[1] | Agnès Bénardeau[3,7]

[1]Interfakultäres Institut für Biochemie (IFIB), University of Tübingen, Tübingen, Germany

[2]Institute of Vegetative Physiology, Charité-Universitätsmedizin Berlin, corporate member of Freie Universität Berlin and Humboldt-Universität zu Berlin, Berlin, Germany

[3]Bayer AG, Cardiovascular Research, Pharma Research Center, Wuppertal, Germany

[4]Institut für Physiologie, Universität Regensburg, Regensburg, Germany

[5]Division of Nephrology and Clinical Immunology, RWTH Aachen University, Aachen, Germany

[6]Institute of Pharmacology, Hannover Medical School, Hannover, Germany

[7]Novo Nordisk A/S, Cardio-Renal Biology, Måløv, Denmark

Correspondence
Peter Sandner, Bayer AG, Cardiovascular Research, Pharma Research Center, 42096 Wuppertal, Germany.
Email: peter.sandner@bayer.com

Present address
Agnès Bénardeau, Novo Nordisk A/S, Cardio-Renal Biology, Måløv, Denmark

Funding information
Deutsche Forschungsgemeinschaft (DFG, German Research Foundation) – FOR 2060 projects, Grant/Award Numbers: FE 438/5-2, FE 438/6-2, 374031971 - TRR 240, 335549539 - GRK 2381

Background and Purpose: Generation of cGMP via NO-sensitive soluble guanylyl cyclase (sGC) has been implicated in the regulation of renal functions. Chronic kidney disease (CKD) is associated with decreased NO bioavailability, increased oxidative stress and oxidation of sGC to its haem-free form, apo-sGC. Apo-sGC cannot be activated by NO, resulting in impaired cGMP signalling that is associated with chronic kidney disease progression. We hypothesised that sGC activators, which activate apo-sGC independently of NO, increase renal cGMP production under conditions of oxidative stress, thereby improving renal blood flow (RBF) and kidney function.

Experimental Approach: Two novel sGC activators, runcaciguat and BAY-543, were tested on murine kidney. We measured cGMP levels in real time in kidney slices of cGMP sensor mice, vasodilation of pre-constricted glomerular arterioles and RBF in isolated perfused kidneys. Experiments were performed at baseline conditions, under L-NAME-induced NO deficiency, and in the presence of oxidative stress induced by ODQ.

Key Results: Mouse glomeruli showed NO-induced cGMP increases. Under baseline conditions, sGC activator did not alter glomerular cGMP concentration or NO-induced cGMP generation. In the presence of ODQ, NO-induced glomerular cGMP signals were markedly reduced, whereas sGC activator induced strong cGMP increases. L-NAME and ODQ pretreated isolated glomerular arterioles were strongly dilated by sGC activator. sGC activator also increased cGMP and RBF in ODQ-perfused kidneys.

Conclusion and Implication: sGC activators increase glomerular cGMP, dilate glomerular arterioles and improve RBF under disease-relevant oxidative stress conditions.

Abbreviations: Ang II, angiotensin II; ANP, atrial natriuretic peptide; CFP, cyan fluorescent protein; DEA/NO, diethylamine NONOate; L-NAME, *N*-nitroarginine methyl ester; ODQ, 1*H*-[1,2,4]oxadiazolo[4,3-a]quinoxalin-1-one; R (cGMP), relative CFP/YFP ratio change of cGMP sensor; RBF, renal blood flow; sGC, soluble guanylyl cyclase; SGLT2i, sodium-glucose-cotransporter 2 inhibitors; SNAP, *S*-nitroso-*N*-acetylpenicillamine; YFP, yellow fluorescent protein; ZSF1, Zucker diabetic fatty/spontaneously hypertensive heart failure F1 hybrid rat.

Therefore, sGC activators represent a promising class of drugs for chronic kidney disease treatment.

LINKED ARTICLES: This article is part of a themed issue on cGMP Signalling in Cell Growth and Survival. To view the other articles in this section visit http://onlinelibrary.wiley.com/doi/10.1111/bph.v179.11/issuetoc

KEYWORDS
cGMP imaging, glomerular arterioles, GC, NO, renal blood flow, sGC activators, vasodilation

1 | INTRODUCTION

Chronic hypertension leads to end-organ damage, which especially affects blood vessels and kidneys. End-organ damage goes along with gradual increase in proteinuria, impaired kidney function including reduced glomerular filtration rate (GFR) and the development of chronic kidney disease (CKD) (Griffin, 2017). Persisting chronic kidney disease often results in end-stage renal disease and ultimately the need for a kidney transplant (Brenner et al., 2001; Coresh, 2017). Currently, the first-line management of chronic kidney disease consists of inhibiting the **renin-angiotensin-aldosterone** system, which is known to play a pivotal role in chronic kidney disease development (Siragy & Carey, 2010). Although therapies inducing reduction of systemic blood pressure (BP) have shown beneficial effects on kidney function in patients with renal disease, these effects are not fully maintained in chronic therapy (Breyer & Susztak, 2016) or in patients with type-2-diabetes and advanced end-stage renal disease (Schievink et al., 2016). Recently, **sodium-glucose-cotransporter 2 (SGLT2)** inhibitors which are approved for the treatment of type-2-diabetes, have been demonstrated to prevent GFR decline in chronic kidney disease patients (Lin et al., 2019; Muskiet et al., 2017). However, despite reduction of cardiovascular risk by SGLT2 inhibitors in chronic kidney disease patients (Briasoulis et al., 2018; Vallon & Thomson, 2017), an initial GFR decrease under SGLT2 inhibitors was reported (Sugiyama et al., 2020). Thus, there is still a need for new chronic kidney disease therapies with a different molecular mode of action, which can overcome limitations of currently used drugs.

The **cGMP** signalling system is a central regulator of cardiovascular homeostasis and has great potential as a target for new effective pharmacological therapies. Recent studies illustrated that genetic variants in components of this pathway significantly influence BP and the risk of cardiovascular and renal disease (Emdin et al., 2018; Erdmann et al., 2013; International Consortium for Blood Pressure, Ehret et al., 2011; Maass et al., 2015). The soluble guanylyl cyclase (**sGC**) generates cGMP upon activation by **NO**. An impairment of the NO/sGC/cGMP pathway and a decline in cGMP contributes to the development vascular dysfunction. Enhanced NO signalling also was associated with a higher GFR as determined via cystatin C and creatinine (Krishnan et al., 2018; Ott et al., 2012). Genetic variants of sGC and **cGMP-dependent protein kinase type I**, a downstream effector of sGC, are causally associated with altered vascular structure and remodelling, and sGC gain of function is associated with a higher GFR and lower risk for chronic kidney disease (Emdin et al., 2018). Therefore, sGC-enhancing drugs might be beneficial for treating chronic kidney disease patients.

Recent studies indicated that oxidative stress, which is triggered by comorbidities in chronic kidney disease, like hypertension, diabetes or obesity, could be one of the drivers of kidney function decline in chronic kidney disease (Coppolino et al., 2018; Samarghandian et al., 2017; Sinha & Dabla, 2015; Su et al., 2019). Oxidative stress is leading to sGC oxidation and ultimately the loss of its **haem** group, resulting in the formation of haem-free apo-sGC. Apo-sGC can no longer bind and be stimulated by the endogenous ligand NO (Stasch et al., 2015). Thus, oxidative stress disrupts NO/sGC/cGMP signalling and, thereby, counteracts physiological regulation of kidney function by NO. sGC activators are small molecules that activate sGC in a haem- and NO-independent manner and, thus, have the potential to restore sGC/cGMP signalling under conditions of oxidative stress. Runcaciguat is a novel potent and selective sGC activator, which activates apo-sGC *in vitro*, *ex vivo* and *in vivo* (Hahn, 2018) and has great potential to prevent the decline of kidney function (Benardeau et al., 2020; Hahn et al., 2021). However, the potential kidney-specific mechanisms behind the renoprotective effects of runcaciguat are not well characterised. Therefore, we aimed to investigate where and under what conditions runcaciguat and its close analogue BAY-543 (Rühle et al., 2020) induce cGMP production in the kidney and how these sGC activators influence the diameter of isolated glomerular arterioles as well as renal blood flow (RBF) in isolated perfused whole kidney preparations.

Our data show that sGC activators increase the glomerular cGMP concentration under oxidative stress conditions. Moreover, sGC activators induce dilation of pre-constricted glomerular afferent and efferent arterioles in the absence of NO and presence of oxidative stress and they significantly improve RBF under oxidative stress conditions. These findings show that sGC activators have direct effects on the renal vasculature and counteract the oxidative stress-induced decline in RBF. Thus, sGC activators could represent a new therapeutic approach for the treatment of chronic kidney disease patients.

2 | METHODS

2.1 | Materials

The sGC activator runcaciguat (BAY 1101042) (Hahn, 2018; Hahn et al., 2021) and its analogue BAY-543 (Rühle et al., 2020) were synthesised by Bayer AG (Wuppertal, Germany) and dissolved in DMSO (Sigma-Aldrich, Darmstadt, Germany). Structurally, runcaciguat and BAY-543 are closely related, differing only in one side group (Figure S1). In the previous studies cited above, their EC_{50} to activate purified sGC (11 nM for both compounds) and their ability to dilate pre-contracted rabbit arteries *ex vivo* (IC_{50} of 199 and 75 nM for runcaciguat and BAY-543, respectively) were found to be very similar.

The sGC oxidant **1H-[1,2,4]oxadiazolo[4,3-a]quinoxaline-1-one (ODQ)** was from Axxora (Ann Arbor, MI, USA; real-time cGMP imaging) or Sigma-Aldrich (all other experiments). **Atrial natriuretic peptide (ANP)** was from Tocris (Minneapolis, MN, USA), **angiotensin II (Ang II)** and **N-nitroarginine methyl ester (L-NAME)** from Sigma-Aldrich, and the L- and N-type calcium channel blocker **cilnidipine** from Cayman Chemical (Ann Arbor, MI, USA). The NO donor diethylamine NONOate (DEA/NO) was from Axxora. (DEA/NO) was stored in 100 mM stock solutions in NaOH (10 mM) and diluted in perfusion buffer immediately before application. Due to its short half-life time (≈16 min at room temperature and pH 7.4), DEA/NO is well-suited to induce fast, transient cGMP increases during real-time cGMP imaging experiments. For analysis of isolated glomerular arterioles and perfused kidneys, the NO-releasing compound *S*-nitroso-*N*-acetylpenicillamine (SNAP; Cayman Chemical) was preferred as it has slower kinetics of NO release (several hours, varies between tissues) as compared with DEA/NO which ensures sustained continuous NO release at 37°C in these experiments.

2.2 | Animals

In the present study, we used mice, because they are amenable to genetic modifications and murine kidneys represent a good model to analyse renal function in mammals. All animal procedures were performed in accordance with the Directive 2010/63/EU, the German Tierschutz-Versuchstierverordnung and the local authorities in Tübingen, Berlin and Regensburg. Animal studies are reported in compliance with the ARRIVE guidelines (Percie du Sert et al., 2020) and with the recommendations made by the *British Journal of Pharmacology* (Lilley et al., 2020). Mice were housed in groups of up to eight animals in open type III cages at 22°C and 50%–60% humidity in a 12 h light/12 h dark cycle with access to standard rodent chow (ssniff; Soest, Germany) and tap water *ad libitum*.

For real-time cGMP imaging, 8- to 18-week-old R26-CAG-cGi500(L1) mice (Thunemann et al., 2013) of either sex on a C57BL/6N genetic background were used. Genotyping of these animals was performed by PCR analysis of ear biopsy DNA using the following primers: P1 (CTCTGCTGCCTCCTGGCTTCT), P2 (CGAGGCGGATCACAAGCAATA) and P3 (TCAATGGGCGGGGG TCGTT). These primers amplify a 330 base pair fragment of the wildtype allele (P1 and P2) and a 250 base pair fragment of the transgene (P1 and P3). These mice were killed with CO_2 followed by cervical dislocation.

Other experiments were performed with C57BL/6N mice (RRID: IMSR_CRL:027; Charles River, Wilmington, MA, USA) at an age of 12–16 weeks. Only male mice were used for these studies to exclude sex-specific variation of arteriole diameters and RBF. If not stated otherwise, experimental animals were killed by cervical dislocation.

2.3 | Preparation of kidney slices

For the preparation of acute tissue slices, kidneys were dissected from R26-CAG-cGi500(L1) mice, and the renal capsule was carefully removed in ice-cold carbogen-gassed Ringer buffer (127.0 mM NaCl, 2.5 mM KCl, 0.5 mM $MgCl_2$, 1.1 mM $CaCl_2$, 1.1 mM NaH_2PO_4, 26.0 mM $NaHCO_3$, 20.0 mM D-glucose). The pH was adjusted by continuous gassing with carbogen. Kidneys were sectioned with a vibratome (VT1200, Leica, Buffalo Grove, IL, USA) to a thickness of 700 µm. Whole kidneys and slices were incubated in ice-cold carbogen-gassed Ringer buffer for up to 8 h until real-time cGMP imaging was performed as described below.

2.4 | Real-time cGMP imaging

Förster resonance energy transfer (FRET)/cGMP imaging was performed as described previously (Thunemann et al., 2013). The set-up consisted of an upright Examiner.Z1 microscope (Zeiss, Oberkochen, Germany), a Yokogawa CSU-X1 spinning disc confocal scanner (Yokogawa Denki, Musashino, Japan), three diode lasers (445, 488 and 561 nm), three water immersion objectives (W N-ACHROMAT 10/0.3, W Plan-APOCHROMAT 20/1.0 DIC [UV] VIS-IR, W Plan-APOCHROMAT 40/1.0 DIC VIS-IR; all from Zeiss) and one air objective (EC Plan-NEOFLUAR 2.5/0.085; Zeiss). Yellow fluorescent protein (YFP) fluorescence of the cGMP sensor cGi500 was detected with a CCD camera (Spot Pursuit, Diagnostic Instruments, Sterling Heights, MI, USA) through a 525/50 nm emission filter after excitation with the 488 nm laser. For FRET-based imaging, the donor fluorophore, cyan fluorescent protein (CFP), was excited with the 445 nm laser, and a Dual-View beam splitter (Photometrics, Tucson, AZ, USA) with 505 nm dichroic mirror, 470/24 nm and 535/30 nm emission filters was used for simultaneous acquisition of CFP and YFP emission. Signals were recorded with an electron-multiplying charged-coupled device (EM-CCD) camera (QuantEM 512SC, Photometrics) at a frame rate of 0.2 Hz and an exposure time of 0.2 s. The system was controlled by VisiView 4.0.0.12 (Visitron Systems, Puchheim, Germany). Kidney slices were continuously superfused with carbogen-gassed Ringer buffer with or without drugs at a flow rate of 1 ml/min at room temperature. The custom-built superfusion system consisted of an fast protein liquid chromatography pump (Pharmacia P-500, GE

Healthcare, Chicago, IL, USA), fast protein liquid chromatography injection valves (Pharmacia V-7, GE Healthcare), a magnetic platform (Warner Instruments, Hamden, CT, USA), a superfusion chamber (RC-26, Warner Instruments), a mesh-assisted Slice Hold-Down (SHD-26H/10, Warner Instruments) and sample loops of different sizes (7 ml for ODQ; 2 ml for other drugs). To ensure that drug exposure was comparable between different tissue slices, the same drug volumes were applied for the same time span. A vacuum pump with adjustable vacuum (Laboport N86, KNF Neuberger, Hamburg, Germany) was connected to the system to constantly remove excess buffer.

2.5 | Image acquisition and post-processing

Online image acquisition was performed with VisiView 4.0.0.12 (Visitron Systems, Puchheim, Germany), and offline post-processing and analysis were performed with Fiji software (RRID:SCR_002285) (Rueden et al., 2017; Schindelin et al., 2012). Images were aligned in *x*/*y* dimension with the Fiji plugin MultiStackReg v1.45 (RRID: SCR_016098). For further evaluation, Excel (RRID:SCR_016137; Office 16; Microsoft, Redmond, WA, USA) and Origin 2019 (RRID: SCR_014212; OriginLab, Northampton, MA, USA) were used. CFP and YFP emission were used to calculate the CFP/YFP ratio. The relative CFP/YFP ratio change (black traces in the respective graphs; referred to as R (cGMP)), which correlates with the cGMP concentration change, was obtained by normalisation to the baseline recorded for ~3 min at the beginning of each experiment. This normalisation is necessary to account for variations in the basal fluorescence intensity between the preparations. For peak evaluation, R (cGMP) traces were smoothed according to the Savitzky–Golay filtering method (smoothing window = 30 points) and the Peak Analyzer tool of Origin was used to calculate the AUC for each signal.

2.6 | Dissection and perfusion of glomerular arterioles

Kidneys were removed and sliced along the corticomedullary axis. Afferent and efferent arterioles were prepared according to procedures detailed by Liu and colleagues (Liu et al., 2012). In short, afferent and efferent arterioles with attached glomeruli were isolated and transferred into a chamber assembled on the stage of an inverted microscope. Arterioles were perfused using a system of pipettes, which allowed to hold and perfuse the vessels. Both, afferent and efferent arterioles were perfused from the free end, so orthograde in case of afferent arterioles and retrograde in case of efferent arterioles. Perfusion pressure was 100 mmHg for afferent arterioles and 40 mmHg for efferent arterioles, and the perfusion rates were in physiological ranges. DMEM (DMEM/F-12, Gibco, Darmstadt, Germany) containing 0.1% BSA (Carl Roth, Karlsruhe, Germany) was used during vessel dissection. The same solution was present in the experimental chamber, whereas the DMEM perfusion solution which was applied to the arteriolar lumen contained 1.0% BSA.

2.7 | Protocols for perfusion of glomerular arterioles

Arterioles were allowed to acclimatise for 10 min after establishing the perfusion. Viability was tested by short-term application of KCl (100 mM). Only vessels which showed full and sustained constriction were used for subsequent experiments. Arterioles were treated for 15 min with the non-specific NOS inhibitor **L-NAME** to induce NO deficiency, or for 10 min with the sGC-oxidising substance ODQ and vehicle (DMSO), respectively. Ang II, which belongs to the strongest vasoconstrictors particularly in the renal vasculature (Patzak et al., 2001), was applied to pre-constrict the vessels. Here, Ang II was applied in ascending concentrations (2 min for each concentration). After application of the highest Ang II concentration, cumulative concentrations of runcaciguat or of the known vasodilators NO (in the form of SNAP; sGC-dependent) and cilnidipine (sGC-independent) were administered to the Ang II-constricted arteries for 2 min each. In the 'L-NAME + vehicle' group, DMSO was applied instead of runcaciguat in corresponding concentrations. To analyse the time course of runcaciguat-induced vasodilation, arterioles pretreated with L-NAME and pre-constricted with Ang II were subjected to a prolonged 10 min treatment with runcaciguat or vehicle.

2.8 | Measurement of arteriole diameters

Perfused arterioles were continuously displayed on the computer screen using a video camera and the respective software (Moticam 2.0, Motic Asia, Kowloon, Hong Kong). Luminal diameters served for the estimation of arteriolar tone and reactivity. For the assessment of concentration–response relationships, pictures were recorded at a frame rate of 1 Hz. Then, the vessel diameter in five pictures was averaged in steady state conditions for each concentration effect to limit the influence of movement artefacts. For long-term investigations of runcaciguat action (10 min), pictures were recorded at a frame rate of 0.1 Hz. Either way, the arteriolar diameters were measured using ImageJ2 (RRID:SCR_003070) (Rueden et al., 2017). For analysis of the Ang II concentration–response relationship, arteriolar diameters were normalised to the initial diameter after L-NAME/ODQ/vehicle and before Ang II application. For evaluation of the dilation of pre-constricted arterioles induced by runcaciguat, SNAP and cilnidipine, diameter changes were normalised to the total constriction induced by L-NAME/ODQ/vehicle + Ang II. Both normalisation procedures are typically applied in vessel physiology to limit the influence of intra- and inter-individual variations of arteriole diameters and thereby focus the evaluation on pharmacological effects. The part of the vessel with the strongest response was chosen for analysis.

2.9 | Preparation and analysis of isolated perfused whole kidneys

Mice were anaesthetised with an intraperitoneal injection of xylazine hydrochloride (10 $mg \cdot kg^{-1}$, Serumwerk Bernburg, Bernburg, Germany) and ketamine HCl (100 $mg \cdot kg^{-1}$; betapharm Arzneimittel, Augsburg, Germany) and placed on a warmed table. Isolation and perfusion of mouse kidneys followed a published method (Schweda et al., 2003). In short, the abdominal cavity was opened by a midline incision, and the aorta was clamped distal to the right renal artery. The mesenteric artery was ligated and a metal perfusion cannula (0.8 mm outer diameter) was inserted into the abdominal aorta. Then, the aorta was ligated proximal to the right renal artery and perfusion was started *in situ* with an initial flow rate of 1 $ml \cdot min^{-1}$. The right kidney was excised, placed in a tempered humid chamber and perfused at constant pressure (100 mmHg). Finally, the renal vein was cannulated (1.5 mm outer diameter polypropylene catheter). The venous effluent was drained outside the humid chamber and collected for determination of venous blood flow. The basic perfusion medium supplied from a 37°C-tempered 200 ml-reservoir consisted of a modified Krebs–Henseleit solution containing amino acids (10 $ml \cdot L^{-1}$ Aminoplasmal B. Braun 10%), 8.7 mM D-glucose, 0.3 mM pyruvate, 2.0 mM L-lactate, 1.0 mM ketoglutarate, 1.0 mM L-malate and 6.0 mM urea. The perfusate was supplemented with 60 $g \cdot L^{-1}$ BSA, 10 $mU \cdot L^{-1}$ vasopressin 8-lysine and freshly washed human red blood cells (10% haematocrit). Ampicillin (30 $mg \cdot L^{-1}$) and flucloxacillin (30 $mg \cdot L^{-1}$) were added to inhibit possible bacterial growth in the medium. To improve the functional preservation of the preparation, the perfusate was continuously dialysed against a 10-fold volume of the same composition, but lacking erythrocytes and BSA. For oxygenation of the perfusion medium, the dialysate was gassed with 94% O_2/6% CO_2.

2.10 | Determination of renal blood flow and cGMP secretion

Perfusate flow from kidneys isolated as described above was calculated by collection and gravimetric determination of the venous effluent. After establishing a constant perfusion pressure (100 mmHg), perfusate flow rates stabilised within 12–15 min. Stock solutions of the indicated drugs were added to the perfusate. For evaluation, the amount of venous effluent was normalised to the perfusate flow under control conditions or after application of 30 μM ODQ as indicated in the respective graphs to exclude differences in baseline perfusion between the preparations. For determination of renal cGMP production, venous effluent was collected over a period of 1 min during four intervals along the study and its cGMP concentration was determined after acetylation of samples using a cGMP enzyme immunoassay Kit (Cat# 581021, Cayman Chemical, Hamburg, Germany). The cGMP secretion was calculated by multiplying cGMP concentration and perfusate flow.

2.11 | Data and statistical analysis

The data and statistical analysis comply with the recommendations of the *British Journal of Pharmacology* on experimental design and analysis in pharmacology (Curtis et al., 2018). Variances in group sizes within individual comparisons are due to exclusion of defective preparations and yields, which were lower than expected. Data are presented as mean ± SD or mean ± SEM as specified in the figure legends. P values <0.05 were considered significant. Randomisation and blinding were not applicable because the experimental setups demanded application of substances in distinct succession. Instead, analysis and evaluation were performed uniformly and were based exclusively on objective parameters.

Statistical analysis was performed with Origin 2019 (OriginLab, Northampton, MA, USA; FRET/cGMP imaging) or GraphPad PRISM 8 (RRID:SCR_002798; GraphPad Software, San Diego, CA, USA; analysis of isolated perfused kidneys). For not normally distributed data sets, statistical differences were analysed non-parametrically by Mann–Whitney U-test. In case of normally distributed data, statistical differences were analysed parametrically by Student's t-test (equal variances) or Welch's t-test (unequal variances). The DEA/NO concentration–response curve was calculated with the sigmoidal 'DoseResp' fitting function of origin.

Time- and concentration-dependent differences of diameter changes of arterioles were statistically assessed with the free software R (RRID:SCR_001905; version 3.6.3) (R Core Team, 2020) using the Brunner test (Brunner & Langer, 1999). Sample sizes subjected to statistical analysis were at least five animals per group ($n = 5$), with n = number of independent values. This test is a non-parametric counterpart of the two-factorial ANOVA and tests the main hypothesis of a global difference between two groups. It is appropriate for the comparison of serial repeated measurements without normal distribution.

2.12 | Nomenclature of targets and ligands

Key protein targets and ligands in this article are hyperlinked to corresponding entries in the IUPHAR/BPS Guide to PHARMACOLOGY http://www.guidetopharmacology.org and are permanently archived in the Concise Guide to PHARMACOLOGY 2019/20 (Alexander et al., 2019).

3 | RESULTS

3.1 | Renal glomeruli express a functional NO/cGMP signalling pathway

To measure the spatiotemporal cGMP dynamics in the kidney, we used transgenic cGMP sensor mice expressing the FRET-based cGMP indicator cGi500 (Russwurm et al., 2007; Thunemann et al., 2013).

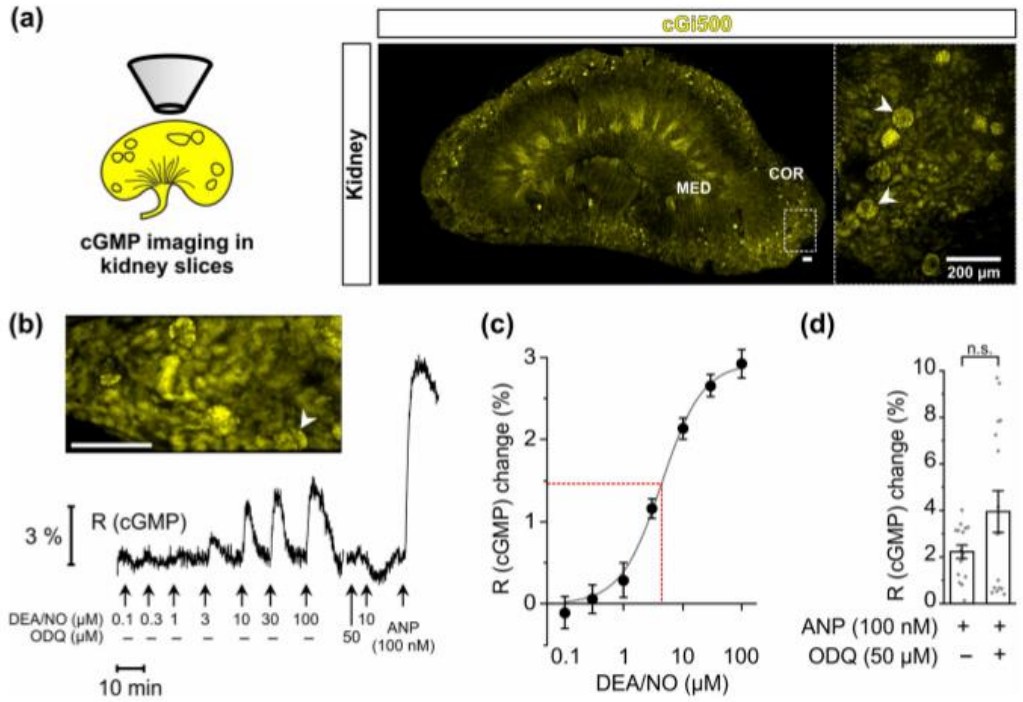

FIGURE 1 NO-induced cGMP generation in real time in glomeruli of kidney slices. FRET-based cGMP imaging was performed with acute kidney slices from R26-CAG-cGi500(L1) mice. (a) Schematic representation and representative images of kidney slices. Yellow colour represents yellow fluorescent protein (YFP) fluorescence of the cGMP sensor cGi500 in renal cells. White arrowheads point towards some glomeruli. Dashed rectangle indicates the magnified region shown to the right. (b) Representative real-time FRET/cGMP measurement of a kidney slice. During recording, increasing concentrations of diethylamine NONOate (DEA/NO) or 100 nM atrial natriuretic peptide (ANP) were applied to the slice for 2 min each. Before the second last stimulation with 10 µM DEA/NO, slices were pre-incubated for 5 min with ODQ (50 µM). Black trace represents the cyan fluorescent protein (CFP)/YFP ratio R, which indicates cGMP concentration changes. The white arrowhead points towards the glomerulus measured in this experiment. (c) Concentration-response curve (solid grey line) based on the relative R (cGMP) changes induced by increasing concentrations of DEA/NO ($n = 19$). The dashed red line indicates EC_{50}. (d) Statistical analysis was performed with the relative R (cGMP) changes induced by ANP (100 nM) in the presence and absence of ODQ ($n = 16$). Data represent mean ± SEM. COR, renal cortex; MED, renal medulla. Scale bars, 200 µm

Specifically, we used the R26-CAG-cGi500(L1) mouse line that expresses the cGMP sensor globally in all tissues. By FRET imaging of live kidney slices *ex vivo*, cGMP signals were recorded in real time in response to the endogenous sGC ligand NO and in response to the sGC activator BAY-543 alone and in combination with NO. The sGC-oxidising agent ODQ was used to mimic chronic kidney disease-related oxidative stress conditions. Slices were kept in carbogen-gassed Ringer buffer during preparation and measurements to keep the tissue vital.

Visual inspection of the sensor-derived fluorescence confirmed that the cGMP sensor was broadly expressed in the kidney of cGMP sensor mice (Figure 1a). Note that the yellow fluorescence seen in the photomicrographs indicates expression of the sensor protein but not the cGMP concentration. The latter is determined by ratiometric analysis of the sensor's CFP and YFP fluorescence as described in Section 2.5. Individual glomeruli were selected as regions of interest and several glomeruli were averaged to quantify the cGMP concentration in the absence and presence of various drugs.

First, we tested the capacity of renal glomeruli to generate cGMP in response to the NO-releasing compound DEA/NO. DEA/NO concentration-dependently increased the cGMP concentration in the glomeruli of cGMP sensor mice with an EC_{50} of 4.4 ± 0.1 µM (Figure 1b,c). Application of ODQ (50 µM) slightly reduced the basal cGMP production and, as expected, abolished NO-induced cGMP generation (Figure 1b). As a control, atrial natriuretic peptide (ANP), which increases cGMP via simulation of the particulate guanylyl cyclase A, was applied to the kidney slices at the end of each experiment. ANP (100 nM) potently increased glomerular cGMP levels independent of ODQ application (Figure 1b,d), indicating that sGC-independent cGMP generation was not affected by ODQ and that the tissue was still vital at the end of each experiment. Together, these data demonstrated the presence of a functional and oxidation-

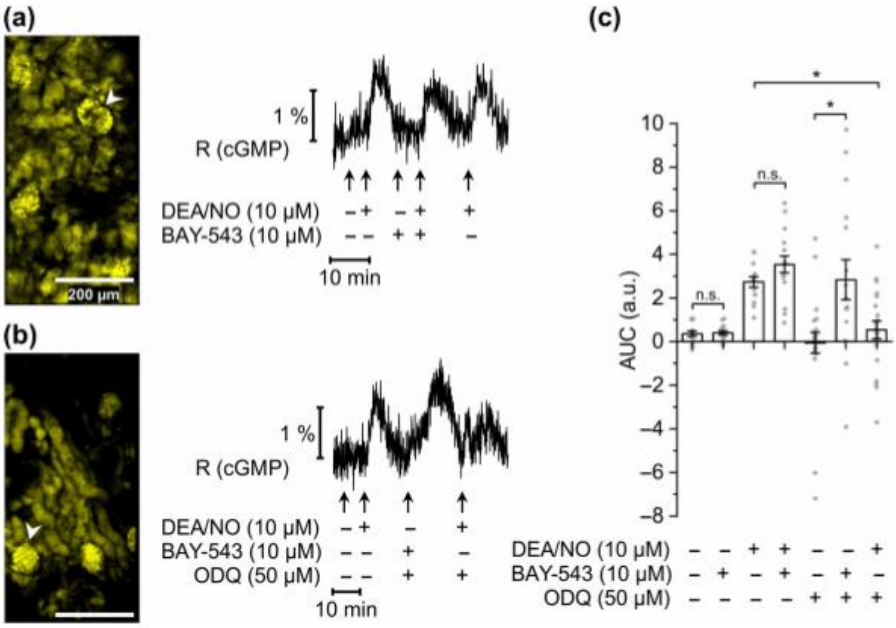

FIGURE 2 sGC activator-induced cGMP generation in glomeruli of ODQ-treated kidney slices. FRET-based cGMP imaging was performed in glomeruli of kidney slices from R26-CAG-cGi500(L1) mice. (a) Representative measurement of a glomerulus without ODQ application. During the recording, diethylamine NONOate (DEA/NO; 10 µM), BAY-543 (10 µM), or a combination of both substances was applied to the slices for 2 min. Black trace represents the cyan fluorescent protein/yellow fluorescent protein (CFP/YFP) ratio R, which indicates cGMP concentration changes. White arrowhead points towards the glomerulus represented in the measurement shown to the right. (b) Representative measurement of a glomerulus with ODQ application. DEA/NO (10 µM), BAY-543 (10 µM), or a combination of both substances was applied with or without 5 min pretreatment with ODQ (50 µM). (c) Statistical analysis was performed with the AUC of the signals. Note that negative AUC values in the presence of ODQ might be due to reduced endogenous cGMP generation compared with baseline conditions. Data represent mean ± SEM (n = 14, 16, 14, 16, 24, 16 and 21 from left to right). Scale bars, 200 µm. *$P < .05$; n.s., not significant

sensitive NO/sGC/cGMP signalling pathway in the glomeruli of murine kidneys. In subsequent FRET imaging experiments, 10 µM DEA/NO was used as a concentration that induces non-saturated cGMP responses.

3.2 | The sGC activator BAY-543 increases glomerular cGMP under oxidative stress

Next, we analysed modulation of glomerular sGC/cGMP signalling by the sGC activator BAY-543, a close analogue of runcaciguat. As expected from our previous results (Figure 1b,c), under baseline conditions (i.e. in the absence of ODQ), application of DEA/NO alone reproducibly induced an increase of cGMP in glomeruli (Figure 2a,c). In the absence of ODQ, application of BAY-543 did not alter the cGMP concentration and did not affect NO-induced cGMP signals. Interestingly, in the presence of ODQ, BAY-543 (10 µM) increased the cGMP concentration to a similar extent as 10 µM DEA/NO (Figure 2b, c). Under the same oxidative stress conditions, that is, in the presence of ODQ, NO no longer increase cGMP (Figure 2b,c), consistent with the findings reported in Figure 1b. Altogether, our data shown in Figures 1 and 2 indicated that the sGC activator BAY-543 stimulates cGMP production in mouse glomeruli under oxidative stress conditions, which have impaired NO-induced cGMP signalling.

3.3 | Runcaciguat induces dilation of renal arterioles

To further explore the physiological effects of cGMP production induced by sGC activators on kidney function, we assessed their effect on the diameters of glomerular vessels in *ex vivo* experiments. Afferent and efferent glomerular arterioles were isolated from mouse kidneys, mounted on pipettes and perfused. The diameter of afferent and efferent arterioles were measured under resting conditions and in the presence of vasoactive agents. For both afferent and efferent arterioles, three groups of vessels were randomly assigned as 'L-NAME + runcaciguat', 'ODQ + runcaciguat' and 'L-NAME + vehicle', which correspond to the groups used for pretreatment with L-NAME or ODQ and subsequent application of runcaciguat or

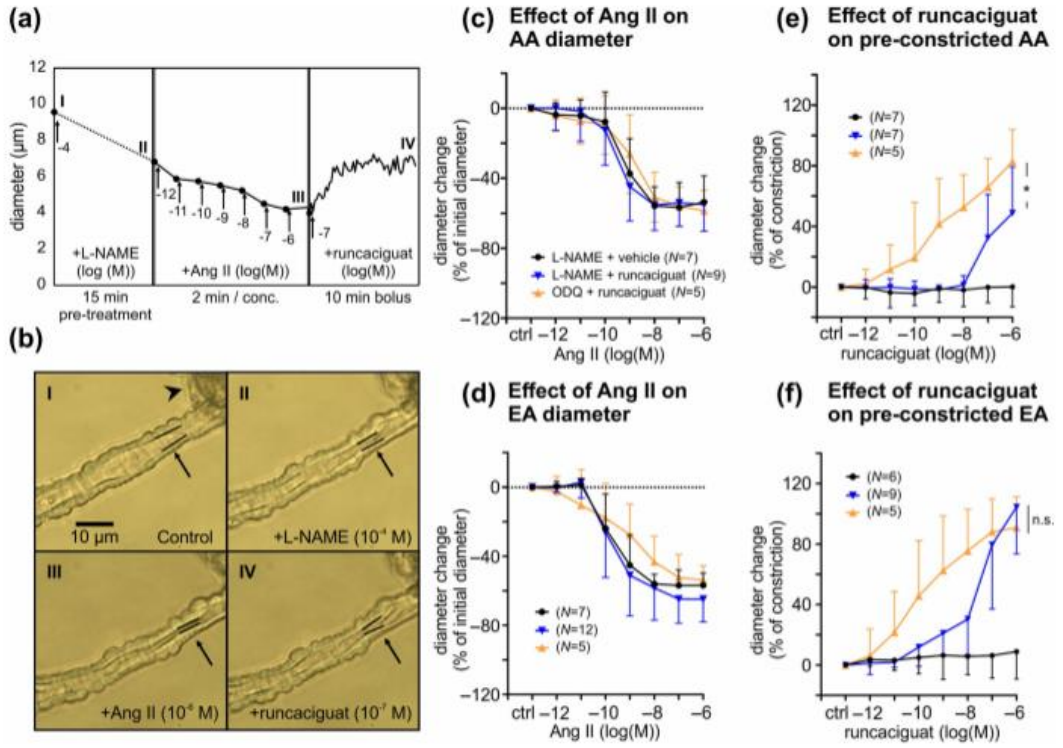

FIGURE 3 Runcaciguat-induced dilation of angiotensin II (Ang II) pre-constricted glomerular arterioles pretreated with L-NAME or ODQ. Diameter changes of afferent (AA) and efferent arterioles (EA) upon application of various substances were monitored. (a) Representative sequence of an afferent arteriole diameter measurement: Endogenous NO generation was inhibited with L-NAME (10^{-4} M) and then the afferent arteriole was pre-constricted with incremental concentrations of Ang II (10^{-12} to 10^{-6} M). The diameter change of the pre-constricted afferent arteriole in response to runcaciguat (10^{-7} M, bolus application) was followed. (b) Images illustrate the monitored vessel during each step of the sequence as indicated by roman numbers. Black arrows point towards the segment subjected to quantitative evaluation. The inner vessel wall in this segment is highlighted with black lines. Black arrowhead points towards the attached glomerulus. (c, d) Resting afferent and efferent arterioles were pretreated with L-NAME ('L-NAME + vehicle' and 'L-NAME + runcaciguat' groups) or ODQ (10^{-5} M; 'ODQ + runcaciguat' group) and then pre-constricted with incremental concentrations of Ang II in presence of L-NAME or ODQ. Values are given as percent change of the initial diameter after L-NAME or ODQ pretreatment and before Ang II application. (e, f) Pre-constricted afferent and efferent arterioles were treated with cumulative concentrations of runcaciguat or vehicle (DMSO). Values are given as percent of the maximal constriction induced by Ang II. Data represent mean ± SD. In panels (c)–(f), *n* values are indicated in parentheses. The colour code given in panels (d)–(f) corresponds to the experimental groups indicated in panel (c). scale bar, 10 µm. *$P < 0.05$

vehicle. The perfusion conditions were strictly identical in these three groups. In one set of experiments, vessels were pretreated with the NOS inhibitor L-NAME (10^{-4} M, 15 min) to induce NO deficiency. Then, increasing concentrations of Ang II were added on top of L-NAME to pre-constrict the vessels, followed by vehicle or runcaciguat ('L-NAME + vehicle' or 'L-NAME + runcaciguat' group; for an example of the experimental protocol, see Figure 3a,b). Another set of experiments was performed in a similar manner, but vessels were pre-incubated with ODQ (10^{-5} M, 10 min) to mimic oxidative stress and oxidise the haem group of sGC ('ODQ + runcaciguat' group). Ang II concentration-dependently decreased the vessel diameter by approximately 60% of the initial diameter at concentrations between 10^{-8} M and 10^{-6} M in both afferent (Figure 3c) and efferent arterioles (Figure 3d). The absolute afferent and efferent arteriole diameters under resting conditions as well as before and after Ang II application were similar throughout the three different groups (Table 1). In addition, superimposition of the Ang II concentration–response curves produced from afferent (Figure 3c) and efferent arterioles (Figure 3d) before application of vehicle or runcaciguat showed similar sensitivity of the vessel preparations to Ang II. Together, these results indicated a good reproducibility of the measurements and similar initial conditions for the subsequent application of vehicle or runcaciguat.

Addition of increasing concentrations of runcaciguat (10^{-12} M to 10^{-6} M) to the pre-constricted afferent (Figure 3e) or efferent arterioles (Figure 3f) for 2 min induced strong vasodilation. ODQ pretreated

TABLE 1 Diameters of glomerular arterioles at different time points during the experiment

	Afferent arteriole diameter (μm)			Efferent arteriole diameter (μm)		
	I	II	III	I	II	III
L-NAME + vehicle	7.7 ± 2.8 ($n = 7$)	7.3 ± 3.0 ($n = 7$)	3.3 ± 1.7 ($n = 7$)	7.7 ± 1.4 ($n = 7$)	6.7 ± 1.6 ($n = 7$)	3.4 ± 1.7 ($n = 7$)
L-NAME + runcaciguat	9.1 ± 1.6 ($n = 9$)	8.6 ± 2.1 ($n = 9$)	3.2 ± 1.0 ($n = 9$)	7.5 ± 1.2 ($n = 12$)	7.0 ± 1.5 ($n = 12$)	2.6 ± 2.0 ($n = 12$)
ODQ + runcaciguat	7.9 ± 1.4 ($n = 5$)	6.7 ± 0.7 ($n = 5$)	2.8 ± 0.8 ($n = 5$)	6.6 ± 1.1 ($n = 5$)	6.2 ± 2.5 ($n = 5$)	2.9 ± 1.1 ($n = 5$)

Note: Afferent and efferent arterioles were pretreated with L-NAME (10^{-4} M; 'L-NAME + vehicle' and 'L-NAME + runcaciguat' groups) or ODQ (10^{-5} M; 'ODQ + runcaciguat' group) and pre-constricted with incremental concentrations of Ang II (10^{-12}–10^{-6} M). Shown are absolute diameters of afferent and efferent arterioles under resting conditions (I), after application of L-NAME or ODQ (II) and after addition of the highest Ang II concentration (III). An example for the procedure is shown in Figure 3a. Data represent mean ± SD. *n* values are indicated in parentheses.

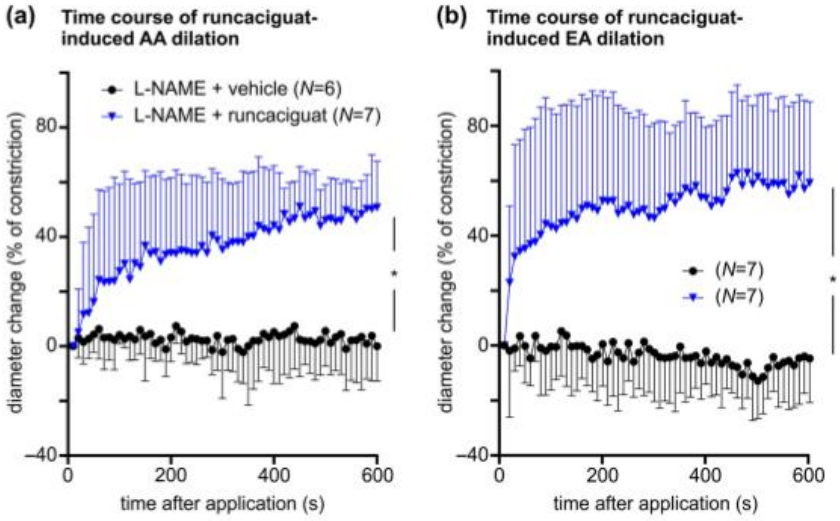

FIGURE 4 Time course of runcaciguat-induced dilation of angiotensin II (Ang II) pre-constricted glomerular arterioles. Glomerular arterioles were pretreated with L-NAME (10^{-4} M) and pre-constricted with Ang II (10^{-12} to 10^{-6} M), as shown before. Then, runcaciguat (10^{-7} M; 'L-NAME + runcaciguat') or DMSO ('L-NAME + vehicle') were applied and diameter changes of (a) afferent arterioles and (b) efferent arteriole were monitored over 10 min. Data represent mean ± SD. *n* values are indicated in parentheses. The colour code given in panel (b) corresponds to the experimental groups indicated in panel (a). *$P < 0.05$

afferent arterioles were significantly more sensitive to runcaciguat than L-NAME pretreated afferent arterioles (Figure 3e,). ODQ pretreated efferent arterioles also showed a trend towards increased sensitivity to runcaciguat as compared with L-NAME pretreated efferent arterioles, but the difference did not reach statistical significance (Figure 3f). The dilating effect of runcaciguat on L-NAME pretreated vessels started at significantly lower concentrations in efferent arterioles than in afferent arterioles but was not significantly different between ODQ pretreated efferent and afferent arterioles (Figure 3e, f). These observations suggested a greater sensitivity for sGC activator of efferent over afferent arterioles under NO deficiency. The highest applied dose of runcaciguat (10^{-6} M) induced significantly stronger dilation of L-NAME pretreated efferent than afferent arterioles (efferent: 110%, afferent: 49%, Figure 3e,f). Maximal dilatations did not differ significantly in vessels pretreated with ODQ (efferent: 91%, afferent: 83%, Figure 3e,f). The dilation induced by runcaciguat (10^{-6} M) in the presence of ODQ was comparable with the maximal dilation that could be achieved by application of the NO donor SNAP or the L- and N-type calcium channel blocker cilnidipine (Figure S2). Further experiments showed that SNAP-induced but not cilnidipine-induced dilation was efficiently blocked by ODQ (Figure S2). Together, these results indicated that runcaciguat is a potent vasodilator of glomerular arterioles under conditions of NO deficiency and oxidative stress.

To further evaluate the time course of sGC activator action, we evaluated how afferent and efferent arteriole diameters changed during prolonged 10 min bolus applications of runcaciguat (10^{-7} M). In these experiments, arterioles were pretreated with L-NAME (10^{-4} M) and pre-constricted with Ang II (10^{-12}–10^{-6} M, not shown). Again, the diameters before application of runcaciguat or vehicle were

similar (data not shown). The maximum vasodilatation achieved 10 min after application of runcaciguat was 50% of constriction in afferent arterioles (Figure 4a) and 60% in efferent arterioles (Figure 4b). Maximal vasodilation and kinetics of diameter changes were not significantly different between afferent and efferent arterioles.

Overall, these data indicated a reduction in renal resistance triggered by the sGC activator runcaciguat under conditions of oxidative stress and NO deficiency. At the tested concentration range, runcaciguat induced dilation of afferent and efferent arterioles. The vasodilating effect of runcaciguat was stronger after pretreatment with ODQ than with L-NAME, suggesting that runcaciguat activates the sGC more potently under conditions of oxidative stress.

3.4 | Runcaciguat increases cGMP and improves RBF in perfused mouse kidneys

To complement the cGMP imaging data generated in kidney slices (Figures 1 and 2) and vascular reactivity measurements with isolated glomerular arterioles (Figures 3 and 4), we went on to analyse RBF and cGMP production under close-to-native conditions in whole kidneys. To do so, mouse kidneys were isolated and perfused at constant pressure (100 mmHg) as described previously (Schweda et al., 2003). Once perfusion of the kidney had stabilised (i.e. after 20 min perfusion), ODQ was infused to mimic NO deficiency and oxidative stress as observed in chronic kidney disease patients (Elshamaa et al., 2011; Martens & Edwards, 2011; Stasch et al., 2015).

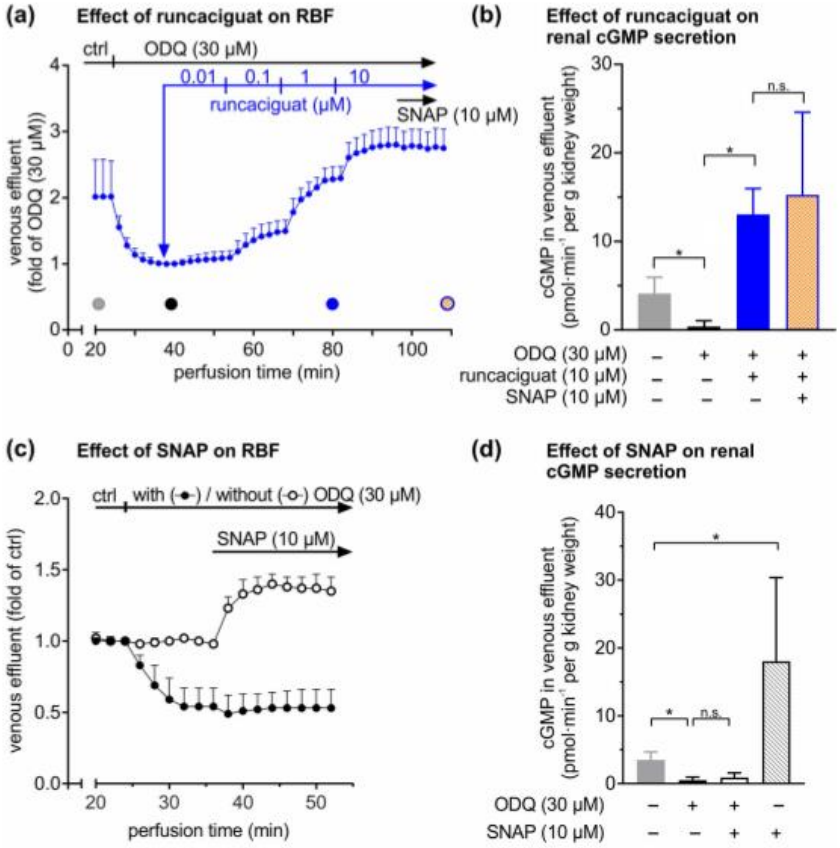

FIGURE 5 Renal blood flow (RBF) and cGMP secretion in perfused mouse kidneys. Kidneys were isolated and perfused at constant pressure (100 mmHg). (a) RBF was analysed by measuring the amount of venous effluent. After stabilization of perfusion (i.e. after 20 min), ODQ (30 µM) followed by incremental concentrations of runcaciguat (0.01, 0.1, 1 and 10 µM) and *S*-nitroso-*N*-acetylpenicillamine (SNAP; 10 µM) were applied sequentially, while the venous effluent was continuously quantified. Filled circles indicate time points at which the cGMP concentration in the venous effluent was determined ($n = 6$). (b) The cGMP concentration in the venous effluent was determined via enzyme immunoassay and multiplied by the perfusate flow to determine cGMP secretion as a measure of intrarenal cGMP formation. (c, d) Similarly, the effects of SNAP (10 µM) in the absence or presence of ODQ (30 µM) on RBF (c) and on renal cGMP secretion (d) were determined ($n = 5$). Data represent mean ± SD. *$P < 0.05$; n.s., not significant; ctrl, control

ODQ (30 μM) strongly reduced RBF to approximately 50% of control (Figure 5a). In line with this finding, ODQ also reduced the cGMP content in the venous effluent as compared with baseline conditions (Figure 5b). Reduction of RBF by ODQ plateaued roughly 10 min after the start of infusion. Under these oxidative stress conditions, runcaciguat (10 μM) increased the cGMP content from 1.21 ± 0.6 to 13.1 ± 0.7 pmol·min^{-1} per g kidney (Figure 5b). At the same time, runcaciguat dose-dependently increased RBF to a level above the baseline recorded in the absence of ODQ at the beginning of the experiment (Figure 5a). After this increase in RBF by runcaciguat, addition of the NO donor SNAP did not significantly change cGMP production (13.1 ± 0.7 versus 15.3 ± 1.2 pmol·min^{-1} per g kidney) (Figure 5b) and did not further change RBF (Figure 5a). In addition, we analysed the effects of SNAP on RBF and cGMP secretion under basal versus oxidative stress conditions (Figure 5c,d). Under basal conditions, SNAP potently increased renal perfusion and cGMP content, while it failed to do so in the presence of ODQ. In summary, these data showed that in the presence of ODQ mimicking chronic kidney disease-related oxidative stress conditions, runcaciguat increases the renal cGMP concentration and RBF in perfused mouse kidneys, whereas NO is no longer able to do so under these conditions.

4 | DISCUSSION

This study showed that sGC activators increase the glomerular cGMP concentration, induce dilation of pre-constricted glomerular arterioles and improve RBF under conditions of NO deficiency and oxidative stress. It is known that oxidation of sGC from its native to the haem-free form, apo-sGC, prevents binding of NO and thereby shuts down the NO/sGC/cGMP signalling pathway (Stasch et al., 2015). This leads to reduced production of cGMP, which is important for the regulation of body homeostasis and kidney function (Krishnan et al., 2018; Wang-Rosenke et al., 2008). As sGC activators act in an NO- and haem-independent manner, these compounds might be able to restore cGMP signalling under pathophysiological conditions involving oxidative stress. Because chronic kidney disease is associated with oxidative stress (Matsuda & Shimomura, 2013; Moon & Won, 2017) and oxidation of sGC might be a critical driver of chronic kidney disease, sGC activators represent a promising new option for chronic kidney disease treatment. However, the mode of action of sGC activators in renal tissue and specifically their impact on renal blood vessels is poorly understood.

To explore the spatiotemporal dynamics of NO- and sGC activator-induced cGMP signals in the kidney, we performed real-time cGMP imaging in kidney slices of transgenic cGMP sensor mice. To our knowledge, this is the first demonstration of cGMP signals in live kidney tissue. We showed that NO and sGC activator increase the cGMP concentration in glomeruli in the absence and presence of oxidative stress, respectively. Furthermore, runcaciguat induced dilation of glomerular arterioles and improved RBF under disease-relevant conditions of oxidative stress and NO depletion. Although the present study did not experimentally distinguish between specific renal cell types, the combined results strongly suggest that runcaciguat acts on apo-sGC in vascular smooth muscle cells of glomerular arterioles, leading to an increase of cGMP, activation of cGMP-dependent protein kinase type I and vasodilation. This model is consistent with the cellular distribution of sGC in the kidney. Using a highly specific antibody against the β1 subunit of sGC, expression of the protein was detected in renal vascular cells, including glomerular arterioles (Theilig et al., 2001). Expression data, however, do not show the functionality of sGC in a specific compartment. It is well known that enzyme activity is regulated by post-translational mechanisms including, in the case of sGC, protein oxidation. Our cGMP imaging data link sGC expression in glomeruli with respective enzyme activity in the absence and presence of oxidative stress. Because the R26-CAG-cGi500(L1) mice used in this study express the cGMP sensor in all cell types, we cannot exclude the possibility that cGMP signals measured in our FRET imaging experiments were also derived from non-vascular smooth muscle cells that express sGC, such as interstitial fibroblasts (Theilig et al., 2001). However, it is unlikely that these cells were involved in sGC activator-induced dilation of renal arterioles. To analyse which specific renal cell types are capable of generating cGMP in response to NO and sGC activators, additional experiments could be performed using transgenic mice with cell type-specific expression of the cGMP sensor (Thunemann et al., 2013). Furthermore, it would be interesting to analyse the effects of sGC activators on cGMP signals in chronic kidney disease kidneys.

Real-time cGMP imaging illustrated that BAY-543 induces cGMP generation in glomeruli specifically in the presence of oxidative stress. This finding complements previous *in vitro* experiments showing that apo-sGC has a higher sensitivity for sGC activators than native sGC (Schmidt et al., 2009). To further dissect the mechanism of sGC activator action on kidney function, we investigated the effects of runcaciguat on the diameter of murine glomerular afferent and efferent arteries. It is known that pre-glomerular resistance and glomerular haemodynamics contribute to the control of the murine GFR (Patzak et al., 2004). Under pathological conditions, such as hypertension and type-2-diabetes, an increase in vascular resistance provokes a reduction of vascular diameter and arterial remodelling in the kidney, leading to impaired vascular reactivity and kidney perfusion (Polichnowski et al., 2013; Touyz et al., 2018). In the present study, we showed that runcaciguat improves vascular reactivity of pre-constricted murine glomerular afferent and efferent arterioles under conditions of NO deficiency and oxidative stress. Runcaciguat induced a concentration-dependent relaxation of pre-constricted glomerular arterioles with an apparent higher sensitivity for ODQ over L-NAME pretreated arterioles. This finding is consistent with a predominant action of sGC activator under oxidative stress as measured in our cGMP imaging experiments with kidney slices. Interestingly, the stronger action of runcaciguat in efferent compared with afferent arterioles indicate an influence on the GFR. This must be investigated in further experiments, for example, via cannulation of the ureter during experiments on isolated perfused kidneys.

To validate the cGMP imaging and vascular reactivity data obtained in kidney slices and isolated arterioles in a more physiological

setting, we evaluated the effects of runcaciguat in perfused whole mouse kidneys. In order to mimic chronic kidney disease-related oxidative stress, ODQ was infused. ODQ rapidly induced stable reduction of kidney perfusion, which could be reversed by runcaciguat in a concentration-dependent manner. In parallel, ODQ induced a significant reduction of the renal cGMP content, which was restored by runcaciguat. At the same time, the improvement of kidney perfusion and cGMP secretion by the NO donor SNAP was completely abolished by ODQ. These data indicate that in contrast to NO, runcaciguat increases cGMP levels and RBF under oxidative stress conditions. Together with the experiments in isolated renal arterioles, these findings strongly suggest a beneficial effect of sGC activators on the perfusion of diseased kidneys by dilating glomerular arterioles under conditions of NO deficiency and oxidative stress. Our study was performed with mouse kidneys, but it is likely that sGC activators have similar effects on human kidney perfusion. Indeed, a recent study reported that the sGC activator BAY 60–2770 relaxes human intrarenal arteries (Frees et al., 2020), indicating that the murine kidney is a suitable model for preclinical studies.

Within the scope of this study, the effect of sGC activators on the renal vasculature was analysed in detail. In addition to their vasodilative effects, sGC activators may also be renoprotective via antifibrotic, antiproliferative and anti-inflammatory effects on vascular and non-vascular compartments of the kidney. In this context, it is interesting to note that the sGC activator BI 703704 (Boustany-Kari et al., 2016) and the sGC stimulator **praliciguat** (Liu et al., 2020) inhibited the progression of diabetic nephropathy in obese ZSF1 rats in doses that did not alter BP, perhaps via suppression of inflammation and apoptosis in tubular cells (Liu et al., 2020). sGC activators may inhibit glomerular remodelling also via direct effects on vascular smooth muscle cells independent of vasodilation. It is well known that NO/sGC/cGMP signalling in vascular smooth muscle cells regulates vascular plasticity and remodelling during diseases like atherosclerosis (Lehners et al., 2018).

In summary, our results indicate that sGC activators increase cGMP production in vascular smooth muscle cells in glomerular arterioles and, thereby, improve kidney perfusion under disease-relevant conditions of oxidative stress and NO depletion. The unique selectivity of sGC activators for oxidised apo-sGC has great potential to limit off-target effects on healthy tissue, where sGC is mainly present in its native reduced form (Sharkovska et al., 2010). Most of the comorbidities in chronic kidney disease are associated with increased oxidative stress burden, leading to endothelial dysfunction with low NO production as well as NO-unresponsive apo-sGC. It is an intriguing concept that sGC activators could overcome the pathophysiological blockade of the endogenous NO/sGC/cGMP in renal tissue. Thus, sGC activators like runcaciguat could provide a novel and effective chronic kidney disease treatment.

ACKNOWLEDGMENTS

The authors like to thank Markus Wolters for his help with initial cGMP imaging of kidney slices, Hana Cernecka for her support in refining the IPK graphs and Maria T. Kristina Zaldivia for reading the manuscript. R.F. and S.F. received grants from the Deutsche Forschungsgemeinschaft (DFG, German Research Foundation) – FOR 2060 projects FE 438/5-2 and FE 438/6-2, Projektnummer 374031971 - TRR 240, and Projektnummer 335549539 - GRK 2381.

AUTHOR CONTRIBUTIONS

T.S., F.S., A.P., R.F. and A.B. designed the project. D.S., M.Z.X., T.S., F.S. and S.F. acquired and analysed the data. T.S., M.G.H., F.E. and P.S. provided novel sGC activators. D.S., J.R.K., A.P., P.S., R.F. and A.B. wrote, and all authors edited and approved the manuscript.

CONFLICT OF INTERESTS

T.S., M.G.H., I.M., J.R.K., F.E. and P.S. are employees of Bayer AG. A.B. has been an employee of Bayer AG and is now employed at Novo Nordisk A/S. D.S., M.Z.X., F.S., S.F., A.P. and R.F. have received a restricted research grant from Bayer AG to conduct experiments.

DECLARATION OF TRANSPARENCY AND SCIENTIFIC RIGOUR

This Declaration acknowledges that this paper adheres to the principles for transparent reporting and scientific rigour of preclinical research as stated in the *British Journal of Pharmacology* guidelines for Design and Analysis and Animal Experimentation, and as recommended by funding agencies, publishers and other organisations engaged with supporting research.

DATA AVAILABILITY STATEMENT

The data that support the findings of this study are available from the corresponding author upon reasonable request. Some data may not be made available because of privacy or ethical restrictions. The authors state that no material from other sources than the presented experiments was used. Citation was indicated according to *British Journal of Pharmacology* guidelines.

ORCID

Daniel Stehle https://orcid.org/0000-0001-9086-2306
Peter Sandner https://orcid.org/0000-0003-2977-7553
Robert Feil https://orcid.org/0000-0002-7335-4841

REFERENCES

Alexander, S. P. H., Fabbro, D., Kelly, E., Mathie, A., Peters, J. A., Veale, E. L., Armstrong, J. F., Faccenda, E., Harding, S. D., Pawson, A. J., & Sharman, J. L. (2019). The Concise Guide to PHARMACOLOGY 2019/20: Catalytic receptors. *British Journal of Pharmacology*, *176*(Suppl 1), S247–S296. https://doi.org/10.1111/bph.14751

Benardeau, A., Hahn, M. G., Gerisch, M., Meyer, M., Menshykau, D., Hetzel, T., Schlender, J., Hartmann, E., Schomber, T., Patzak, A., Schweda, F., Kraehling, J. R., Sandner, P., & Eitner, F. (2020). The novel soluble guanylyl cyclase (sGC) activator runcaciguat induced renal vasodilation and attenuated kidney damage in a rat CKD model. *Journal of the American Society of Nephrology*, *31*(Suppl), PO0600, 232.

Boustany-Kari, C. M., Harrison, P. C., Chen, H., Lincoln, K. A., Qian, H. S., Clifford, H., Wang, H., Zhang, X., Gueneva-Boucheva, K., Bosanac, T.,

Wong, D., Fryer, R. M., Richman, J. G., Sarko, C., & Pullen, S. S. (2016). A soluble guanylate cyclase activator inhibits the progression of diabetic nephropathy in the ZSF1 rat. *The Journal of Pharmacology and Experimental Therapeutics*, *356*(3), 712–719. https://doi.org/10.1124/jpet.115.230706

Brenner, B. M., Cooper, M. E., de Zeeuw, D., Keane, W. F., Mitch, W. E., Parving, H. H., Remuzzi, G., Snapinn, S. M., Zhang, Z., & Shahinfar, S. (2001). Effects of losartan on renal and cardiovascular outcomes in patients with type 2 diabetes and nephropathy. *The New England Journal of Medicine*, *345*(12), 861–869. https://doi.org/10.1056/NEJMoa011161

Breyer, M. D., & Susztak, K. (2016). Developing treatments for chronic kidney disease in the 21st century. *Seminars in Nephrology*, *36*(6), 436–447. https://doi.org/10.1016/j.semnephrol.2016.08.001

Briasoulis, A., Al Dhaybi, O., & Bakris, G. L. (2018). SGLT2 inhibitors and mechanisms of hypertension. *Current Cardiology Reports*, *20*(1), 1–7. https://doi.org/10.1007/s11886-018-0943-5

Brunner, E., & Langer, F. (1999). *Nichtparametrische analyse longitudinaler Daten*. München, Wien: R. Oldenbourg Verlag.

Coppolino, G., Leonardi, G., Andreucci, M., & Bolignano, D. (2018). Oxidative stress and kidney function: A brief update. *Current Pharmaceutical Design*, *24*(40), 4794–4799. https://doi.org/10.2174/1381612825666190112165206

R Core Team. (2020). R: a language and environment for statistical computing. Available from https://www.R-project.org (accessed 24 November 2020)

Coresh, J. (2017). Update on the burden of CKD. *Journal of the American Society of Nephrology*, *28*(4), 1020–1022. https://doi.org/10.1681/ASN.2016121374

Curtis, M. J., Alexander, S., Cirino, G., Docherty, J. R., George, C. H., Giembycz, M. A., Hoyer, D., Insel, P. A., Izzo, A. A., Ji, Y., MacEwan, D. J., Sobey, C. G., Stanford, S. C., Teixeira, M. M., Wonnacott, S., & Ahluwalia, A. (2018). Experimental design and analysis and their reporting II: Updated and simplified guidance for authors and peer reviewers. *British Journal of Pharmacology*, *175*(7), 987–993. https://doi.org/10.1111/bph.14153

Elshamaa, M. F., Sabry, S., Badr, A., El-Ahmady, M., Elghoroury, E. A., Thabet, E. H., Kandil, D., & Kamel, S. (2011). Endothelial nitric oxide synthase gene intron4 VNTR polymorphism in patients with chronic kidney disease. *Blood Coagulation & Fibrinolysis*, *22*(6), 487–492. https://doi.org/10.1097/MBC.0b013e328346ef71

Emdin, C. A., Khera, A. V., Klarin, D., Natarajan, P., Zekavat, S. M., Nomura, A., Haas, M., Aragam, K., Ardissino, D., Wilson, J. G., Schunkert, H., McPherson, R., Watkins, H., Elosua, R., Bown, M. J., Samani, N. J., Baber, U., Erdmann, J., Gormley, P., … Kathiresan, S. (2018). Phenotypic consequences of a genetic predisposition to enhanced nitric oxide signaling. *Circulation*, *137*(3), 222–232. https://doi.org/10.1161/CIRCULATIONAHA.117.028021

Erdmann, J., Stark, K., Esslinger, U. B., Rumpf, P. M., Koesling, D., de Wit, C., Kaiser, F. J., Braunholz, D., Medack, A., Fischer, M., & Zimmermann, M. E. (2013). Dysfunctional nitric oxide signalling increases risk of myocardial infarction. *Nature*, *504*(7480), 432–436. https://doi.org/10.1038/nature12722

Frees, A., Assersen, K. B., Jensen, M., Hansen, P. B. L., Vanhoutte, P. M., Madsen, K., Federlein, A., Lund, L., Toft, A., & Jensen, B. L. (2020). Natriuretic peptides relax human intrarenal arteries through natriuretic peptide receptor type—A recapitulated by soluble guanylyl cyclase agonists. *Acta Physiologica (Oxford, England)*, *231*, e13565. https://doi.org/10.1111/apha.13565

Griffin, K. A. (2017). Hypertensive kidney injury and the progression of chronic kidney disease. *Hypertension*, *70*(4), 687–694. https://doi.org/10.1161/HYPERTENSIONAHA.117.08314

Hahn, M. G. (2018). BAY-1101042: A potent NO- and heme-independent sGC activator suitable for oral dosing. *Drugs of the Future*, *43*(10), 783–792.

Hahn, M. G., Lampe, T., Sheikh, S. E., Griebenow, N., Woltering, E., Schlemmer, K.-H., Dietz, L., Gerisch, M., Wunder, F., Becker-Pelster, E. M., Mondritzki, T., Tinel, H., Knorr, A., Kern, A., Lang, D., Hueser, J., Schomber, T., Benardeau, A., Eitner, F., … Stasch, J. P. (2021). Discovery of the soluble guanylate cyclase activator runcaciguat (BAY 1101042). *Journal of Medicinal Chemistry*, *64*(9), 5323–5344. https://doi.org/10.1021/acs.jmedchem.0c02154

International Consortium for Blood Pressure Genome-Wide Association Studies, Ehret, G. B., Munroe, P. B., Rice, K. M., Bochud, M., Johnson, A. D., Smith, A. V., Psaty, B. M., Abecasis, G. R., Chakravarti, A., Elliott, P., van Duijn, C. M., Newton-Cheh, C., Levy, D., Caulfield, M. J., & Johnson, T. (2011). Genetic variants in novel pathways influence blood pressure and cardiovascular disease risk. *Nature*, *478*(7367), 103–109. https://doi.org/10.1038/nature10405

Krishnan, S. M., Kraehling, J. R., Eitner, F., Benardeau, A., & Sandner, P. (2018). The impact of the nitric oxide (NO)/soluble guanylyl cyclase (sGC) signaling cascade on kidney health and disease: A preclinical perspective. *International Journal of Molecular Sciences*, *19*(6), 1–18. 1712. https://doi.org/10.3390/ijms19061712

Lehners, M., Dobrowinski, H., Feil, S., & Feil, R. (2018). cGMP signaling and vascular smooth muscle cell plasticity. *Journal of Cardiovascular Development and Disease*, *5*(2), 20, 1–18. https://doi.org/10.3390/jcdd5020020

Lilley, E., Stanford, S. C., Kendall, D. E., Alexander, S. P., Cirino, G., Docherty, J. R., George, C. H., Insel, P. A., Izzo, A. A., Ji, Y., Panettieri, R. A., Sobey, C. G., Stefanska, B., Stephens, G., Teixeira, M., & Ahluwalia, A. (2020). ARRIVE 2.0 and the *British Journal of Pharmacology*: Updated guidance for 2020. *British Journal of Pharmacology*, *177*(16), 3611–3616. https://doi.org/10.1111/bph.15178

Lin, Y. H., Huang, Y. Y., Hsieh, S. H., Sun, J. H., Chen, S. T., & Lin, C. H. (2019). Renal and glucose-lowering effects of empagliflozin and dapagliflozin in different chronic kidney disease stages. *Frontiers in Endocrinology*, *22*(10), 1–11, 820. https://doi.org/10.3389/fendo.2019.00820

Liu, G., Shea, C. M., Jones, J. E., Price, G. M., Warren, W., Lonie, E., Yan, S., Currie, M. G., Profy, A. T., Masferrer, J. L., & Zimmer, D. P. (2020). Praliciguat inhibits progression of diabetic nephropathy in ZSF1 rats and suppresses inflammation and apoptosis in human renal proximal tubular cells. *American Journal of Physiology. Renal Physiology*, *319*(4), F697–F711. https://doi.org/10.1152/ajprenal.00003.2020

Liu, Z. Z., Viegas, V. U., Perlewitz, A., Lai, E. Y., Persson, P. B., Patzak, A., & Sendeski, M. M. (2012). Iodinated contrast media differentially affect afferent and efferent arteriolar tone and reactivity in mice: A possible explanation for reduced glomerular filtration rate. *Radiology*, *265*(3), 762–771. https://doi.org/10.1148/radiol.12120044

Maass, P. G., Aydin, A., Luft, F. C., Schachterle, C., Weise, A., Stricker, S., Lindschau, C., Vaegler, M., Qadri, F., Toka, H. R., Schulz, H., & Bahring, S. (2015). PDE3A mutations cause autosomal dominant hypertension with brachydactyly. *Nature Genetics*, *47*(6), 647–653. https://doi.org/10.1038/ng.3302

Martens, C. R., & Edwards, D. G. (2011). Peripheral vascular dysfunction in chronic kidney disease. *Cardiology Research and Practice*, *2011*, 267257–267259. https://doi.org/10.4061/2011/267257

Matsuda, M., & Shimomura, I. (2013). Increased oxidative stress in obesity: Implications for metabolic syndrome, diabetes, hypertension, dyslipidemia, atherosclerosis, and cancer. *Obesity Research & Clinical Practice*, *7*(5), e330–e341. https://doi.org/10.1016/j.orcp.2013.05.004

Moon, J. S., & Won, K. C. (2017). Oxidative stress: Link between hypertension and diabetes. *The Korean Journal of Internal Medicine*, *32*(3), 439–441. https://doi.org/10.3904/kjim.2017.153

Muskiet, M. H. A., Heerspink, H. J. L., & van Raalte, D. H. (2017). SGLT2 inhibition: A new era in renoprotective medicine? *The Lancet Diabetes and Endocrinology*, *5*(8), 569–571. https://doi.org/10.1016/S2213-8587(17)30222-X

Ott, I. M., Alter, M. L., von Websky, K., Kretschmer, A., Tsuprykov, O., Sharkovska, Y., Krause-Relle, K., Raila, J., Henze, A., Stasch, J. P., & Hocher, B. (2012). Effects of stimulation of soluble guanylate cyclase on diabetic nephropathy in diabetic eNOS knockout mice on top of angiotensin II receptor blockade. *PLoS ONE*, *7*(8), e42623. https://doi.org/10.1371/journal.pone.0042623

Patzak, A., Lai, E. Y., Mrowka, R., Steege, A., Persson, P. B., & Persson, A. E. (2004). AT1 receptors mediate angiotensin II-induced release of nitric oxide in afferent arterioles. *Kidney International*, *66*(5), 1949–1958. https://doi.org/10.1111/j.1523-1755.2004.00981.x

Patzak, A., Mrowka, R., Storch, E., Hocher, B., & Persson, P. B. (2001). Interaction of angiotensin II and nitric oxide in isolated perfused afferent arterioles of mice. *Journal of the American Society of Nephrology*, *12*(6), 1122–1127. https://doi.org/10.1681/ASN.V1261122

Percie du Sert, N., Hurst, V., Ahluwalia, A., Alam, S., Avey, M. T., Baker, M., Browne, W. J., Clark, A., Cuthill, I. C., Dirnagl, U., Emerson, M., Garner, P., Holgate, S. T., Howells, D. W., Karp, N. A., Lazic, S. E., Lidster, K., MacCallum, C. J., Macleod, M., … Würbel, H. (2020). The ARRIVE guidelines 2.0: Updated guidelines for reporting animal research. *PLoS Biology*, *18*(7), 1–65, e3000411. https://doi.org/10.1371/journal.pbio.3000410

Polichnowski, A. J., Griffin, K. A., Long, J., Williamson, G. A., & Bidani, A. K. (2013). Blood pressure-renal blood flow relationships in conscious angiotensin II- and phenylephrine-infused rats. *American Journal of Physiology. Renal Physiology*, *305*(7), F1074–F1084. https://doi.org/10.1152/ajprenal.00111.2013

Rueden, C. T., Schindelin, J., Hiner, M. C., DeZonia, B. E., Walter, A. E., Arena, E. T., & Eliceiri, K. W. (2017). ImageJ2: ImageJ for the next generation of scientific image data. *BMC Bioinformatics*, *18*(1), 1–26, 529. https://doi.org/10.1186/s12859-017-1934-z

Rühle, A., Elgert, C., Hahn, M. G., Sandner, P., & Behrends, S. (2020). Tyrosine 135 of the beta1 subunit as binding site of BAY-543: Importance of the Y-x-S-x-R motif for binding and activation by sGC activator drugs. *European Journal of Pharmacology*, *881*, 173203. https://doi.org/10.1016/j.ejphar.2020.173203

Russwurm, M., Mullershausen, F., Friebe, A., Jager, R., Russwurm, C., & Koesling, D. (2007). Design of fluorescence resonance energy transfer (FRET)-based cGMP indicators: A systematic approach. *The Biochemical Journal*, *407*(1), 69–77. https://doi.org/10.1042/BJ20070348

Samarghandian, S., Azimi-Nezhad, M., Farkhondeh, T., & Samini, F. (2017). Anti-oxidative effects of curcumin on immobilization-induced oxidative stress in rat brain, liver and kidney. *Biomedicine & Pharmacotherapy*, *87*, 223–229. https://doi.org/10.1016/j.biopha.2016.12.105

Schievink, B., Kropelin, T., Mulder, S., Parving, H. H., Remuzzi, G., Dwyer, J., Vemer, P., de Zeeuw, D., & Lambers Heerspink, H. J. (2016). Early renin-angiotensin system intervention is more beneficial than late intervention in delaying end-stage renal disease in patients with type 2 diabetes. *Diabetes, Obesity & Metabolism*, *18*(1), 64–71. https://doi.org/10.1111/dom.12583

Schindelin, J., Arganda-Carreras, I., Frise, E., Kaynig, V., Longair, M., Pietzsch, T., Preibisch, S., Rueden, C., Saalfeld, S., Schmid, B., Tinevez, J. Y., White, D. J., Hartenstein, V., Eliceiri, K., Tomancak, P., & Cardona, A. (2012). Fiji: An open-source platform for biological-image analysis. *Nature Methods*, *9*(7), 676–682. https://doi.org/10.1038/nmeth.2019

Schmidt, H. H., Schmidt, P. M., & Stasch, J. P. (2009). NO- and haem-independent soluble guanylate cyclase activators. *Handbook of Experimental Pharmacology*, *191*, 309–339. https://doi.org/10.1007/978-3-540-68964-5_14

Schweda, F., Wagner, C., Kramer, B. K., Schnermann, J., & Kurtz, A. (2003). Preserved macula densa-dependent renin secretion in A1 adenosine receptor knockout mice. *American Journal of Physiology. Renal Physiology*, *284*(4), F770–F777. https://doi.org/10.1152/ajprenal.00280.2002

Sharkovska, Y., Kalk, P., Lawrenz, B., Godes, M., Hoffmann, L. S., Wellkisch, K., Geschka, S., Relle, K., Hocher, B., & Stasch, J. P. (2010). Nitric oxide-independent stimulation of soluble guanylate cyclase reduces organ damage in experimental low-renin and high-renin models. *Journal of Hypertension*, *28*(8), 1666–1675. https://doi.org/10.1097/HJH.0b013e32833b558c

Sinha, N., & Dabla, P. K. (2015). Oxidative stress and antioxidants in hypertension-a current review. *Current Hypertension Reviews*, *11*(2), 132–142. https://doi.org/10.2174/1573402111666150529130922

Siragy, H. M., & Carey, R. M. (2010). Role of the intrarenal renin-angiotensin-aldosterone system in chronic kidney disease. *American Journal of Nephrology*, *31*(6), 541–550. https://doi.org/10.1159/000313363

Stasch, J. P., Schlossmann, J., & Hocher, B. (2015). Renal effects of soluble guanylate cyclase stimulators and activators: A review of the preclinical evidence. *Current Opinion in Pharmacology*, *21*, 95–104. https://doi.org/10.1016/j.coph.2014.12.014

Su, H., Wan, C., Song, A., Qiu, Y., Xiong, W., & Zhang, C. (2019). Oxidative stress and renal fibrosis: Mechanisms and therapies. *Advances in Experimental Medicine and Biology*, *1165*, 585–604. https://doi.org/10.1007/978-981-13-8871-2_29

Sugiyama, S., Yoshida, A., Hieshima, K., Kurinami, N., Jinnouchi, K., Tanaka, M., Suzuki, T., Miyamoto, F., Kajiwara, K., Jinnouchi, T., & Jinnouchi, H. (2020). Initial acute decline in estimated glomerular filtration rate after sodium-glucose cotransporter-2 inhibitor in patients with chronic kidney disease. *Journal of Clinical Medical Research*, *12*(11), 724–733. https://doi.org/10.14740/jocmr4351

Theilig, F., Bostanjoglo, M., Pavenstadt, H., Grupp, C., Holland, G., Slosarek, I., Gressner, A. M., Russwurm, M., Koesling, D., & Bachmann, S. (2001). Cellular distribution and function of soluble guanylyl cyclase in rat kidney and liver. *Journal of the American Society of Nephrology*, *12*(11), 2209–2220. https://doi.org/10.1681/ASN.V12112209

Thunemann, M., Wen, L., Hillenbrand, M., Vachaviolos, A., Feil, S., Ott, T., Han, X., Fukumura, D., Jain, R. K., Russwurm, M., de Wit, C., & Feil, R. (2013). Transgenic mice for cGMP imaging. *Circulation Research*, *113*(4), 365–371. https://doi.org/10.1161/CIRCRESAHA.113.301063

Touyz, R. M., Alves-Lopes, R., Rios, F. J., Camargo, L. L., Anagnostopoulou, A., Arner, A., & Montezano, A. C. (2018). Vascular smooth muscle contraction in hypertension. *Cardiovascular Research*, *114*(4), 529–539. https://doi.org/10.1093/cvr/cvy023

Vallon, V., & Thomson, S. C. (2017). Targeting renal glucose reabsorption to treat hyperglycaemia: The pleiotropic effects of SGLT2 inhibition. *Diabetologia*, *60*(2), 215–225. https://doi.org/10.1007/s00125-016-4157-3

Wang-Rosenke, Y., Neumayer, H. H., & Peters, H. (2008). NO signaling through cGMP in renal tissue fibrosis and beyond: Key pathway and novel therapeutic target. *Current Medicinal Chemistry*, *15*(14), 1396–1406. https://doi.org/10.2174/092986708784567725

SUPPORTING INFORMATION

Additional supporting information may be found online in the Supporting Information section at the end of this article.

How to cite this article: Stehle, D., Xu, M. Z., Schomber, T., Hahn, M. G., Schweda, F., Feil, S., Kraehling, J. R., Eitner, F., Patzak, A., Sandner, P., Feil, R., & Bénardeau, A. (2022). Novel soluble guanylyl cyclase activators increase glomerular cGMP, induce vasodilation and improve blood flow in the murine kidney. *British Journal of Pharmacology*, *179*(11), 2476–2489. https://doi.org/10.1111/bph.15586

Eingesetzt wird dafür im einleitenden Text ein DOI-Link zum Artikel:

https://doi.org/10.1152/ajprenal.00272.2020

Curriculum Vitae

My curriculum vitae does not appear in the electronic version of my paper for reasons of data protection.

Publication list

Original papers:

1. Fei L, **Xu M**, Wang H, Zhong C, Jiang S, Lichtenberger FB, Erdoğan C, Wang H, Bonk JS, Lai EY, Persson PB, Kovács R, Zheng Z, Patzak A, Khedkar PH. Piezo1 Mediates Vasodilation Induced by Acute Hyperglycemia in Mouse Renal Arteries and Microvessels. Hypertension. 2023 Aug;80(8):1598-1610. IF: 9.9
2. Sholokh A, Walter S, Markó L, McMurray BJ, Sunaga-Franze DY, **Xu M**, Zühlke K, Russwurm M, Bartolomaeus TUP, Langanki R, Qadri F, Heuser A, Patzak A, Forslund SK, Bähring S, Borodina T, Persson PB, Maass PG, Bader M, Klussmann E. Mutant phosphodiesterase 3A protects the kidney from hypertension-induced damage. Kidney Int. 2023 Aug;104(2):388-393. IF: 19.6
3. **Xu M**, Lichtenberger FB, Erdoğan C, Lai E, Persson PB, Patzak A, Khedkar PH. Nitric Oxide Signalling in Descending Vasa Recta after Hypoxia/Re-Oxygenation. Int J Mol Sci. 2022 Jun 24;23(13):7016 IF: 5.6
4. Stehle D, **Xu MZ**, Schomber T, Hahn MG, Schweda F, Feil S, Kraehling JR, Eitner F, Patzak A, Sandner P, Feil R, Bénardeau A. Novel soluble guanylyl cyclase activators increase glomerular cGMP, induce vasodilation and improve blood flow in the murine kidney. Br J Pharmacol. 2022 Jun;179(11):2476-2489. IF: 9.5
5. Zhong C, **Xu M**, Boral S, Summer H, Lichtenberger FB, Erdoğan C, Gollasch M, Golz S, Persson PB, Schleifenbaum J, Patzak A, Khedkar PH. Age Impairs Soluble Guanylyl Cyclase Function in Mouse Mesenteric Arteries. Int J Mol Sci. 2021 Oct 22;22(21):11412. IF: 6.2
6. Wennysia IC, Zhao L, Schomber T, Braun D, Golz S, Summer H, Benardeau A, Lai EY, Lichtenberger FB, Schubert R, Persson PB, **Xu MZ**, Patzak A. Role of soluble guanylyl cyclase in renal afferent and efferent arterioles. Am J Physiol Renal Physiol. 2021 Feb 1;320(2):F193-F202. IF: 4.1
7. Liu ZZ, Mathia S, Pahlitzsch T, Wennysia IC, Persson PB, Lai EY, Högner A, **Xu MZ**, Schubert R, Rosenberger C, Patzak A. Myoglobin facilitates angiotensin II-induced constriction of renal afferent arterioles. Am J Physiol Renal Physiol. 2017 May 1;312(5):F908-F916. IF: 3.2

Acknowledgments

I would like to express my deepest gratitude to my supervisor, Professor Andreas Patzak, for his unwavering support and mentorship throughout my doctoral studies. I still remember how he helped me navigate the initial challenging period when I first came here to Berlin. Moreover, when I felt lost and uncertain about my future, he helped me break through the barriers and continue my study. As for me, he is not only a supervisor, but also a guiding elder who supports me not only in my academic part but also in various aspects of my life. I learned not only the knowledge but also the attitude to treat my life from him.

I am also grateful to Professor Enyin Lai for his invaluable help. It is his assistance that provided me with the opportunity to study abroad, and he has offered guidance during moments of personal confusion, helping me find the right direction.

I would like to express my heartfelt appreciation to my parents, Hongwei Xu, and Xiaofu Zhou. Their selfless support and unwavering encouragement have been the pillars that have propelled me forward. In my moments of anguish, while studying and living abroad, they have been my refuge and the guiding light that has illuminated my path.

To my beloved wife, Yuejia Wang. I am deeply grateful for her unwavering encouragement and companionship. The happy moments we share together are the most important source of energy that sustains my academic pursuits and daily life. Her tender care has helped me overcome many difficulties, and I feel very lucky to have such a caring companion to accompany me through my study abroad and future journeys.

I am grateful to all my friends for enriching my life during my time abroad. Their presence has been essential, bringing happiness, shared adventures, and heartfelt conversations. They have added vibrant colors to my overseas experience, acting as both seasoning and the main source of joy in my life.

I would also like to express my gratitude to my colleagues for their assistance during the experiments and their support throughout my time abroad.

To all those who have played a significant role in my academic and personal development, I offer my heartfelt thanks. Your guidance, support, and companionship have shaped my journey and contributed to my growth as a scholar and an individual.